

AD-A160 991

NUMERICAL MODELING OF TWO-DIMENSIONAL WIDTH-AVERAGED
FLOWS USING BOUNDARY (U) MISSISSIPPI STATE UNIV
MISSISSIPPI STATE DEPT OF AEROPHYSICS A

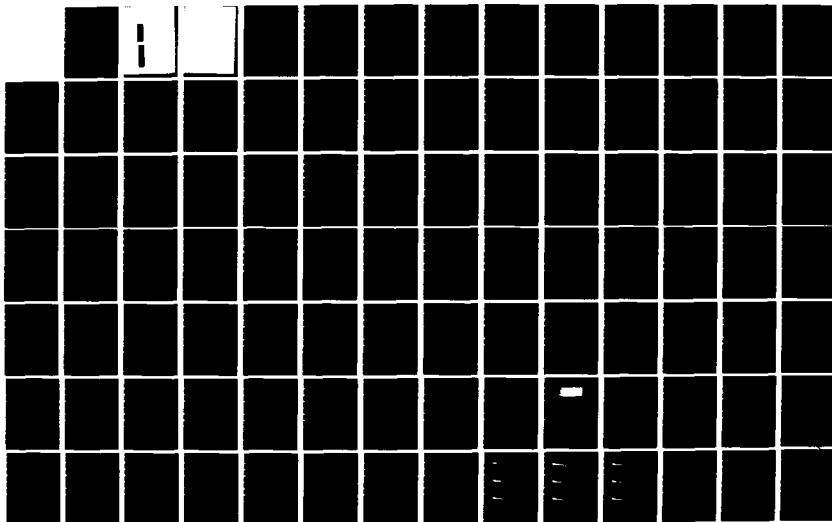
1/2

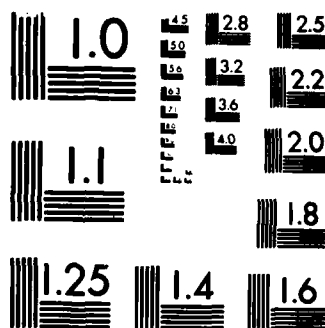
UNCLASSIFIED

J F THOMPSON ET AL AUG 85 WES/TR/E-85-9

F/G 20/4

NL

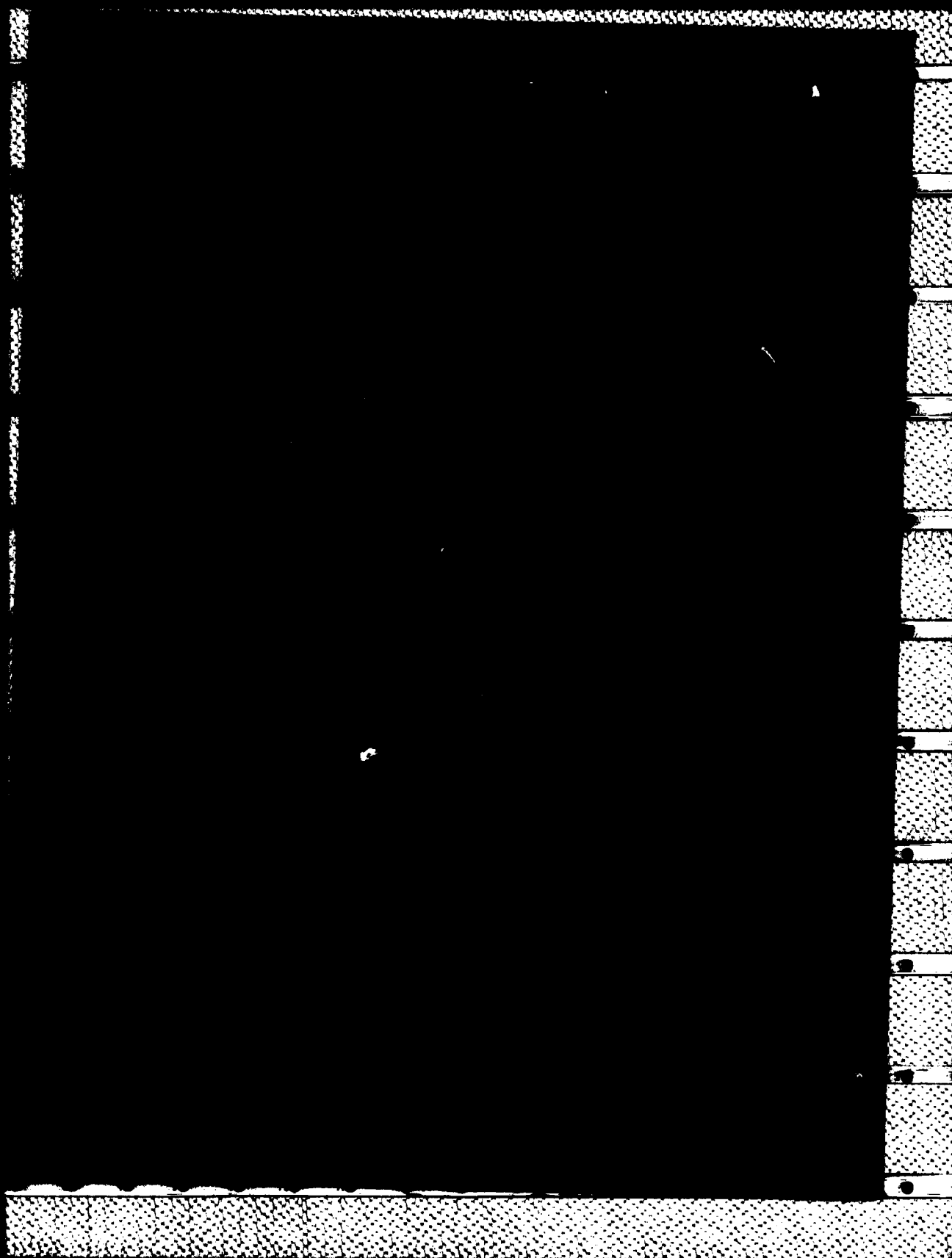




MICROCOPY RESOLUTION TEST CHART
NATIONAL BUREAU OF STANDARDS-1963-A

AD-A160 991

DTIC FILE COPY



Unclassified

2

SECURITY CLASSIFICATION OF THIS PAGE (When Data Entered)

REPORT DOCUMENTATION PAGE		READ INSTRUCTIONS BEFORE COMPLETING FORM
1. REPORT NUMBER Technical Report E-85-9	2. GOVT ACCESSION NO. AD-A160771	RECIPIENT'S CATALOG NUMBER
4. TITLE (and Subtitle) NUMERICAL MODELING OF TWO-DIMENSIONAL WIDTH-AVERAGED FLOWS USING BOUNDARY-FITTED COORDINATE SYSTEMS		5. TYPE OF REPORT & PERIOD COVERED Final report
7. AUTHOR(s) Joe F. Thompson, Robert S. Bernard		6. PERFORMING ORG. REPORT NUMBER
9. PERFORMING ORGANIZATION NAME AND ADDRESS Mississippi State University, Department of Aerospace Engineering, Drawer A, Mississippi State, Mississippi 39762; US Army Engineer Waterways Experiment Station, Hydraulics Laboratory, PO Box 631, Vicksburg, Mississippi 39180-0631		8. CONTRACT OR GRANT NUMBER(s) Contract No. DACW39-78-C-0054
11. CONTROLLING OFFICE NAME AND ADDRESS DEPARTMENT OF THE ARMY US Army Corps of Engineers Washington, DC 20314-1000		10. PROGRAM ELEMENT, PROJECT, TASK AREA & WORK UNIT NUMBERS CWIS No. 31604 (EWQOS Task IIIA.4)
14. MONITORING AGENCY NAME & ADDRESS (if different from Controlling Office) US Army Engineer Waterways Experiment Station Environmental Laboratory PO Box 631, Vicksburg, Mississippi 39180-0631		12. REPORT DATE August 1985
		13. NUMBER OF PAGES 122
		15. SECURITY CLASS. (of this report) Unclassified
		15a. DECLASSIFICATION/DOWNGRADING SCHEDULE
16. DISTRIBUTION STATEMENT (of this Report) Approved for public release; distribution unlimited.		
17. DISTRIBUTION STATEMENT (of the abstract entered in Block 20, if different from Report) E		
18. SUPPLEMENTARY NOTES Available from National Technical Information Service, 5285 Port Royal Road, Springfield, Virginia 22161.		
19. KEY WORDS (Continue on reverse side if necessary and identify by block number) Boundary-fitted coordinates Reservoirs Hydrodynamics Selective withdrawal Numerical modeling Stratified flow		
20. ABSTRACT (Continue on reverse side if necessary and identify by block number) Finite-difference solution of two-dimensional (2D), time-dependent width-averaged Navier-Stokes equations, including an algebraic turbulence model, based on a numerically generated boundary-fitted coordinate system, is discussed. This solution, implemented by the WESSEL computer code, is applicable to 2D regions of arbitrary shape, with multiple inlets and outlets, and with obstacles in the interior. A choice of central, upwind, or ZIP		

(Continued)

DD FORM 1 JAN 73 1473 EDITION OF 1 NOV 65 IS OBSOLETE

Unclassified

SECURITY CLASSIFICATION OF THIS PAGE (When Data Entered)

Unclassified

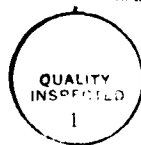
SECURITY CLASSIFICATION OF THIS PAGE(When Data Entered)

20. ABSTRACT (Continued).

differencing of the convective terms is provided. One-sided differencing is used for the continuity equation. The density is taken to be a function of the temperature, and the system of equations forming the model consists of the continuity equation, the two momentum equations, and the energy equation. Arbitrary distribution of velocity and temperature (or density) can be specified on the inlets and outlets. The solution is implicit in time, with the difference equations being solved simultaneously by SOR (successive over-relaxation) iteration at each time step. Pressure is calculated via Chorin's method. *Revised 10/10*

The WESSEL code permits analysis of hydrodynamics for a variety of applications to Civil Works projects.

Accession For	
NTIS GRA&I	<input checked="checked" type="checkbox"/>
DTIC TAB	<input type="checkbox"/>
Unannounced	<input type="checkbox"/>
Justification	
By	
Distribution/	
Availability Codes	
Dist	Avail and/or Special
A-1	



Unclassified

SECURITY CLASSIFICATION OF THIS PAGE(When Data Entered)

PREFACE

The study reported herein was sponsored by the Office, Chief of Engineers (OCE), US Army, under the Environmental and Water Quality Operational Studies (EWQOS) Program, through the work unit (CWIS No. 31604) entitled "Techniques to Meet Environmental Quality Objectives for Reservoir Releases." The effort was supported by Task IIIA.4, "Selective Withdrawal Characteristics of Various Outlet Configurations."

This study was conducted during the period June 1979 to September 1983 as part of Contract No. DACW39-78-C-0054 with Mississippi State University (MSU) to develop a boundary-fitted coordinate numerical hydrodynamic code for reservoir selective withdrawal. The research and development were carried out by Dr. Joe F. Thompson of the Department of Aerospace Engineering, MSU, and by Dr. Robert S. Bernard of the Reservoir Water Quality Branch (RWQB), Hydraulics Laboratory (HL), US Army Engineer Waterways Experiment Station (WES). Drs. Thompson and Bernard prepared this report.

The OCE Technical Monitors were Mr. Earl E. Eiker, Dr. John Bushman, and Mr. James L. Gottesman. The EWQOS Program Manager at WES was Dr. J. L. Mahloch. Mr. H. B. Simmons, Chief, HL, and Mr. J. L. Grace, Jr., Chief of the Hydraulic Structures Division, directed the effort. Immediate supervision was provided by Mr. J. P. Holland, Chief, RWQB, and Dr. D. R. Smith, former Chief, RWQB. Mr. Mark S. Dortch, formerly of the RWQB, and Dr. Billy H. Johnson of the Mathematical Modeling Group, HL, monitored the contract.

During the preparation of this report, COL Tilford C. Creel, CE, and COL Robert C. Lee, CE, were Commanders and Directors of WES and Mr. F. R. Brown was Technical Director. At the time of publication, COL Allen F. Grum, USA, was Director and Dr. Robert W. Whalin was Technical Director.

This report should be cited as follows:

Thompson, J. F., and Bernard, R. S. 1985. "Numerical Modeling of Two-Dimensional Width-Averaged Flows Using Boundary-Fitted Coordinate Systems," Technical Report E-85-9, US Army Engineer Waterways Experiment Station, Vicksburg, Miss.

CONTENTS

	<u>Page</u>
PREFACE	1
CONVERSION FACTORS, NON-SI TO SI (METRIC)	
UNITS OF MEASUREMENT	4
PART I: INTRODUCTION	5
PART II: EQUATIONS OF MOTION	9
Integral Form of the Equations	10
Differential Form of the Equations	16
PART III: EQUATIONS OF MOTION IN GENERAL CURVILINEAR COORDINATE SYSTEMS	19
General Curvilinear Coordinates	19
Transformed Equations of Motion	27
Mod Set	36
PART IV: MODIFICATIONS TO THE EQUATIONS OF MOTION	37
Removal of Hydrostatic Pressure	37
Mass Residual Correction	38
Lateral Averaging	38
Incompressible Flow	46
Final Equations	47
PART V: DISCRETE REPRESENTATION	51
Solution Grid	51
Difference Representation	52
Difference Equations	54
Calculation Procedure	64
Acceleration Parameters	65
Turbulence Model	68
PART VI: RESULTS	71
Selective Withdrawal from a Rectangular Channel with Linear Stratification	72
Cold Inflow into a Flume with Nonuniform Width and Depth	78
Flow over a Crested Weir	83
PART VII: CONCLUSION	117
REFERENCES	118
APPENDIX A: NOTATION	A1

CONVERSION FACTORS, NON-SI TO SI (METRIC)
UNITS OF MEASUREMENT

NON-SI units of measurement used in this report can be converted to SI (metric) units as follows:

<u>Multiply</u>	<u>By</u>	<u>To Obtain</u>
cubic feet per second	0.02831685	cubic metres per second
Fahrenheit degrees	5/9	Celsius degrees*
feet	0.3048	metres
feet per second	0.3048	metres per second
slugs per cubic foot	515.50336	kilograms per cubic metre

* To obtain Celsius (C) temperature readings from Fahrenheit (F) readings, use the following formula: $C = (5/9)(F - 32)$.

NUMERICAL MODELING OF TWO-DIMENSIONAL WIDTH-AVERAGED FLOWS
USING BOUNDARY-FITTED COORDINATE SYSTEMS

PART I: INTRODUCTION

1. The use of numerically generated boundary-fitted curvilinear coordinate systems as the basis for numerical solution of partial differential equations on arbitrary regions is now well established. A comprehensive survey of the generation and use of these coordinate systems has recently appeared (Thompson, Warsi, and Mastin 1983), and the proceedings of a recent symposium devoted to this area (Thompson 1982a) cover the basic techniques involved.

2. Such coordinate systems have the property that some coordinate line is coincident with each segment of the boundary in the physical region, so that the complication of boundary shape is effectively removed from the problem. In the past decade, the numerical generation of curvilinear coordinate systems has provided the key to the development of finite-difference solutions of partial differential equations on regions with arbitrarily shaped boundaries. Although much of the impetus for these developments has come from fluid dynamics, the techniques are equally applicable to heat transfer, electromagnetics, structures, and all other areas involving field solutions.

3. With coordinate systems that make coordinate lines (surfaces in three dimensions) coincident with the boundaries, finite-difference codes can be written which are applicable to general configurations without the need of special procedures at the boundaries. Even when the boundaries are in motion, the use of such coordinate systems allows all computation to be done on a fixed grid with a uniform rectangular mesh in the transformed (computational) plane. This greatly simplifies the coding with regard to boundary conditions, which can now be represented without need of interpolation. It is also possible to distribute the curvilinear grid lines in the physical plane with concentration of lines

in regions of high gradients while maintaining the square grid in the transformed plane.

4. With such systems, the grid points may be thought of as a finite set of observers of the physical solution, stationed so as to be most effective in covering all of the action on the field. The structure of an intersecting net of families of coordinate lines allows the observers to be readily identified in relation to each other. This results in more simplified coding than would the use of a triangular structure or a random distribution of points. The grid generation system provides some influence of each observer on the others so that when one moves to get into a better position, its neighbors will follow in order to maintain smooth coverage of the field. The curvilinear coordinate system thus should cover the field, with coordinate lines coincident with all boundaries. The distribution of lines should be smooth, with concentration in regions of high gradient.

5. Numerical solutions of partial differential equations are done on the curvilinear coordinate system by first transforming all partial derivatives (or integrals) analytically from cartesian to curvilinear coordinates, so that the latter become the independent variables.* Normal and tangential derivatives at boundaries are similarly transformed. (These transformation relations are given in Thompson 1982b). The result is a set of partial differential equations and boundary conditions in which all derivatives (or integrals) are taken with respect to the curvilinear coordinates. These equations may then be expressed as difference equations on a rectangular grid in the transformed plane. Thus, there is no need for interpolation, regardless of the shape of the boundaries or the distribution of the curvilinear coordinate lines in the field.

6. A finite-difference solution is given for the two-dimensional (2D), time-dependent, width-averaged Navier-Stokes equations, including an algebraic turbulence model, based on such a numerically generated

* A simple example would be a conversion from cartesian to polar coordinates.

boundary-fitted coordinate system. This solution is applicable to 2D regions of arbitrary shape, with multiple inlets and outlets, and with obstacles in the interior. The density is taken to be a function of the temperature, and the system of equations to be satisfied consists of the continuity equation, the two momentum equations, and the energy equation.

7. The solution provides for a choice of central, upwind, or ZIP differencing of the convective terms. Viscous terms and heat-conduction terms are represented by second-order central difference expressions. The time derivatives may be represented as either first- or second-order backward difference expressions. The finite volume formulation is used so that the equations are fully conservative. The solution is implicit in time, with all the difference equations being solved iteratively by successive overrelaxation in each time step.

8. The input allows any portions of the boundary (external or obstacles) to be designated as inlets, outlets, no-slip surfaces, or slip surfaces. Arbitrary specification of velocity and temperature (or density) on inlets and/or outlets is allowed. The output is in the form of field arrays of the velocity components, pressure, and temperature. All computation is done in metric units, but the input and output units may be specified otherwise. The code for this solution (WESSEL) and the code that generates the boundary-fitted coordinate system (WESCOR) are described in detail in Thompson and Bernard (1985) and Thompson (1983), respectively. The coordinate system is generated from the numerical solution of a system of elliptic partial differential equations with provision for controlling the spacing of the coordinate lines in the field (Thompson 1982c). The transformed region is rectangular, with the obstacles and intrusions transformed to slits and/or slabs. A complete discussion of the relation between the physical and transformed planes is given in Thompson (1983).

9. The mathematical development of this solution and the finite volume formulation thereof on a general boundary-fitted coordinate system are discussed in the following sections. This solution is designed

specifically to include the modeling of the water quality in selective withdrawal from reservoirs, and results for one configuration related to that application are given.

PART II: EQUATIONS OF MOTION

10. Since numerical solutions are inherently descriptions of physical properties interpreted either as values at a finite collection of points or as average values over finite regions, it is natural to write the governing equations of motion in the form of integral conservation equations. In this form, the equations express time rates of change in a finite volume in terms of the resultant fluxes through the boundary of the volume. Such equations make no assumptions regarding behavior inside the volume, and naturally provide only average values of the solution over the volume.

11. It is, in fact, in this integral form that the physical laws of dynamics and thermodynamics must be originally postulated for a fluid, since the concept of density is strictly definable only through an integral expression. Only if the fluid medium is assumed to be continuous can such integral relations as the Divergence Theorem be used to obtain partial differential equations by applying the integral conservation equations to an arbitrarily small volume. In this case, the integral form that represents the difference in fluxes on opposite sides of the volume becomes a partial derivative at a point.

12. While the integral and differential forms are analytically equivalent for a continuum, the two forms can have different implications in a numerical solution, which is necessarily carried out on a finite set of points or volumes. This is particularly true when the solution uses points on a non-cartesian grid or, equivalently, volumes that are not cubes. It is also true when physical "discontinuities" such as fronts and shocks occur in the field. In each of these cases, the numerical representation of derivatives may not always be accurate, while it may be possible to represent fluxes through the volume sides with sufficient accuracy.

13. For these reasons, the equations of motion are given below, first, in the integral conservation form. The analytically equivalent differential form is then given for reference and some later use, but

the developments of numerical procedures that follow are based primarily on the integral form. Throughout the presentation of the equations, subscripts indicate cartesian coordinate directions in tensor notation, with repeated indices indicating summation as usual. The Kronecker delta appears with its usual meaning, as well. The common symbols for the physical variables are used.*

Integral Form of the Equations

Continuity equation

14. The continuity equation, expressing conservation of mass for an arbitrary moving volume, is

$$\frac{d}{dt} \iiint_{V(t)} \rho dV + \iint_{S(t)} \rho (\mathbf{u}_j - \mathbf{U}_j) n_j dS = 0 \quad (1)$$

Here, the first term measures the rate of change of mass in the volume, while the second term, being a surface integral over the entire closed boundary of the volume, is the resultant flux of mass out of the volume through its boundary. In the second term, u_j is the fluid velocity, while U_j is the local surface velocity, so that $u_j - U_j$ is the fluid velocity relative to the surface. Note that $(u_j - U_j) n_j$ is simply the dot product $(\mathbf{u} - \mathbf{U}) \cdot \mathbf{n}$ and hence the relative velocity normal to the local increment of bounding surface, so that the product $\rho (\mathbf{u}_j - \mathbf{U}_j) n_j dS$ is the flux of mass through this surface increment. If the surface is moving with the fluid, then the relative velocity, $u_j - U_j$, vanishes and the equation states simply that the mass in the volume must be constant.

Momentum equation

15. Newton's Second Law, that the time rate of change of momentum equals the sum of the impressed forces, applies to a particular mass,

* For convenience, symbols are listed and defined in the Notation (Appendix A).

not to an arbitrary volume. Therefore, the volume used in this relation must always contain the same particles of the fluid, and its boundary surface must move with the local fluid velocity. Since the fluid velocity relative to the surface then vanishes, the expression of the Second law is as follows:

$$\frac{d}{dt} \iiint_{V_F(t)} \rho u_i dV = \iint_{S_F(t)} \tau_{ij} n_j dS + \iiint_{V_F(t)} \rho g_i dV \quad (2)$$

Here the subscript F is attached to the volume and its bounding surface to indicate that the volume is being defined to always contain the same portion of fluid. The left side then is the time rate of change of the x_i component of momentum of the particular mass of fluid within the volume. The forces impressed on this mass are of two types, as expressed by the two terms on the right side. The first term represents the forces acting on the surface of the fluid volume. These forces arise from pressure and viscosity and are expressed in terms of the stress tensor τ_{ij} (force per unit area) in which the subscripts indicate, respectively, the direction of the force and the direction of the normal to the surface on which it acts. The product $\tau_{ij} n_j$ then is the surface force in x_i direction acting on the local surface increment $dS^{(j)}$. The second term on the right is the body force, such as gravity, acting on the mass in the volume, the vector g_i being the body force per unit mass. This body force could include electromagnetic forces as well as gravity, of course.

16. The momentum equation (Equation 2) may be converted to apply to an arbitrary moving volume through the Reynolds Transport Theorem, which states that for any moving volume and any function f :

$$\frac{d}{dt} \iiint_{V(t)} f dV = \iiint_{V(t)} \frac{\partial f}{\partial t} dV + \iint_{S(t)} f U_j n_j dS \quad (3a)$$

Applied to the fluid volume V_F this becomes

$$\frac{d}{dt} \iiint_{V_F(t)} f dV = \iiint_{V_F(t)} \frac{\partial f}{\partial t} dV + \iint_{S_F(t)} f u_j n_j dS \quad (3b)$$

Now consider an arbitrary volume $V(t)$ that instantaneously is identical to the fluid volume $V_F(t)$. When the two volumes coincide, the first terms on the right sides of Equations 3a and 3b become identical so that we have at that instant

$$\frac{d}{dt} \iiint_{V_F(t)} f dV = \frac{d}{dt} \iiint_{V(t)} f dV + \iint_{S(t)} f (u_j - U_j) n_j dS \quad (4)$$

Since any arbitrary moving volume will coincide with some fluid volume at any instant, this last equation may be used to replace the left side of Equation 2, with the substitution $\rho u_i = f$. The momentum equation may be written for an arbitrary moving volume as:

$$\begin{aligned} \frac{d}{dt} \iiint_{V(t)} \rho u_i dV + \iint_{S(t)} \rho u_i (u_i - U_j) n_j dS \\ = \iint_{S(t)} \tau_{ij} n_j dS + \iiint_{V(t)} \rho g_i dV \end{aligned} \quad (5)$$

Now the first term on the left is the time rate of change of momentum in the volume, and the second term on the left is the resultant flux of momentum through the bounding surface.

Energy equation

17. The energy equation expresses conservation of energy for an arbitrary moving volume, and can be written directly as

$$\begin{aligned} \frac{d}{dt} \iiint_{V(t)} \rho \left(e + \frac{1}{2} u_i u_i \right) dV + \iint_{S(t)} \rho \left(e + \frac{1}{2} u_i u_i \right) (u_j - U_j) n_j dS \\ = \iint_{S(t)} u_i \tau_{ij} n_j dS + \iiint_{V(t)} \rho u_j g_j dV - \iint_{S(t)} q_j n_j dS \end{aligned} \quad (6)$$

Analogous to the other equations, the first term on the left represents the time rate of change of total energy (internal, measured by temperature, and kinetic) in the volume, and the second gives the resultant flux of total energy through the bounding surface. The first two terms on the right are the work done by the surface and body forces, respectively, while the last term is the resultant heat transfer through the bounding surface. In this equation, the energy release by internal reactions has been omitted. The surface heat transfer vector q_i could include radiation as well as conduction.

Stress and heat conduction

18. In these equations, the stress tensor and the conduction heat transfer vector are given by, respectively,

$$\tau_{ij} = -p\delta_{ij} + \mu \left(\frac{\partial u_i}{\partial x_j} + \frac{\partial u_j}{\partial x_i} \right) + \left(\mu' - \frac{2}{3}\mu \right) \frac{\partial u_k}{\partial x_k} \delta_{ij} \quad (7)$$

$$q_i = -\kappa \frac{\partial T}{\partial x_i} \quad (8)$$

where δ_{ij} is the Kronecker delta. Both of these quantities are inherently differential, being dependent on gradients in the fluid, so the assumption of continuity of the medium is necessary for their definition. However, average values of derivatives can be defined using the Divergence Theorem which states, for a general vector \underline{A} ,

$$\iiint_V \frac{\partial A_j}{\partial x_j} dV = \iint_S A_j n_j dS \quad (9)$$

If \underline{A} is taken as $\underline{k}^{(1)} f$, where $\underline{k}^{(1)}$ is the unit vector in the x_1 direction, then Equation 9 becomes, for any function f ,

$$\iiint_V \frac{\partial f}{\partial x_1} dV = \iint_S f [\underline{k}^{(1)} \cdot \underline{n}] dS \quad (10)$$

which can be used to define an average value of $\frac{\partial f}{\partial x_i}$ over the volume in terms of an integral over the bounding surface.

Summary of equations

19. Equations 1, 5, and 6, together with 7 and 8 and an equation of state and relations for the viscosities and conductivity, constitute a closed system of equations of motion in integral form.

20. With the portion of the stress tensor due to viscous forces written as

$$\sigma_{ij} = \mu \left(\frac{\partial u_i}{\partial x_j} + \frac{\partial u_j}{\partial x_i} \right) + \left(\mu' - \frac{2}{3} \mu \right) \frac{\partial u_k}{\partial x_k} \delta_{ij} \quad (11)$$

these equations are collected here as follows:

Continuity:

$$\frac{d}{dt} \iiint_{V(t)} \rho dV + \iint_{S(t)} \rho (u_j - U_j) n_j dS = 0 \quad (12)$$

Momentum:

$$\begin{aligned} & \frac{d}{dt} \iiint_{V(t)} \rho u_i dV + \iint_{S(t)} \rho u_i (u_j - U_j) n_j dS \\ &= - \iint_{S(t)} p n_i dS + \iint_{S(t)} \sigma_{ij} n_j dS + \iiint_{V(t)} \rho g_i dV \end{aligned} \quad (13)$$

Energy:

$$\begin{aligned}
 & \frac{d}{dt} \iiint_{V(t)} \rho \left(e + \frac{1}{2} u_i u_i \right) dV + \iint_{S(t)} \rho \left(e + \frac{1}{2} u_i u_i \right) (u_j - U_j) n_j dS \\
 & = - \iint_{S(t)} p u_j n_j dS + \iint_{S(t)} u_i \sigma_{ij} n_j dS \\
 & + \iiint_{V(t)} \rho u_j g_j dV - \iint_{S(t)} q_j n_j dS \quad (14)
 \end{aligned}$$

Energy equation in terms of enthalpy

21. The energy equation can also be written in terms of enthalpy, rather than the energy, by substituting

$$h = e + \frac{p}{\rho}$$

to obtain for the left side of the energy equation

$$\begin{aligned}
 & \frac{d}{dt} \iiint_{V(t)} \rho \left(h + \frac{1}{2} u_i u_i \right) dV + \iint_{S(t)} \rho \left(h + \frac{1}{2} u_i u_i \right) (u_j - U_j) n_j dS \\
 & - \frac{d}{dt} \iiint_{V(t)} p dV - \iint_{S(t)} p (u_j - U_j) n_j dS
 \end{aligned}$$

Fixed volume

22. For a fixed volume, $U_j = 0$ and the time derivative passes inside the volume integral. For example, the first term of the momentum equation becomes

$$\iiint_V \frac{\partial (\rho u_i)}{\partial t} dV$$

with similar changes in the other equations.

Differential Form of the Equations

Basic equations

23. The differential form of these equations is obtained by applying the Divergence Theorem (Equation 9) to convert all surface integrals to volume integrals and then reasoning that, since the result must apply for any fixed volume no matter how small, the integrand must vanish. This yields the following equations from Equations 12, 13, and 14 for the continuity, momentum, and energy equations, respectively,

Continuity:

$$\frac{\partial \rho}{\partial t} + \frac{\partial (\rho u_j)}{\partial x_j} = 0 \quad (15)$$

Momentum:

$$\frac{\partial (\rho u_i)}{\partial t} + \frac{\partial (\rho u_i u_j)}{\partial x_j} = - \frac{\partial p}{\partial x_i} + \frac{\partial \sigma_{ij}}{\partial x_j} + \rho g_i \quad (16)$$

Energy:

$$\begin{aligned} \frac{\partial}{\partial t} \left[\rho \left(e + \frac{1}{2} u_i u_i \right) \right] + \frac{\partial}{\partial x_j} \left[\rho \left(e + \frac{1}{2} u_i u_i \right) u_j \right] \\ = - \frac{\partial (p u_j)}{\partial x_j} + \frac{\partial (u_i \sigma_{ij})}{\partial x_j} + \rho u_j g_j - \frac{\partial q_j}{\partial x_j} \end{aligned} \quad (17)$$

The differential form of the equations implies the assumption of continuity of the medium, of course, since it was necessary to apply the integral equations to an arbitrarily small volume to obtain this form.

Alternate form of the energy equation

24. In the differential form, the mechanical energy contribution to the energy equation (Equation 17) may be removed by multiplying the momentum equation (Equation 16) by u_j and subtracting the result from the energy equation, the result being

$$\frac{\partial(\rho e)}{\partial t} + \frac{\partial(\rho e u_j)}{\partial x_j} = -p \frac{\partial u_j}{\partial x_j} + \sigma_{ij} \frac{\partial u_i}{\partial x_j} - \frac{\partial q_j}{\partial x_j} \quad (18)$$

or in terms of enthalpy,

$$\frac{\partial(\rho h)}{\partial t} + \frac{\partial(\rho h u_j)}{\partial x_j} = \frac{\partial p}{\partial t} + u_j \frac{\partial p}{\partial x_j} + \sigma_{ij} \frac{\partial u_i}{\partial x_j} - \frac{\partial q_j}{\partial x_j} \quad (19)$$

Thus, Equations 15, 16, and one of the Equations 17-19, together with equations of state, etc., constitute a closed system.

25. These forms of the energy equation with mechanical energy removed can be put in integral form by integrating over the volume and reversing the use of the Divergence Theorem (Equation 9) and the Reynolds Transport Theorem (Equation 3) with the result

$$\begin{aligned} \frac{d}{dt} \iiint_{V(t)} \rho e dV + \iint_{S(t)} \rho e (u_j - U_j) n_j dS \\ = \iiint_{V(t)} \left(\sigma_{ij} \frac{\partial u_i}{\partial x_j} - p \frac{\partial u_j}{\partial x_j} \right) dV - \iint_{S(t)} q_j n_j dS \end{aligned} \quad (20)$$

or, with the enthalpy,

$$\begin{aligned}
& \frac{d}{dt} \iiint_{V(t)} \rho h dV + \iint_{S(t)} \rho h (u_j - U_j) n_j dS \\
& = \frac{d}{dt} \iiint_{V(t)} p dV + \iint_{S(t)} p (u_j - U_j) n_j dS \\
& + \iiint_{V(t)} \sigma_{ij} \frac{\partial u_i}{\partial x_j} dV - \iint_{S(t)} q_j n_j dS \quad (21)
\end{aligned}$$

Therefore, in integral form, the energy equation (Equation 14) can be replaced by either Equation 20 or 21.

Set of equations for present model

26. The set of equations chosen for the present model is composed of the continuity equation (Equation 12), the momentum equation (Equation 13), and the energy equation (Equation 20), together with the stress and heat flux relations, Equations 11 and 8, with the bulk viscosity μ' set to zero. These equations are applied on a fixed curvilinear coordinate system so that the surface velocity U_j vanishes. The time derivatives then appear as partial derivatives inside the integrals.

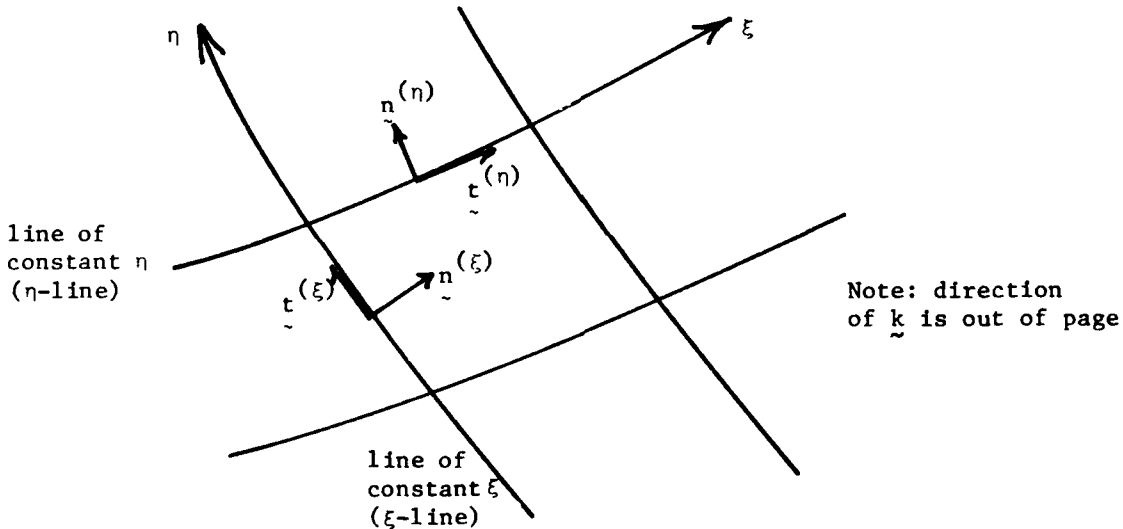
PART III: EQUATIONS OF MOTION IN GENERAL CURVILINEAR COORDINATE SYSTEMS

27. In order to treat completely arbitrary configurations, the equations of motion must now be transformed from the cartesian system of the preceding section to a general 2D curvilinear coordinate system.

General Curvilinear Coordinates

Unit tangents and normals

28. To establish the terminology, consider the following general element bounded by four curved sides, on each of which one of the curvilinear coordinates is constant:



29. With the position vector $\underline{r} = \underline{i}x + \underline{j}y$, we have the following relations. The unit tangent to a line of constant η is given by

$$\underline{t}^{(\eta)} = \frac{\frac{d\underline{r}}{d\xi}}{\left| \frac{d\underline{r}}{d\xi} \right|} = \frac{\underline{i}x_{\xi} + \underline{j}y_{\xi}}{\sqrt{x_{\xi}^2 + y_{\xi}^2}} = \frac{1}{\sqrt{\gamma}} (\underline{i}x_{\xi} + \underline{j}y_{\xi}) \quad (22)$$

with $\gamma \equiv x_\xi^2 + y_\xi^2$, and the unit normal to a line of constant η is

$$\underline{n}^{(\eta)} = \underline{k} \times \underline{t}^{(\eta)} = \frac{1}{\sqrt{\gamma}} (\underline{j}x_\xi - \underline{i}y_\xi) \quad (23)$$

Similarly, for a constant- ξ line, the unit tangent and normal are

$$\underline{t}^{(\xi)} = \frac{\frac{d\underline{r}}{d\eta}}{\left| \frac{d\underline{r}}{d\eta} \right|} = \frac{\underline{i}x_\eta + \underline{j}y_\eta}{\sqrt{x_\eta^2 + y_\eta^2}} = \frac{1}{\sqrt{\alpha}} (\underline{i}x_\eta + \underline{j}y_\eta) \quad (24)$$

with $\alpha \equiv x_\eta^2 + y_\eta^2$. The normal is

$$\underline{n}^{(\xi)} = \underline{t}^{(\xi)} \times \underline{k} = \frac{1}{\sqrt{\alpha}} (-\underline{j}x_\eta + \underline{i}y_\eta) \quad (25)$$

Area and volume

30. Then the area of a face on an η -line between two ξ -lines is given by

$$\begin{aligned} dS^{(\eta)} &= \left| \underline{k} \times \frac{d\underline{r}}{d\xi} \right| = \left| \underline{k} \times (\underline{i}x_\xi + \underline{j}y_\xi) \right| \\ &= |\underline{j}x_\xi - \underline{i}y_\xi| = \sqrt{x_\xi^2 + y_\xi^2} = \sqrt{\gamma} \end{aligned} \quad (26)$$

and the area of a face on a ξ -line between two η -lines is

$$dS^{(\xi)} = \left| \underline{k} \times \frac{d\underline{r}}{d\eta} \right| = \sqrt{\alpha} \quad (27)$$

Then on an η -line,

$$\underline{n}^{(\eta)} dS^{(\eta)} = \underline{j}x_{\xi} - \underline{i}y_{\xi} \quad (28)$$

and on a ξ -line,

$$\underline{n}^{(\xi)} dS^{(\xi)} = -\underline{j}x_{\eta} + \underline{i}y_{\eta} \quad (29)$$

Also, for any vector $\underline{A} = \underline{i}A_1 + \underline{j}A_2$, we have on an η -line,

$$\underline{A} \cdot \underline{n}^{(\eta)} dS^{(\eta)} = -A_1 y_{\xi} + A_2 x_{\xi} \quad (30)$$

while on a ξ -line,

$$\underline{A} \cdot \underline{n}^{(\xi)} dS^{(\xi)} = A_1 y_{\eta} - A_2 x_{\eta} \quad (31)$$

31. The volume of a cell is given by

$$\begin{aligned} dV &= \left| \underline{k} \cdot \left(\frac{d\underline{r}}{d\xi} \times \frac{d\underline{r}}{d\eta} \right) \right| \\ &= \left| \underline{k} \cdot [(\underline{i}x_{\xi} + \underline{j}y_{\xi}) \times (\underline{i}x_{\eta} + \underline{j}y_{\eta})] \right| \\ &= \left| \underline{k} \cdot (\underline{k}x_{\xi}y_{\eta} - \underline{k}x_{\eta}y_{\xi}) \right| \\ &= |x_{\xi}y_{\eta} - x_{\eta}y_{\xi}| = J \end{aligned} \quad (32)$$

where J is the Jacobian of the transformation.

Divergence

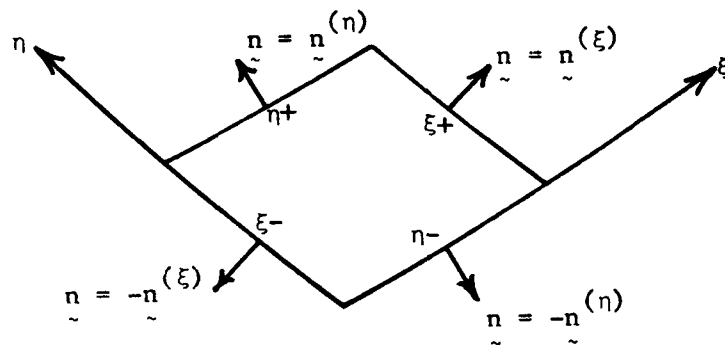
32. Now by the Divergence Theorem, we have for any vector \underline{A} ,

$$\iiint \nabla \cdot \underline{\underline{A}} dV = \iint \underline{\underline{A}} \cdot \underline{\underline{n}} dS$$

Application of the Divergence Theorem to the cell yields

$$(\nabla \cdot \underline{\underline{A}})J = \left[\underline{\underline{A}} \cdot \underline{\underline{n}}^{(\eta)} dS^{(\eta)} \right]_{\eta+} - \left[\underline{\underline{A}} \cdot \underline{\underline{n}}^{(\eta)} dS^{(\eta)} \right]_{\eta-} + \left[\underline{\underline{A}} \cdot \underline{\underline{n}}^{(\xi)} dS^{(\xi)} \right]_{\xi+} - \left[\underline{\underline{A}} \cdot \underline{\underline{n}}^{(\xi)} dS^{(\xi)} \right]_{\xi-}$$

Here, the following notation is used:



Thus

$$(\nabla \cdot \underline{\underline{A}})J = (-A_1 y_\xi + A_2 x_\xi)_{\eta+} - (-A_1 y_\xi + A_2 x_\xi)_{\eta-} + (A_1 y_\eta - A_2 x_\eta)_{\xi+} - (A_1 y_\eta - A_2 x_\eta)_{\xi-}$$

Note that, in the limit, this could be written in derivative form

$$(\nabla \cdot \underline{\underline{A}})J = (-A_1 y_\xi + A_2 x_\xi)_\eta + (A_1 y_\xi - A_2 x_\eta)_\xi$$

where the subscripts now indicate partial differentiation.

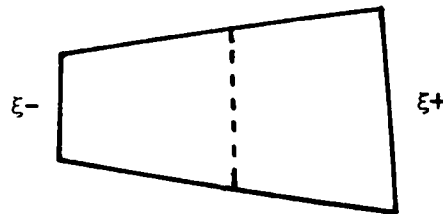
33. This then becomes a relation for the divergence:

$$\nabla \cdot \underline{A} = \frac{1}{J} \left[(-A_1 y_\xi + A_2 x_\xi)_\eta + A_1 y_\eta - A_2 x_\eta \right]_\xi \quad (33)$$

If the derivatives are expanded, there is a cancellation of cross derivatives of x and y so that

$$\nabla \cdot \underline{A} = \frac{1}{J} \left(-A_{1\eta} y_\xi + A_{2\eta} x_\xi + A_{1\xi} y_\eta - A_{2\xi} x_\eta \right) \quad (34)$$

34. Both Equations 33 and 34 are valid expressions for divergence, and the two are equivalent analytically. They are not equivalent numerically, however, since the latter involves the expansion of derivatives. The form of Equation 33 is the geometrically conservative form (after multiplication through by the Jacobian). Note that the difference between these two forms is that in the geometrically conservative form, Equation 33, the "area" through which the flux of A flows is that of the bounding faces through which the flux occurs. In Equation 34, however, the area is evaluated at the cell center rather than on the boundary. For a sharply deformed cell, such as is illustrated below,



the fluxes through $\xi+$ and $\xi-$ sides would both be computed using the area on the dotted line in Equation 34. With Equation 33, however, the actual areas of the $\xi+$ and $\xi-$ sides would be used. Thus, the fully conservative form should be much more tolerant of deformed coordinate systems.

Geometrically conservative
derivatives and surface integral

35. If \underline{A} is taken to be $\underline{j}f$, then by Equation 33,

$$f_x = \frac{1}{J} \left[(fy_\eta)_\xi - (fy_\xi)_\eta \right] \quad (35)$$

which gives the geometrically conservative representation of the partial derivative with respect to x . Similarly, with $\underline{A} = \underline{j}f$ we have

$$f_y = \frac{1}{J} \left[-(fx_\eta)_\xi - (fx_\xi)_\eta \right] \quad (36)$$

36. Recall also for later use that the right side of Equation 33, except for the $\frac{1}{J}$, is the surface integral,

$$\begin{aligned} \iint A_j n_j dS &= \iint \underline{A} \cdot \underline{n} dS = (A_1 y_\eta - A_2 x_\eta)_\xi + (-A_1 y_\xi + A_2 x_\xi)_\eta \\ &= (\tilde{A}_1)_\xi + (\tilde{A}_2)_\eta \end{aligned} \quad (37)$$

where

$$\tilde{A}_1 \equiv A_1 y_\eta - A_2 x_\eta \quad (38a)$$

$$\tilde{A}_2 \equiv -A_1 y_\xi + A_2 x_\xi \quad (38b)$$

Here \tilde{A}_1 and \tilde{A}_2 are the fluxes of \underline{A} through the ξ and η faces, respectively. In fact, note that by Equations 23 and 25,

$$\tilde{A}_1 = \sqrt{\alpha} \, \underline{n}^{(\xi)} \cdot \underline{A}$$

$$\tilde{A}_2 = \sqrt{\gamma} \, \underline{n}^{(\eta)} \cdot \underline{A}$$

Thus \tilde{A}_1 is the component of \underline{A} normal to a ξ -line multiplied by the area of the ξ -face ($\sqrt{\alpha}$). Similarly, \tilde{A}_2 is the normal component of \underline{A} on an η -line multiplied by the area of the η -face.

37. Comparing Equations 33 and 37, it is clear that the equations of motion can be put in geometrically conservative form either by applying the integral form to the cells of the curvilinear coordinate system, i.e., using Equation 37, or by simply representing the derivatives in the differential form by the geometrically conservative expression, i.e., using Equation 33.

Geometrically nonconservative derivatives

38. In geometrically nonconservative form we have, with the derivatives expanded in Equations 35 and 36,

$$f_x = \frac{1}{J} (y_\eta f_\xi - y_\xi f_\eta) \quad (39)$$

$$f_y = \frac{1}{J} (x_\xi f_\eta - x_\eta f_\xi) \quad (40)$$

39. The second derivatives are, by repeated application of these relations,

$$f_{xx} = \frac{1}{J^2} \left(y_\eta^2 f_{\xi\xi} - 2y_\xi y_\eta f_{\xi\eta} + y_\xi^2 f_{\eta\eta} \right) - \frac{1}{J^2} \left(\overline{DDYY} f_y + \overline{DDYX} f_x \right) \quad (41)$$

with

$$\overline{DDYY} \equiv y_n^2 y_{\xi\xi} - 2y_\xi y_n y_{\xi n} + y_\xi^2 y_{nn}$$

$$\overline{DDYX} \equiv y_n^2 x_{\xi\xi} - 2y_\xi y_n x_{\xi n} + y_\xi^2 x_{nn}$$

and

$$f_{yy} = \frac{1}{J^2} \left(x_n^2 f_{\xi\xi} - 2x_\xi x_n f_{\xi n} + x_\xi^2 f_{nn} \right) - \frac{1}{J^2} \left(\overline{DDXY} f_y + \overline{DDXX} f_x \right) \quad (42)$$

with

$$\overline{DDXY} \equiv x_n^2 y_{\xi\xi} - 2x_\xi x_n y_{\xi n} + x_\xi^2 y_{nn}$$

$$\overline{DDXX} \equiv x_n^2 x_{\xi\xi} - 2x_\xi x_n x_{\xi n} + x_\xi^2 x_{nn}$$

and

$$f_{xy} = \frac{1}{J^2} \left[x_n y_n f_{\xi\xi} + x_\xi y_\xi f_{nn} - (x_\xi y_n + x_n y_\xi) f_{\xi n} \right] + \frac{1}{J^2} \left(\overline{DDXYX} f_y + \overline{DDXYX} f_x \right) \quad (43)$$

with

$$\overline{DDXYX} \equiv x_n y_n y_{\xi\xi} + x_\xi y_\xi y_{nn} - (x_\xi y_n + x_n y_\xi) y_{\xi n}$$

$$\overline{DDXYX} \equiv x_n y_n x_{\xi\xi} + x_\xi y_\xi x_{nn} - (x_\xi y_n + x_n y_\xi) x_{\xi n}$$

40. Finally, the Laplacian is, from Equations 41 and 42,

$$\nabla^2 f = \frac{1}{J^2} \left(\alpha f_{\xi\xi} - 2\beta f_{\xi\eta} + \gamma f_{\eta\eta} \right) - \frac{1}{J^2} \left(\overline{DDY} f_y + \overline{DDX} f_x \right) \quad (44)$$

with

$$\overline{DDY} \equiv \alpha y_{\xi\xi} - 2\beta y_{\xi\eta} + \gamma y_{\eta\eta}$$

$$\overline{DDX} \equiv \alpha x_{\xi\xi} - 2\beta x_{\xi\eta} + \gamma x_{\eta\eta}$$

$$\beta \equiv x_{\xi} x_{\eta} + y_{\xi} y_{\eta}$$

and α and γ as defined earlier:

$$\alpha = x_{\eta}^2 + y_{\eta}^2$$

$$\gamma = x_{\xi}^2 + y_{\xi}^2$$

Transformed Equations of Motion

Continuity equation

41. Using Equation 37 we have

$$\iint \rho u_j n_j dS = (\rho \tilde{u})_{\xi} + (\rho \tilde{v})_{\eta}$$

where by Equation 38

$$\tilde{u} = uy_{\eta} - vx_{\eta} \quad (45a)$$

$$\tilde{v} = vx_{\xi} - uy_{\xi} \quad (45b)$$

Here \tilde{u} and \tilde{v} are the velocities normal to the ξ and η lines, respectively, multiplied by the area of the faces through which the flow occurs ($\sqrt{\alpha}$ and $\sqrt{\gamma}$, respectively). Then, since

$$\iiint \rho_t dV = \rho_t J$$

the continuity equation (Equation 12) becomes

$$\rho_t J + (\rho \tilde{u})_{\xi} + (\rho \tilde{v})_{\eta} = 0 \quad (46)$$

As noted above, this form could also have been obtained by using the geometrically conservative expressions for the derivatives, i.e., Equations 35 and 36, in the differential form of the continuity equation (Equation 15). The same applies for the geometrically conservative forms of the momentum and energy equations developed below.

Momentum equation

42. In the momentum equation (Equation 13) we have, by Equation 37,

$$\begin{aligned} \iint \rho u_i u_j n_j dS &= (\rho u_i \tilde{u})_{\xi} + (\rho u_i \tilde{v})_{\eta} \\ \iint \sigma_{ij} n_j dS &= (\tilde{\sigma}_{i1})_{\xi} + (\tilde{\sigma}_{i2})_{\eta} \end{aligned}$$

where, by Equation 38,

$$\tilde{\sigma}_{11} = \sigma_{11}y_{\eta} - \sigma_{12}x_{\eta} \quad (47a)$$

$$\tilde{\sigma}_{12} = \sigma_{12}x_{\xi} - \sigma_{11}y_{\xi} \quad (47a)$$

The pressure term is a bit different. We have

$$\begin{aligned} \iint p n dS &= \left[p n^{(\eta)} dS^{(\eta)} \right]_{\eta+} - \left[p n^{(\eta)} dS^{(\eta)} \right]_{\eta-} \\ &+ \left[p n^{(\xi)} dS^{(\xi)} \right]_{\xi+} - \left[p n^{(\xi)} dS^{(\xi)} \right]_{\xi-} \\ &= \left[p(jx_{\xi} - iy_{\xi}) \right]_{\eta} + \left[p(jx_{\eta} + iy_{\eta}) \right]_{\xi} \end{aligned}$$

by Equations 28 and 29. Then

$$\iint p n dS = i \left[(py_{\eta})_{\xi} - (py_{\xi})_{\eta} \right] + j \left[-(px_{\eta})_{\xi} + (px_{\xi})_{\eta} \right]$$

Finally, the gravity term becomes

$$\iiint \rho g_1 dV = \rho g_1 J$$

The entire momentum equation then is

$$(\rho u)_t J + (\rho u \tilde{u} - \tilde{\sigma}_{11} + py_{\eta})_{\xi} + (\rho u \tilde{v} - \tilde{\sigma}_{12} - py_{\xi})_{\eta} - \rho g_1 J = 0 \quad (48a)$$

$$(\rho v)_t J + (\rho v \tilde{u} - \tilde{\sigma}_{21} - px_{\eta})_{\xi} + (\rho v \tilde{v} - \tilde{\sigma}_{22} + px_{\xi})_{\eta} - \rho g_2 J = 0 \quad (48b)$$

with

$$\tilde{\sigma}_{11} = \sigma_{11}y_n - \sigma_{12}x_n \quad (49a)$$

$$\tilde{\sigma}_{12} = \sigma_{12}x_\xi - \sigma_{11}y_\xi \quad (49b)$$

$$\tilde{\sigma}_{21} = \sigma_{21}y_n - \sigma_{22}x_n \quad (49c)$$

$$\tilde{\sigma}_{22} = \sigma_{22}x_\xi - \sigma_{21}y_\xi \quad (49d)$$

Energy equation

43. For the energy equation (Equation 20) we have, by Equation 37,

$$\iint \rho e u_j n_j dS = (\rho e \tilde{u})_\xi + (\rho e \tilde{v})_\eta$$

$$\iint q_j n_j dS = (\tilde{q}_1)_\xi + (\tilde{q}_2)_\eta$$

with, by Equation 38

$$\tilde{q}_1 = q_1 y_n - q_2 x_n \quad (50a)$$

$$\tilde{q}_2 = q_2 x_\xi - q_1 y_\xi \quad (50b)$$

The energy equation then becomes,

$$(\rho e)_t J + (\rho e \tilde{u} + \tilde{q}_1)_\xi + (\rho e \tilde{v} + \tilde{q}_2)_\eta - \left(\sigma_{ij} \frac{\partial u_j}{\partial x_i} - p \frac{\partial u_j}{\partial x_j} \right) J = 0 \quad (51)$$

Stress and heat conduction terms

44. Using Equations 35 and 36 we have

$$j_x = \frac{1}{J} \left[(uy_\eta)_\xi - (uy_\xi)_\eta \right] \quad (52a)$$

$$u_y = \frac{1}{J} \left[-(ux_\eta)_\xi + (ux_\xi)_\eta \right] \quad (52b)$$

$$v_x = \frac{1}{J} \left[(vy_\eta)_\xi - (vy_\xi)_\eta \right] \quad (52c)$$

$$v_y = \frac{1}{J} \left[-(vx_\eta)_\xi + (vx_\xi)_\eta \right] \quad (52d)$$

$$T_x = \frac{1}{J} \left[(Ty_\eta)_\xi - (Ty_\xi)_\eta \right] \quad (52e)$$

$$T_y = \frac{1}{J} \left[-(Tx_\eta)_\xi + (Tx_\xi)_\eta \right] \quad (52f)$$

With these relations, we then calculate from Equation 11, with $\mu' = 0$,

$$\sigma_{11} = \frac{4}{3} \mu u_x - \frac{2}{3} \mu v_y \quad (53a)$$

$$\sigma_{22} = \frac{4}{3} \mu v_y - \frac{2}{3} \mu u_x \quad (53b)$$

$$\sigma_{12} = \sigma_{21} = \mu(u_y + v_x) \quad (53c)$$

and from Equation 8,

$$q_1 = -\kappa T_x \quad (54a)$$

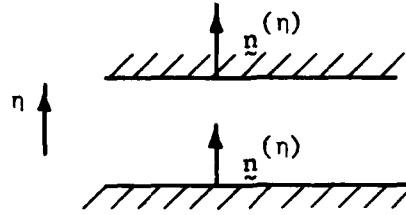
$$q_2 = -\kappa T_y \quad (54b)$$

Also, for the last term in the energy equation (Equation 51) we have

$$\sigma_{ij} \frac{\partial u_i}{\partial x_j} - p \frac{\partial u_j}{\partial x_j} = (\sigma_{11} - p)u_x + (\sigma_{22} - p)v_y + \sigma_{12}(v_x + u_y) \quad (55)$$

Wall heat transfer

45. When a cell side coincides with a wall, the wall heat transfer supplies the value of \tilde{q} on that side as follows:

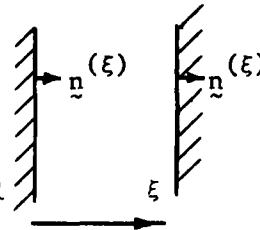


For an η -line wall we have, using the normal as given in Equation 23,

$$\begin{aligned} q_{\text{wall}} &= \tilde{q} \cdot [\pm \underline{n}^{(\eta)}] = \frac{\pm 1}{\sqrt{\gamma}} (q_2 x_\xi - q_1 y_\xi) \\ &= \frac{\pm 1}{\sqrt{\gamma}} \tilde{q}_2 \end{aligned}$$

where the $+$ applies to the lower wall and the $-$ to the upper. Thus

$$\tilde{q}_2 = \pm \sqrt{\gamma} q_{\text{wall}} \quad (56)$$



46. Similarly, for a ξ -line wall we have

$$\tilde{q}_1 = \pm \sqrt{\alpha} q_{\text{wall}} \quad (57)$$

with the $+$ corresponding to the left wall and the $-$ to the right.

Wall temperature

47. For an η -line wall, $\tilde{q}_2 = \pm \sqrt{\gamma} q_{\text{wall}}$ from Equation 56. Then, using Equations 50b, 54a-b, and 52e-f we have

$$\begin{aligned} \pm \sqrt{\gamma} q_{\text{wall}} &= \tilde{q}_2 = q_2 x_\xi - q_1 y_\xi \\ &= -\kappa (T_y x_\xi - T_x y_\xi) \\ &= -\frac{\kappa}{J} \left\{ \left[-(Tx_\eta)_\xi + (Tx_\xi)_\eta \right] x_\xi - \left[(Ty_\eta)_\xi - (Ty_\xi)_\eta \right] y_\xi \right\} \end{aligned}$$

or,

$$(Tx_\xi)_\eta x_\xi + (Ty_\xi)_\eta y_\xi = (Tx_\eta)_\xi x_\xi + (Ty_\eta)_\xi y_\xi \mp \frac{J}{\kappa} \sqrt{\gamma} q_{\text{wall}} \quad (58)$$

The wall temperature can be evaluated from this equation using one-sided differences for the η derivatives.

48. For a ξ -line wall,

$$(Tx_\eta)_\xi x_\eta + (Ty_\eta)_\xi y_\eta = (Tx_\xi)_\eta x_\eta + (Ty_\xi)_\eta y_\eta \mp \frac{J}{\kappa} \sqrt{\alpha} q_{\text{wall}} \quad (59)$$

Here one-sided ξ derivatives are used.

49. With the derivatives expanded, the nonconservative forms of these conditions are, from Equations 58 and 59, respectively,

$$\gamma T_\eta = \beta T_\xi \mp \frac{J}{\kappa} \sqrt{\gamma} q_{\text{wall}} \quad (60)$$

for an η -line, wall and

$$\alpha T_{\xi} = \beta T_{\eta} + \frac{J}{\kappa} \sqrt{\alpha} q_{\text{wall}} \quad (61)$$

for a ξ -line wall.

Slip boundary conditions

50. On a boundary with free slip, the normal velocity component and the vorticity must vanish. These two conditions serve to determine the two velocity components on such a boundary as follows.

51. The vorticity is given by

$$\omega = v_x - u_y = 0 \quad (62)$$

or in curvilinear coordinates, using Equations 52a-c,

$$(vy_{\eta})_{\xi} - (vy_{\xi})_{\eta} + (ux_{\eta})_{\xi} - (ux_{\xi})_{\eta} = 0 \quad (63)$$

52. On an η -line boundary, the vanishing of the normal velocity is expressed from Equation 45b as

$$vx_{\xi} - uy_{\xi} = 0 \quad (64)$$

and in the above expression of vanishing vorticity, we have, in discrete form, with the upper sign applying to the lower wall w , etc.

$$(vy_{\xi})_{\eta} = \mp \left[F_1 (vy_{\xi}) + F_2 (vy_{\xi})_{w \pm 1} + F_3 (vy_{\xi})_{w \pm 2} \right]$$

where (F_1, F_2, F_3) are $(1, -1, 0)$ and $\left(\frac{3}{2}, -2, \frac{1}{2}\right)$ for first and second order, respectively. Then

$$\begin{aligned}
(vy_{\eta})_{\xi} \pm [F_1(vy_{\xi}) + F_2(vy_{\xi})_{w\pm 1} + F_3(vy_{\xi})_{w\pm 2}] \\
+ (ux_{\eta})_{\xi} \pm [F_1(ux_{\xi}) + F_2(ux_{\xi})_{w\pm 1} + F_3(ux_{\xi})_{w\pm 2}] = 0
\end{aligned}$$

Thus

$$\begin{pmatrix} -y_{\xi} & x_{\xi} \\ F_1 x_{\xi} & F_1 y_{\xi} \end{pmatrix} \begin{pmatrix} u \\ v \end{pmatrix} = \left\{ \begin{array}{c} 0 \\ \pm [(vy_{\eta})_{\xi} + (ux_{\eta})_{\xi}] - F_2 [(vy_{\xi})_{w\pm 1} + (ux_{\xi})_{w\pm 1}] - F_3 [(vy_{\xi})_{w\pm 2} + (ux_{\xi})_{w\pm 2}] \end{array} \right\}$$

Then, with

$$\begin{aligned}
\Gamma^{(\eta)} \equiv \mp [(vy_{\eta})_{\xi} + (ux_{\eta})_{\xi}] - F_2 [(vy_{\xi})_{w\pm 1} + (ux_{\xi})_{w\pm 1}] \\
- F_3 [(vy_{\xi})_{w\pm 2} + (ux_{\xi})_{w\pm 2}]
\end{aligned}$$

we have

$$u = \frac{x_{\xi}}{\gamma F_1} \Gamma^{(\eta)} \quad (65a)$$

$$v = \frac{y_{\xi}}{\gamma F_1} \Gamma^{(\eta)} \quad (65b)$$

53. Similarly on a ξ -line boundary, we have, by Equation 45a,

$$uy_{\eta} - vx_{\eta} = 0 \quad (66)$$

so that with

$$\Gamma^{(\xi)} \equiv \frac{1}{\alpha} \left[(vy_{\xi})_{\eta} + (ux_{\xi})_{\eta} \right] - F_2 \left[(vy_{\eta})_{w\pm 1} + (ux_{\eta})_{w\pm 1} \right] \\ - F_3 \left[(vy_{\eta})_{w\pm 2} + (ux_{\eta})_{w\pm 2} \right]$$

we have

$$u = \frac{x_{\eta}}{\alpha F_1} \Gamma^{(\xi)} \quad (67a)$$

$$v = \frac{y_{\eta}}{\alpha F_1} \Gamma^{(\xi)} \quad (67b)$$

Model Set

54. The set of equations in general curvilinear coordinates used in the present model are the continuity equation (Equation 46), the momentum equation (Equation 48), the energy equation (Equation 51), together with the expressions given by Equations 52-55 and the applicable boundary conditions given by Equations 56 and 57 for the heat transfer, Equations 60 and 61 for the wall temperature, and Equations 65 and 67 for the wall slip velocity. Additional relations and some modifications to these equations are presented in Part IV.

PART IV: MODIFICATIONS TO THE EQUATIONS OF MOTION

Removal of Hydrostatic Pressure

55. One modification is made by subtracting out the hydrostatic pressure p_H which satisfies, by Equation 13 with zero velocity, the equation

$$0 = - \iint p_H n_i dS + \iiint \rho_s g_i dV$$

where ρ_s is the initial density. The momentum equation (Equation 13) then can be written, for a fixed volume, as

$$\begin{aligned} \iiint \frac{\partial(\rho u_i)}{\partial t} dV + \iint \rho u_i u_j n_j dS \\ = - \iint (p - p_H) n_i dS + \iint \sigma_{ij} n_j dS + \iiint (\rho - \rho_s) g_i dV \end{aligned} \quad (68)$$

with the hydrostatic pressure calculated from

$$p_H = p_0 + \int_{x_0}^x \rho_s g \cdot d\mathbf{x} \quad (69)$$

Here p_0 is the pressure at some reference point x_0

56. This modification is reflected in the momentum equation (Equation 48) by the replacement of the pressure with the difference between the true pressure and the hydrostatic pressure, and replacement of the density in the gravity term by the difference from the initial value. This is valid only if the fluid is initially in a condition of static equilibrium.

Mass Residual Correction

57. As a stabilizing measure, the products of the discrete residual of the continuity equation (Equation 12) and the velocity and energy are added to the right sides of the momentum and energy equations, Equations 48 and 51, respectively, as corrective source terms. These terms are, respectively, $u_1 D$ and $e D$, where D is the residual evaluated from Equation 46:

$$\begin{aligned} D &= \iiint \frac{\partial \rho}{\partial t} dV + \iint \rho u_j n_j dS \\ &= \rho_t J + (\rho \tilde{u})_\xi + (\rho \tilde{v})_\eta \end{aligned} \tag{70}$$

58. It may be noted that the analytical effect of this corrective use of the continuity equation in the momentum and energy equations would be to reduce the equations in the nonconservative form if the equations were converted to differential form and terms were cancelled where possible. However, the effect is not the same in the difference expressions since the use of different points in the various expressions prevents such cancellations on the discrete grid. The numerical effect of these corrective terms is to resist the tendency of large outflow from a cell to catastrophically deplete the cell contents, and similarly to lessen the effects of large inflow.

Lateral Averaging

59. Variable width is accounted for in the present model by the procedure of lateral averaging, which has seen much use in hydrodynamic problems to introduce some three-dimensional effects into two-dimensional computational models. With this procedure, the equations of motion are integrated laterally, and the dependent variables are

replaced by lateral averages thereof. Thus, with the z -direction being the lateral direction, we have the definition of the lateral average of a quantity f given as

$$\bar{f}(x,y) \equiv \frac{1}{B(x,y)} \int_{z_1(x,y)}^{z_2(x,y)} f(x,y,z) dz \quad (71)$$

where B is the width, i.e., $B(x,y) \equiv z_2(x,y) - z_1(x,y)$. Then, with f' a perturbation from this average value, we have

$$f(x,y,z) = \bar{f}(x,y) + f'(x,y,z) \quad (72)$$

In all that follows, such perturbations will be assumed to be small in comparison with the average value. Thus $|f'| \ll |\bar{f}|$.

Continuity equation

60. Applying this procedure to the continuity equation (Equation 15), we have

$$\int_{z_1}^{z_2} \left[\frac{\partial \rho}{\partial t} + \frac{\partial(\rho u)}{\partial x} + \frac{\partial(\rho v)}{\partial y} + \frac{\partial(\rho w)}{\partial z} \right] dz = 0$$

Now

$$\int_{z_1}^{z_2} \frac{\partial \rho}{\partial t} dz = \frac{\partial}{\partial t} \int_{z_1}^{z_2} \rho dz = B \frac{\partial \bar{\rho}}{\partial t}$$

and

$$\int_{z_1}^{z_2} \frac{\partial(\rho u)}{\partial x} dz = \frac{\partial}{\partial x} \int_{z_1}^{z_2} \rho u dz - \left(\rho u \frac{\partial z}{\partial x} \right)_{z_1}^{z_2}$$

and

$$\int_{z_1}^{z_2} \frac{\partial(\rho v)}{\partial y} dz = \frac{\partial}{\partial y} \int_{z_1}^{z_2} \rho v dz - \left(\rho v \frac{\partial z}{\partial y} \right)_{z_1}^{z_2}$$

and

$$\int_{z_1}^{z_2} \frac{\partial(\rho w)}{\partial z} dz = \left(\rho w \right)_{z_1}^{z_2}$$

But $w = u \frac{\partial z}{\partial x} + v \frac{\partial z}{\partial y}$ on z_1 and z_2 in order for the flow to be parallel to the boundary. Therefore, the brackets cancel and we have

$$B \frac{\partial \bar{\rho}}{\partial t} + \frac{\partial}{\partial x} \int_{z_1}^{z_2} (\bar{\rho} + \rho') (\bar{u} + u') dz + \frac{\partial}{\partial y} \int_{z_1}^{z_2} (\bar{\rho} + \rho') (\bar{v} + v') dz = 0$$

or

$$B \frac{\partial \bar{\rho}}{\partial t} + \frac{\partial}{\partial x} (B \bar{\rho} \bar{u}) + \frac{\partial}{\partial y} (B \bar{\rho} \bar{v}) + \frac{\partial}{\partial x} \int_{z_1}^{z_2} \rho' u' dz + \frac{\partial}{\partial y} \int_{z_1}^{z_2} \rho' v' dz = 0$$

Neglecting the quadratic prime terms, we then have for the laterally averaged continuity equation

$$B \frac{\partial \bar{\rho}}{\partial t} + \frac{\partial}{\partial x} (B \bar{\rho} \bar{u}) + \frac{\partial}{\partial y} (B \bar{\rho} \bar{v}) = 0 \quad (73)$$

The effect of the lateral averaging on the continuity equation in geometrically conservative form (Equation 46) is thus to multiply the density by the width B in all terms.

Momentum equation

61. Applying the same procedure to the x -momentum equation from Equation 16, we have, with subscripts indicating components, not derivatives,

$$\int_{z_1}^{z_2} \left[\frac{\partial(\rho u)}{\partial t} + \frac{\partial(\rho u^2)}{\partial x} + \frac{\partial(\rho uv)}{\partial y} + \frac{\partial(\rho uw)}{\partial z} + \frac{\partial p}{\partial x} - \frac{\partial \sigma_{xx}}{\partial x} - \frac{\partial \sigma_{xy}}{\partial y} - \frac{\partial \sigma_{xz}}{\partial z} - \rho g_x = 0 \right] dz$$

Now

$$\int_{z_1}^{z_2} \frac{\partial(\rho u)}{\partial t} dz = \frac{\partial}{\partial t} \int_{z_1}^{z_2} \rho u dz = B \frac{\partial(\bar{\rho} \bar{u})}{\partial t} + \frac{\partial}{\partial t} \int_{z_1}^{z_2} \rho' u' dz$$

and

$$\int_{z_1}^{z_2} \frac{\partial(\rho u^2)}{\partial x} dz = \frac{\partial}{\partial x} \int_{z_1}^{z_2} \rho u^2 dz - \left(\rho u^2 \frac{\partial z}{\partial x} \right)_{z_1}^{z_2}$$

Similar terms occur for the other convective terms. The brackets cancel as in the continuity equation. The convective terms then become

$$\frac{\partial (\overline{B\rho u^2})}{\partial x} + \frac{\partial (\overline{B\rho uv})}{\partial y} + \text{prime terms}$$

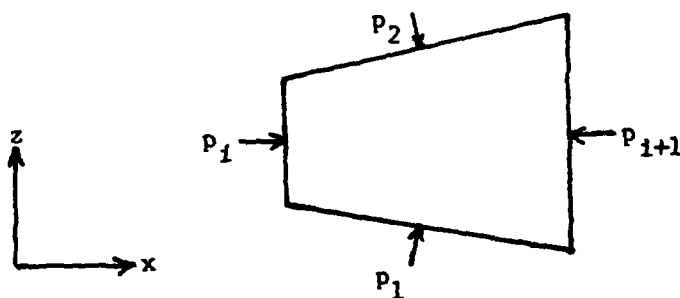
Neglecting the ρ' terms, we obtain for the remaining prime terms:

$$\frac{\partial}{\partial x} \left(\overline{\rho} \int_{z_1}^{z_2} u'^2 dz \right) + \frac{\partial}{\partial y} \left(\overline{\rho} \int_{z_1}^{z_2} u'v' dz \right)$$

62. Also, for the pressure terms,

$$\begin{aligned} \int_{z_1}^{z_2} \frac{\partial p}{\partial x} dz &= \frac{\partial}{\partial x} \int_{z_1}^{z_2} p dz - \left(p \frac{\partial z}{\partial x} \right)_{z_1}^{z_2} \\ &= \frac{\partial (\overline{Bp})}{\partial x} - p_2 \frac{\partial z_2}{\partial x} + p_1 \frac{\partial z_1}{\partial x} \end{aligned}$$

Now consider the pressures impressed on the volume:



If p_1 and p_2 are written $p_1 = p_2 = \frac{1}{2} (p_1 + p_{1+1})$, then

$$- p_2 \frac{\partial z_2}{\partial x} + p_1 \frac{\partial z_1}{\partial x} = - \frac{1}{2} (p_1 + p_{1+1}) \frac{\Delta B}{\Delta x}$$

which cancels the $\bar{p} \frac{\partial B}{\partial x}$ from the first term. Therefore,

$$\int_{z_1}^{z_2} \frac{\partial p}{\partial x} dz = B \frac{\partial \bar{p}}{\partial x}$$

63. For the stress terms we have,

$$\int_{z_1}^{z_2} \frac{\partial \sigma_{xx}}{\partial x} dz = \frac{\partial}{\partial x} (B \bar{\sigma}_{xx}) - \left(\sigma_{xx} \frac{\partial z}{\partial x} \right)_{z_1}^{z_2}$$

and

$$\int_{z_1}^{z_2} \frac{\partial \sigma_{xy}}{\partial y} dz = \frac{\partial}{\partial y} (B \bar{\sigma}_{xy}) - \left(\sigma_{xy} \frac{\partial z}{\partial y} \right)_{z_1}^{z_2}$$

Also

$$\int_{z_1}^{z_2} \frac{\partial \sigma_{xz}}{\partial z} dz = \left(\sigma_{xz} \right)_{z_1}^{z_2}$$

64. The gravity term becomes simply

$$\int_{z_2}^{z_1} \rho g_x dz = B \bar{\rho} g_x$$

65. Then the laterally averaged momentum equations, with the ρ' terms neglected, are for the x-direction,

$$\begin{aligned} B \frac{\partial(\bar{\rho} \bar{u})}{\partial t} + \frac{\partial(B \bar{\rho} \bar{u}^2)}{\partial x} + \frac{\partial(B \bar{\rho} \bar{u} \bar{v})}{\partial y} + B \frac{\partial \bar{p}}{\partial x} - \frac{\partial(B \bar{\sigma}_{xx})}{\partial x} - \frac{\partial(B \bar{\sigma}_{xy})}{\partial y} \\ - B \bar{\rho} g_x + \frac{\partial}{\partial x} \left(\bar{\rho} \int_{z_1}^{z_2} u'^2 dz \right) + \frac{\partial}{\partial y} \left(\bar{\rho} \int_{z_1}^{z_2} u' v' dz \right) \\ + \left(\sigma_{xx} \frac{\partial z}{\partial x} \right)_{z_1}^{z_2} + \left(\sigma_{xy} \frac{\partial z}{\partial y} \right)_{z_1}^{z_2} - \left(\sigma_{xz} \right)_{z_1}^{z_2} = 0 \end{aligned} \quad (74a)$$

and for the y-direction,

$$\begin{aligned} B \frac{\partial(\bar{\rho} \bar{v})}{\partial t} + \frac{\partial(B \bar{\rho} \bar{u} \bar{v})}{\partial x} + \frac{\partial(B \bar{\rho} \bar{v}^2)}{\partial y} + B \frac{\partial \bar{p}}{\partial y} - \frac{\partial(B \bar{\sigma}_{xy})}{\partial x} - \frac{\partial(B \bar{\sigma}_{yy})}{\partial y} \\ - B \bar{\rho} g_y + \frac{\partial}{\partial x} \left(\bar{\rho} \int_{z_1}^{z_2} u' v' dz \right) + \frac{\partial}{\partial y} \left(\bar{\rho} \int_{z_1}^{z_2} v'^2 dz \right) \\ + \left(\sigma_{yy} \frac{\partial z}{\partial y} \right)_{z_1}^{z_2} + \left(\sigma_{xy} \frac{\partial z}{\partial x} \right)_{z_1}^{z_2} - \left(\sigma_{yz} \right)_{z_1}^{z_2} = 0 \end{aligned} \quad (74b)$$

66. In the present model, the effect of the correlation terms is incorporated into the averaged stress terms through turbulence models as discussed in a later section. The stresses on the lateral boundaries are neglected. The hydrostatic pressure is removed from the above equations by simply defining the pressure in the above equations to be the difference between the true pressure and the hydrostatic pressure and replacing the density in the gravitational terms with the difference from the reference value.

67. In the geometrically conservative forms of the momentum equation (Equation 48), the effect of the lateral averaging is to multiply the first terms, the pressure terms, and the gravity terms by the width B , and to insert B in the ξ and η derivatives for the convective and stress terms.

Energy equation

68. In a similar manner, the lateral averaged energy equation is, using Equation 18,

$$\begin{aligned}
 & B \frac{\partial(\bar{\rho}\bar{e})}{\partial t} + \frac{\partial(B\bar{\rho}u\bar{e})}{\partial x} + \frac{\partial(B\bar{\rho}v\bar{e})}{\partial y} + \bar{p} \left[\frac{\partial(B\bar{u})}{\partial x} + \frac{\partial(B\bar{v})}{\partial y} \right] \\
 & - \left[\bar{\sigma}_{xx} \frac{\partial(B\bar{u})}{\partial x} + \bar{\sigma}_{xy} \left(\frac{\partial(B\bar{v})}{\partial x} + \frac{\partial(B\bar{u})}{\partial y} \right) + \bar{\sigma}_{yy} \frac{\partial(B\bar{v})}{\partial y} \right] \\
 & + \frac{\partial(B\bar{q}_x)}{\partial x} + \frac{\partial(B\bar{q}_y)}{\partial y} = 0
 \end{aligned} \tag{75}$$

The correlation terms between velocity and energy have been neglected, along with the stress work and heat transfer on the lateral boundaries.

69. The effect of the lateral averaging on the energy equation in geometrically conservative form (Equation 51) is to multiply the first term by the width B and to insert a B inside the ξ and η derivatives and inside the derivatives in the last term.

Effect on hydrostatic
pressure and mass residual

70. Since the width B is multiplied by the pressure and gravity terms in the laterally averaged momentum equation (Equation 74), the lateral averaging has no effect on the hydrostatic pressure in Equation 69.

71. The laterally averaged mass residual is obtained by inference from Equations 70 and 73. Dropping the bars indicating average, and using the transformed derivatives, this quantity becomes

$$D = B\rho_t J + (B\rho\tilde{u})_\xi + (B\rho\tilde{v})_\eta \quad (76)$$

Incompressible Flow

72. Of particular interest in the present work are situations in which the density variations are negligible in all terms except the gravity term ρg . Attention is further restricted to cases in which density may vary with temperature but not with pressure. (That is, the temperature gradients are large enough to affect the density, but the pressure gradients are not.) Thus, from a practical standpoint, the fluid is mechanically incompressible and the laterally averaged continuity equation reduces to

$$(Bu)_x + (Bv)_y = (B\tilde{u})_\xi + (B\tilde{v})_\eta = 0$$

which represents the well-known Boussinesq approximation for variable-density flow. Note that this removes the pressure term from the laterally averaged energy equation (Equation 75).

Final Equations

73. The final set of equations to be solved in the present model then consists of the momentum equation, the energy equation, and the continuity equation (discussed later) together with the relations for the stress and heat conduction and the boundary conditions. This set is summarized as follows:

Momentum equation

74. From Equation 48 with the modifications indicated above we have

$$\begin{aligned} B\rho_o u_t J + \left[B(\rho_o u\tilde{u} - \tilde{\sigma}_{11}) \right]_{\xi} + \left[B(\rho_o u\tilde{v} - \tilde{\sigma}_{12}) \right]_{\eta} \\ + B(P_{\xi}y_{\eta} - P_{\eta}y_{\xi}) - B(\rho - \rho_s)g_1 J - uD = 0 \end{aligned} \quad (77a)$$

and

$$\begin{aligned} B\rho_o v_t J + \left[B(\rho_o v\tilde{u} - \tilde{\sigma}_{21}) \right]_{\xi} + \left[B(\rho_o v\tilde{v} - \tilde{\sigma}_{22}) \right]_{\eta} \\ + B(-P_{\xi}x_{\eta} + P_{\eta}x_{\xi}) - B(\rho - \rho_s)g_2 J - vD = 0 \end{aligned} \quad (77b)$$

where $P \equiv p - p_H$ is the difference from the hydrostatic pressure, ρ_s is the initial density, ρ is the present density, and ρ_o is a constant reference density. Nonconservative expressions have been used for the pressure terms, for reasons that will be explained later.

Energy equation

75. From Equation 51 with the modifications we have

$$B\rho_o e_t J + \left[B(\rho_o e\tilde{u} + \tilde{q}_1) \right]_{\xi} + \left[B(\rho_o e\tilde{v} + \tilde{q}_2) \right]_{\eta} - J \sigma_{ij} \frac{\partial (Bu_1)}{\partial x_j} - eD = 0 \quad (78)$$

Continuity equation and mass residual

76. Subject to the Boussinesq approximation, the continuity equation is

$$(B\tilde{u})_{\xi} + (B\tilde{v})_{\eta} = 0 \quad (79)$$

and the mass residual is now given by

$$D = \rho_o \left[(B\tilde{u})_{\xi} + (B\tilde{v})_{\eta} \right] \quad (80)$$

Boundary conditions

77. The boundary conditions are as follows:

- a. Wall heat transfer: Equations 56-57.
- b. Wall temperature: Equations 60-61.
- c. Slip wall velocity: Equations 65 and 67.

78. The following choices of boundary conditions are incorporated:

- a. Thermal.
 - (1) Specified boundary temperature, with the boundary heat transfer calculated from Equations 56 or 57.
 - (2) Specified heat transfer, with boundary temperature calculated from Equations 60 or 61.
 - (3) Extrapolated boundary temperature from interior, i.e., equal to the interior value adjacent to the boundary.
- b. Velocity.
 - (1) Specified boundary velocity.

(2) Slip, with the boundary velocity calculated from Equations 65 and 66.

(3) Extrapolated boundary velocity from interior.

Solid walls are treated with thermal and velocity boundary condition (1) or (2). Inlets have thermal and velocity boundary condition (1) or (3). Outlets have thermal and velocity boundary condition (1) or (3). Free surfaces are approximately simulated with thermal and velocity boundary condition (3).

79. The normal velocities on all inlets and outlets must be such that the total outflow exactly balances the total inflow. The mass flow rate through an η -line boundary is, by Equation 45 with cognizance of the width B , simply $\rho_o \tilde{B} \tilde{v}$ while that through a ξ -line boundary is $\rho_o \tilde{B} \tilde{u}$. Outflow through a lower (upper) η -line boundary is then $-(+)$ $\rho_o \tilde{B} \tilde{v}$, and inflow is $+(-)$ $\rho_o \tilde{B} \tilde{v}$. Similarly, outflow through a left (right) ξ -line boundary is $-(+)$ $\rho_o \tilde{B} \tilde{u}$, while inflow is $+(-)$ $\rho_o \tilde{B} \tilde{u}$. The total flow rates are calculated by summing over all points on the appropriate boundary segments.

Auxiliary relations

80. In the above equations, the following auxiliary relations are used:

- a. \tilde{u} and \tilde{v} from Equation 45.
- b. $\tilde{\sigma}_{ij}$ from Equation 49.
- c. \tilde{q}_i from Equation 50.
- d. σ_{ij} from Equation 53.
- e. q_i from Equation 54.
- f. Velocity and temperature derivatives for stress and heat conduction from Equation 52.
- g. The relation Equation 55, with u and v multiplied by B .
- h. p_H from Equation 69.
- i. D from Equation 81.

In addition, the conservative derivative expressions are used for the x_j - derivatives in the energy equation. The metric components are repeated here for completeness:

$$\alpha = x_{\eta}^2 + y_{\eta}^2$$

$$\gamma = x_{\xi}^2 + y_{\xi}^2$$

$$\beta = x_{\xi}x_{\eta} + y_{\xi}y_{\eta}$$

$$J = x_{\xi}y_{\eta} - x_{\eta}y_{\xi}$$

PART V: DISCRETE REPRESENTATION

81. The present model is a finite-difference solution based on the integral form of the equations of motion, i.e., with the equations in geometrically conservative form. The solution is implemented on a boundary-fitted coordinate system which allows boundaries of arbitrary shape to be treated.

82. The boundary-fitted coordinate system is generated numerically by solving a system of elliptic partial differential equations as discussed in general in Thompson (1982c), and in detail for this present application in Thompson (1983). The latter reference also discusses the operation and input of the coordinate code used. The essential feature of this curvilinear coordinate system is that some coordinate line segment is coincident with each segment of the physical boundary, including interior obstacles. This allows all difference expressions to be taken along coordinate lines regardless of the boundary shape.

83. With such a coordinate system, all computation can be done on a square grid on the rectangular transformed region regardless of the shape of the physical region. This allows the physical configuration to be changed via the input without modification to the code.

Solution Grid

84. The coordinate system is generated with twice as many points in each direction as is intended for use in the flow solution. Thus, the grid system for the flow solution is formed by taking every other coordinate line. The physical variables are all defined at the grid points on this grid. Values needed between grid points are determined by simple linear averages. However, since the coordinate values are available at points between these grid points, coordinate derivatives at points between the grid points, as well as at the grid points, may be calculated without averaging the coordinate values. This is important in achieving a conservative difference form, since averaging the

coordinate values can cause different sets of coordinate values to be used in equivalent representations of certain derivatives with a consequent introduction of spurious effective gradients in uniform functions.

Difference Representation

85. The points surrounding a point of calculation, i.e., point C in Figure 1, are identified in relation to the compass directions. As noted above, the coordinate derivatives at any of the 25 points on this figure can be calculated directly from the coordinate values at adjacent points, e.g.,

$$(x_{\xi})_C = x_E - x_W$$

$$(x_{\xi})_{NE} = x_{EENE} - x_N$$

$$(x_{\eta})_C = x_N - x_S$$

$$(x_{\eta})_{NE} = x_{NNNE} - x_E, \text{ etc.}$$

since the coordinate system is generated using twice as many points in each direction as will be used in the flow solution.

86. The flow solution, however, is represented only at grid points, so that averages must be used at other points. Thus

$$f_E = \frac{1}{2} (f_C + f_{EE})$$

$$f_{NE} = \frac{1}{4} (f_C + f_{EE} + f_{NN} + f_{NENE})$$

$$f_N = \frac{1}{2} (f_C + f_{NN}), \text{ etc.}$$

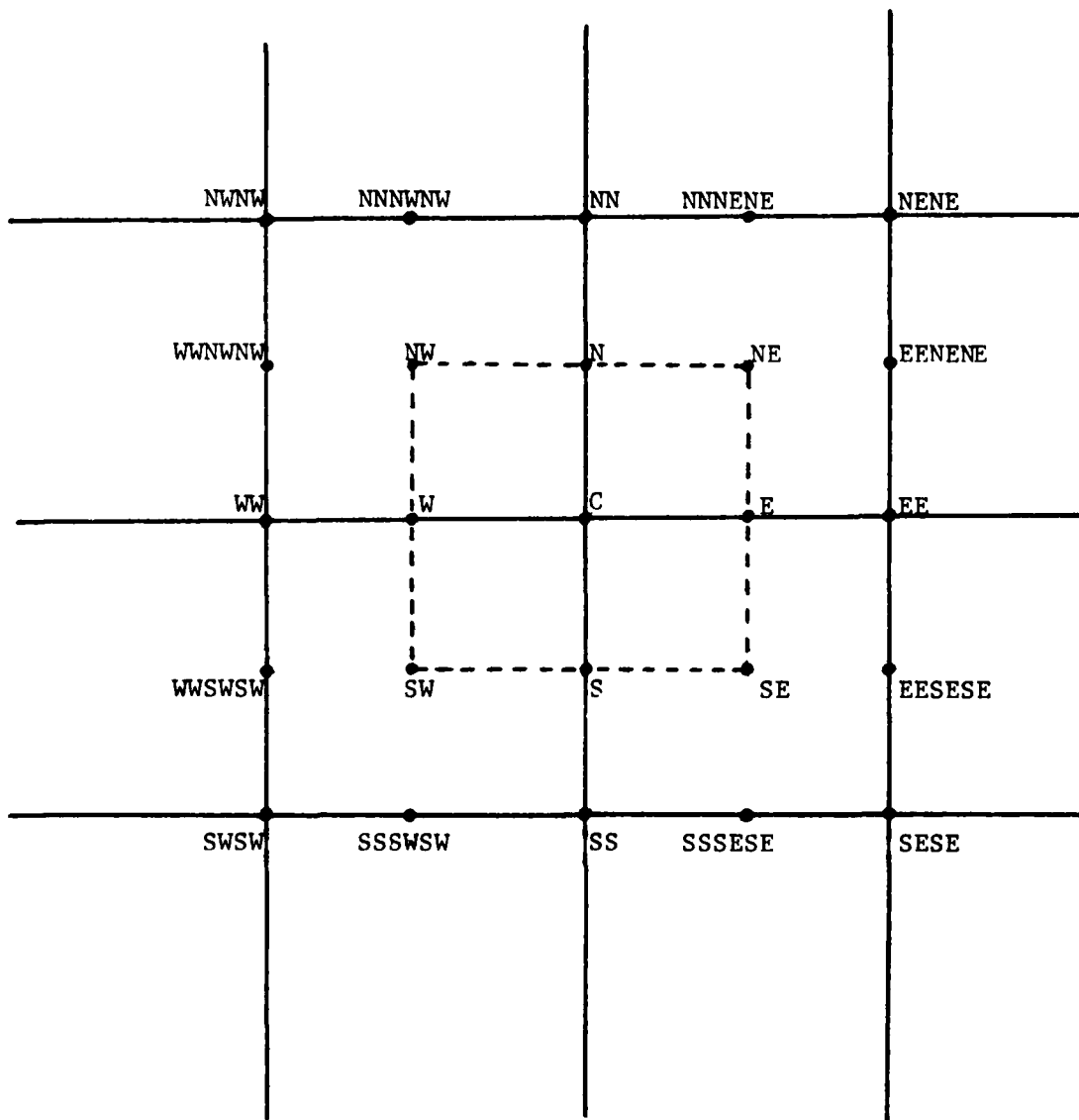


Figure 1. Coordinate scheme for finite-difference representation

With these values one can calculate the derivatives of the flow variable at all points, as illustrated for the coordinates above.

87. The flow variables are stored in 2D arrays, so that the following correspondencies apply:

$$f_C = F(I, J)$$

$$f_{EE} = F(I + 1, J)$$

$$f_{NN} = F(I, J + 1)$$

$$f_{NENE} = F(I + 1, J + 1), \text{ etc.}$$

88. The volume of integration used is that indicated by dotted lines in the figure, and the Jacobian J thus represents the area of the four-sided area in physical space corresponding to this square in the transformed plane. The fluxes must therefore be represented on the sides of this square in the transformed plane, meaning that the ξ and η derivatives in the momentum, energy, and mass residual equations (Equations 77, 78, and 80) are represented as

$$(f_\xi)_C = f_E - f_W$$

$$(f_\eta)_C = f_N - f_S$$

Difference Equations

89. The finite-difference representations for the various terms in the equations are discussed below. All types of terms are covered, but the full equations are not given here because the code (Thompson and Bernard 1985) is written with all terms identified therein.

Time derivatives

90. All time derivatives are represented by first- or second-order backward difference expressions:

$$(f_t)^n = \frac{1}{\Delta t} \left(c_1 f^n + c_2 f^{n-1} + c_3 f^{n-2} \right) \quad (81)$$

where the superscript indicates the time level and the coefficients (c_1, c_2, c_3) are $(1, -1, 0)$ for the first order and $(\frac{3}{2}, -2, \frac{1}{2})$ for second order. Second order is used for all but the first step, where the first order must be used to start the solution.

Convective terms

91. The convective terms are of the form $(B\rho_o \tilde{f}u)_\xi$ or $(B\rho_o \tilde{f}v)_\eta$, where f is 1 for continuity, u and v for momentum, and e for energy. These terms can be represented by central or upwind differencing, the choice being designated in the input. Central differences are second order while upwind is first order. Although the conservative form $B\rho_o f_t J + (B\rho_o \tilde{f}u)_\xi + (B\rho_o \tilde{f}v)_\eta$ is standard, it is also possible to choose the nonconservative form $B\rho_o J f_t + B\rho_o \tilde{u}f)_\xi + (B\rho_o \tilde{v}f)_\eta$ obtained by using the continuity equation in the momentum and energy equations, or the ZIP form (Zalesak 1981), via an input parameter.

92. The conservative central difference expressions are of the form

$$\left[(B\rho_o \tilde{f}u)_\xi \right]_C = (B\rho_o \tilde{f}u)_E - (B\rho_o \tilde{f}u)_W \quad (82a)$$

$$\left[(B\rho_o \tilde{f}v)_\eta \right]_C = (B\rho_o \tilde{f}v)_N - (B\rho_o \tilde{f}v)_S \quad (82b)$$

while the nonconservative central forms are

$$(B\rho_o \tilde{u}f_\xi)_C = (B\rho_o \tilde{u})_C (f_E - f_W) \quad (83a)$$

$$(B\rho_o \tilde{v}f_\eta)_C = (B\rho_o \tilde{v})_C (f_N - f_S) \quad (83b)$$

The conservative upwind forms are

$$\left[(B\rho_o \tilde{u}f)_{\xi} \right]_C = (B\rho_o \tilde{u})_E f_R - (B\rho_o \tilde{u})_W f_L \quad (84a)$$

$$\left[(B\rho_o \tilde{v}f)_{\eta} \right]_C = (B\rho_o \tilde{v})_N f_T - (B\rho_o \tilde{v})_S f_B \quad (84b)$$

where

$$R = \begin{cases} EE & \tilde{u}_E < 0 \\ C & \tilde{u}_E > 0 \end{cases} \quad L = \begin{cases} C & \tilde{u}_W < 0 \\ WW & \tilde{u}_W > 0 \end{cases}$$

$$T = \begin{cases} NN & \tilde{v}_N < 0 \\ C & \tilde{v}_N > 0 \end{cases} \quad B = \begin{cases} C & \tilde{v}_S < 0 \\ SS & \tilde{v}_S > 0 \end{cases}$$

The nonconservative upwind forms are

$$(B\rho_o \tilde{u}f_{\xi})_C = (B\rho_o \tilde{u})_C (f_R - f_L) \quad (85a)$$

$$(B\rho_o \tilde{v}f_{\eta})_C = (B\rho_o \tilde{v})_C (f_T - f_B) \quad (85b)$$

with the definitions of the subscripts R, L, T, and B as above, except that all the decisions are based on the values \tilde{u}_C and \tilde{v}_C .

93. The ZIP form is

$$\left[(B\rho_o \tilde{u}f)_{\xi} \right]_C = (B\rho_o \tilde{u}f)_R - (B\rho_o \tilde{u}f)_L \quad (86a)$$

$$\left[(B\rho_o \tilde{v}f)_{\eta} \right]_C = (B\rho_o \tilde{v}f)_T - (B\rho_o \tilde{v}f)_B \quad (86b)$$

where here the term $(B\tilde{o}_0\tilde{u}f)_R$ represents the sum of four terms, in each of which one of the four variables is evaluated at point E and the other three are evaluated at point C. The other terms in Equation 86 have analogous meanings, the subscripts L, T, and B being associated with points W, N, and S, respectively, in the same manner.

94. Regardless of the mode selected for the convective terms, the central form is always used for the evaluation of mass residual (Equation 80) in the momentum and energy equations.

Stress and heat conduction terms

95. The stress terms are evaluated using second-order central differences as follows. The term $(B\tilde{\sigma}_{11})_\xi$ in Equation 77a is given by

$$(B\tilde{\sigma}_{11})_\xi = (B\tilde{\sigma}_{11})_E - (B\tilde{\sigma}_{11})_W \quad (87)$$

Now, by Equation 49a,

$$(\tilde{\sigma}_{11})_E = (\sigma_{11}y_\eta - \sigma_{12}x_\eta)_E$$

and, by Equation 53,

$$(\sigma_{11})_E = \left(\frac{4}{3} \mu u_x - \frac{2}{3} \mu v_y \right)_E$$

$$(\sigma_{12})_E = (\mu u_y + \mu v_x)_E$$

Finally, by Equation 52a,

$$(u_x)_E = \frac{1}{J_E} \left[(uy_\eta)_\xi - (uy_\xi)_\eta \right]_E$$

with

$$\left[(uy_\eta)_\xi \right]_E = (uy_\eta)_{EE} - (uy_\eta)_C$$

$$\left[(uy_\xi)_\eta \right]_E = (uy_\xi)_{NE} - (uy_\xi)_{SE}$$

and analogous expressions for the other terms involved. This pattern is followed for all the stress terms in the momentum equation.

96. In the energy equation (Equation 78), the dissipation term $\sigma_{ij} \frac{\partial (Bu_1)}{\partial x_j}$ is evaluated in a similar fashion. Thus, for this term, which only occurs at point C, we have

$$(\sigma_{11})_C = \left(\frac{4}{3} \mu u_x - \frac{2}{3} \mu v_y \right)_C$$

with

$$(u_x)_C = \frac{1}{J_C} \left[(uy_\eta)_\xi - (uy_\xi)_\eta \right]_C$$

and

$$\left[(uy_\eta)_\xi \right]_C = (uy_\eta)_{E} - (uy_\eta)_W$$

$$\left[(uy_\xi)_\eta \right]_C = (uy_\xi)_N - (uy_\xi)_S$$

Also, for this term, the derivatives $\left. \frac{\partial (Bu_1)}{\partial x_j} \right|_C$ are evaluated as is done for $(u_x)_C$ above.

97. The heat conduction terms in the energy equation (Equation 78) are evaluated analogously to the stress terms in the momentum equations, using second-order central differences. Thus

$$(B\tilde{q}_1)_\xi = (B\tilde{q}_1)_E - (B\tilde{q}_1)_W$$

with, by Equation 50a,

$$(\tilde{q}_1)_E = (q_1 y_\eta - q_2 x_\eta)_E$$

and, by Equation 54a,

$$(q_1)_E = -(\kappa T_x)_E$$

with

$$(T_x)_E = \frac{1}{J_E} \left[(Ty_\eta)_\xi - (Ty_\xi)_\eta \right]_E$$

and

$$\left[(Ty_\eta)_\xi \right]_E = (Ty_\eta)_{EE} - (Ty_\eta)_C$$

$$\left[(Ty_\xi)_\eta \right]_E = (Ty_\xi)_{NE} - (Ty_\xi)_{SE}$$

etc.

Pressure terms

98. The pressure terms in the momentum equations are of the following forms, which are evaluated using first-order backward differences:

$$(BP_{\xi} y_\eta)_C = B_C (y_\eta)_C (P_C - P_{WW}) \quad (88a)$$

$$(BP_{\eta} y_\xi)_C = B_C (y_\xi)_C (P_C - P_{SS}) \quad (88b)$$

The reason for the one-sided differencing is explained below.

Chorin's method for
calculating pressure

99. For incompressible flow, the pressure gradient serves one purpose: it prevents loss or gain of mass within a fluid volume. Thus, the pressure and the continuity equation are directly related. In curvilinear coordinates, the desired condition for conservation of mass is given by Equation 79, which is the same thing as saying

$$D = 0$$

with the mass residual D given by Equation 80. The question, of course, is how to find a pressure distribution that maintains this condition.

100. Consider the divergence of the width-averaged momentum equation, obtained by summing the x -derivative of Equation 48a and the y -derivative of Equation 48b:

$$D_t + \frac{\partial}{\partial \xi} (B_{\eta} P_x - B_{\xi} P_y) + \frac{\partial}{\partial \eta} (B_{\xi} P_y - B_{\eta} P_x) = \text{RHS} \quad (89a)$$

Note that all terms not involving the pressure or the mass residual have been placed anonymously in the right-hand side (RHS). The expressions for P_x and P_y are the nonconservative forms given by Equations 39 and 40. Employing a backward time-differencing scheme for D_t , Equation 89a can be rewritten as

$$\frac{c_1}{\Delta t} D + \frac{\partial}{\partial \xi} (B_{\eta} P_x - B_{\xi} P_y) + \frac{\partial}{\partial \eta} (B_{\xi} P_y - B_{\eta} P_x) = \text{RHS} \quad (89b)$$

with D representing the current mass residual, RHS containing the values of D from previous time steps, and c_1 being the leading coefficient in Equation 81.

101. Now suppose that the left-hand side (LHS) of Equation 89b is calculated by a convergent iteration scheme such that

$$\text{LHS}^{(m)} \approx \text{LHS}^{(m-1)} \quad (89c)$$

where the superscript (m) indicates the iteration count. If the scheme is truly convergent, the condition $D = 0$ can be achieved by setting

$$D^{(m)} = 0$$

in each successive calculation of the left side of Equation 89c. This in itself defines an iteration scheme, namely

$$\begin{aligned} & \frac{\partial}{\partial \xi} \left[B_{y_{\eta}} P_x^{(m)} - B_{x_{\eta}} P_y^{(m)} \right] + \frac{\partial}{\partial \eta} \left[B_{x_{\xi}} P_y^{(m)} - B_{y_{\xi}} P_x^{(m)} \right] \\ &= \frac{C_1}{\Delta t} D^{(m-1)} + \frac{\partial}{\partial \xi} \left[B_{y_{\eta}} P_x^{(m-1)} - B_{x_{\eta}} P_y^{(m-1)} \right] \\ &+ \frac{\partial}{\partial \eta} \left[B_{x_{\xi}} P_y^{(m-1)} - B_{y_{\xi}} P_x^{(m-1)} \right] \end{aligned} \quad (89d)$$

Equation 89d is a Poisson equation for pressure that must be solved at each iteration for the entire flow field. What remains is to select the difference expressions that will represent the quantities P_x , P_y , and D .

102. In the numerical solution of the momentum equations (Equations 77a and 77b), one can choose upwind, central, or ZIP differencing for the advective terms, with central differencing for the viscous terms. Experience has shown, however, that central differencing for the pressure terms in the momentum equation, and for the mass residual in the continuity equation, promotes numerical oscillation on regular grids. The way to avoid the latter problem is to use a staggered grid (pressure and velocity calculated at alternate grid points) or, for the present work, to use one-sided differencing for the pressure gradient and for the continuity equation. While this does not reduce the

accuracy of the momentum calculation, it does reduce the conservation of mass to a first-order approximation.

103. Assuming the coordinate derivatives constant to first order, but retaining B as a variable, the pressure terms in Equation 89b reduce to

$$\frac{\partial}{\partial \xi} (B y_{\eta} P_x - B x_{\eta} P_y) \approx \frac{\alpha}{J} \frac{\partial}{\partial \xi} (B P_{\xi}) - \frac{\beta}{J} \frac{\partial}{\partial \xi} (B P_{\eta})$$

$$\frac{\partial}{\partial \eta} (B x_{\xi} P_y - B y_{\xi} P_x) \approx \frac{\gamma}{J} \frac{\partial}{\partial \eta} (B P_{\eta}) - \frac{\beta}{J} \frac{\partial}{\partial \eta} (B P_{\xi})$$

The one-sided difference approximations for the mass residual in Equation 89d, and for the pressure derivatives in Equations 82a, 82b, and 89d, are as follows

$$P_{\xi} = P_C - P_{WW}$$

$$P_{\eta} = P_C - P_{SS}$$

$$\frac{\partial}{\partial \xi} (B P_{\xi}) = (B P_{\xi})_{EE} - (B P_{\xi})_C$$

$$\frac{\partial}{\partial \xi} (B P_{\eta}) = (B P_{\eta})_{EE} - (B P_{\eta})_C$$

$$\frac{\partial}{\partial \eta} (B P_{\xi}) = (B P_{\xi})_{NN} - (B P_{\xi})_C$$

$$\frac{\partial}{\partial \eta} (B P_{\eta}) = (B P_{\eta})_{NN} - (B P_{\eta})_C$$

$$\frac{\partial}{\partial \xi} (B \tilde{u}) = (B \tilde{u})_{EE} - (B \tilde{u})_C$$

$$\frac{\partial}{\partial \eta} (B\tilde{v}) = (B\tilde{v})_{NN} - (B\tilde{v})_C$$

These approximations reduce Equation 89d to

$$\begin{aligned} (OT)^{(m)} - \frac{2}{J_C} (\alpha_C B_E - \beta_C B_C + \gamma_C B_N) P_C^{(m)} \\ = \rho_o \frac{c_1}{\Delta t} \left[(B\tilde{u})_{EE} - (B\tilde{u})_C + (B\tilde{v})_{NN} - (B\tilde{v})_C \right] \\ + (OT)^{(m-1)} - \frac{2}{J_C} (\alpha_C B_E - \beta_C B_C + \gamma_C B_N) P_C^{(m-1)} \quad (89e) \end{aligned}$$

where OT represents pressure terms other than the central pressure P_C .

104. The final step in defining the iteration scheme for pressure is to equate the OT terms on each side of Equation 89e, such that

$$\begin{aligned} P_C^{(m)} = P_C^{(m-1)} - \frac{\rho_o c_1 J_C}{2\Delta t (\alpha_C B_E - \beta_C B_C + \gamma_C B_N)} \\ \left[(B\tilde{u})_{EE} - (B\tilde{u})_C + (B\tilde{v})_{NN} - (B\tilde{v})_C \right]^{(m-1)} \end{aligned}$$

Numerical experimentation has shown that, for nonsquare grids, this scheme converges only with underrelaxation, i.e.,

$$\begin{aligned} P_C^{(m)} = P_C^{(m-1)} - \frac{\omega \rho_o c_1 J_C}{2\Delta t (\alpha_C B_E - \beta_C B_C + \gamma_C B_N)} \\ \left[(B\tilde{u})_{EE} - (B\tilde{u})_C + (B\tilde{v})_{NN} - (B\tilde{v})_C \right]^{(m-1)} \quad (89f) \end{aligned}$$

where

$$0 < \omega < 1 \quad (89g)$$

Equations 89f and 89g constitute a variation of Chorin's (1967) method for calculating pressure. The scheme is applied on boundary points and field points alike.

Boundary conditions

105. In all expressions for temperature and velocity boundary conditions, second-order central differences are used for derivatives along the boundary, and first-order one-sided differences are used for derivatives off the boundary. Thus, for example, on an η -line boundary with the field to the north, we have

$$(f_{\xi})_C = f_E - f_W \quad (90a)$$

$$(f_{\eta})_C = 2(f_N - f_C) \quad (90b)$$

Corners

106. Convex corners in the transformed plane are treated by averaging the results of separate applications of the temperature and velocity boundary conditions on the two faces of the corner.

107. Concave corners are treated simply by averaging the extrapolated values along the two faces of the corner, using first- or second-order extrapolation as selected on the input.

Calculation Procedure

108. The momentum and energy equations are solved simultaneously at each time step by successive overrelaxation (SOR) iteration. In the difference representation, all coefficients of values at the central point C are factored (i.e. grouped) together to speed up the iterative convergence. In the energy equation, this requires a short inner

iteration since the energy and temperature at the central point both appear in the equation. The SOR iteration involves first calculating new values from the difference equations and then taking the new iterative values of velocity and temperature as weighted averages of these values and the values from the previous iteration, the weight assigned to the newly calculated value being the acceleration parameter ω . The field is swept repetitively, calculating new velocities, temperature, and pressure at each point in succession. Before each field sweep, the boundary values are updated. These iterative sweeps are continued until convergence occurs or until a prescribed number of iterations has been completed. In the latter case, the solution may be directed to stop and store the partially converged results or to continue to the next time step. Output is provided in the form of plotted velocity vectors and contours of density, temperature, or pressure, as well as printed field values.

Acceleration Parameters

109. The acceleration parameters for the SOR iteration are calculated locally for the momentum and energy equations (see Thompson, Thames, and Mastin 1977). With these equations represented by the general form

$$A_1 f_{\xi\xi} + A_2 f_{\eta\eta} + B_1 f_{\xi} + B_2 f_{\eta} + C f + D = 0 \quad (91)$$

where D (not to be confused with the mass residual here) contains all cross-derivative terms and all other terms not represented explicitly. In the case where convection dominates diffusion, or vice versa, in both directions, the optimum acceleration parameters are given by

$$\omega = \frac{2}{1 + \sqrt{1 - \rho_J^2}} \text{ if } 4A_1^2 \geq B_1^2 \text{ and } 4A_2^2 \geq B_2^2 \quad (92a)$$

$$\omega = \frac{2}{1 + \sqrt{1 + \rho_J^2}} \text{ if } 4A_1^2 \leq B_1^2 \text{ and } 4A_2^2 \leq B_2^2 \quad (92b)$$

where

$$\rho_J = \frac{\sqrt{|4A_1^2 - B_1^2|}}{|C - 2(A_1 + A_2)|} \cos\left(\frac{\pi}{I + 1}\right) + \frac{\sqrt{|4A_2^2 - B_2^2|}}{|C - 2(A_1 + A_2)|} \cos\left(\frac{\pi}{J + 1}\right) \quad (93)$$

In all other cases, the underrelaxation represented by the second of these situations is used. Here I and J are the field dimensions.

110. In the momentum equations (Equations 77a and 77b) we have, neglecting derivatives of the width B and defining $F \equiv 4/3$,

$$\begin{aligned} (\sigma_{11}y_\eta - \sigma_{12}x_\eta)_\xi &= \frac{F\mu}{J} \left(u_\xi y_\eta^2 - u_\eta y_\xi y_\eta \right)_\xi \\ &\quad - \frac{\mu}{J} \left(u_\eta x_\xi x_\eta - u_\xi x_\eta^2 + v_\xi x_\eta y_\eta - v_\eta x_\eta y_\xi \right)_\xi \\ &= \frac{F\mu}{J} \left[y_\eta^2 u_{\xi\xi} \dots + u_\xi (y_\eta^2)_\xi - u_\eta (y_\xi y_\eta)_\xi \right] \\ &\quad - \frac{\mu}{J} \left[\dots - x_\eta^2 u_{\xi\xi} + (x_\xi x_\eta)_\xi u_\eta - (x_\eta^2)_\xi u_\xi \dots \right] \\ (\sigma_{12}x_\xi - \sigma_{11}y_\xi)_\eta &= \frac{\mu}{J} \left(u_\eta x_\xi^2 - u_\xi x_\xi x_\eta + \dots \right)_\eta - \frac{F\mu}{J} \left(u_\xi y_\xi y_\eta - u_\eta y_\xi^2 \right)_\eta \\ &= \frac{\mu}{J} \left[x_\xi^2 u_{\eta\eta} + (x_\xi^2)_\eta u_\eta - (x_\xi x_\eta)_\eta u_\xi \dots \right] \\ &\quad - \frac{F\mu}{J} \left[-y_\xi^2 u_{\eta\eta} + (y_\xi y_\eta)_\eta u_\xi - (y_\xi^2)_\eta u_\eta \dots \right] \end{aligned}$$

Then the stress terms in x-momentum are

$$\begin{aligned}
 & -\frac{\mu}{J} \left[y_n^2 u_{\xi\xi} + (y_n^2)_\xi u_\xi - (y_\xi y_n)_\xi u_n \right] + \frac{\mu}{J} \left[-x_n^2 u_{\xi\xi} + (x_\xi x_n)_\xi u_n - (x_n^2)_\xi u_\xi \right] \\
 & -\frac{\mu}{J} \left[x_\xi^2 u_{nn} + (x_\xi^2)_n u_n - (x_\xi x_n)_n u_\xi \right] + \frac{\mu}{J} \left[-y_\xi^2 u_{nn} + (y_\xi y_n)_n u_\xi - (y_\xi^2)_n u_n \right] \cdot \cdot \cdot \\
 & = \frac{\mu}{J} \left\{ -\left(Fy_n^2 + x_n^2 \right) u_{\xi\xi} - \left(Fy_\xi^2 + x_\xi^2 \right) u_{nn} - \left[F(y_n^2)_\xi + (x_n^2)_\xi - (x_\xi x_n)_n - F(y_\xi y_n)_n \right] u_\xi \right. \\
 & \quad \left. - \left[-F(y_\xi y_n)_\xi - (x_\xi x_n)_\xi + (x_\xi^2)_n + F(y_\xi^2)_n \right] u_n \cdot \cdot \cdot \right\}
 \end{aligned}$$

Then, for the x-momentum equation,

$$A_1 = -\frac{\mu}{J} \left(x_n^2 + Fy_n^2 \right)$$

$$A_2 = -\frac{\mu}{J} \left(x_\xi^2 + Fy_\xi^2 \right)$$

$$B_1 = \rho \tilde{u} - \frac{\mu}{J} \left[\left(x_n^2 + Fy_n^2 \right)_\xi - \left(x_\xi x_n + Fy_\xi y_n \right)_n \right]$$

$$B_2 = \rho \tilde{v} - \frac{\mu}{J} \left[\left(x_\xi^2 + Fy_\xi^2 \right)_n - \left(x_\xi x_n + Fy_\xi y_n \right)_\xi \right]$$

$$C = J\rho \frac{G}{\Delta t}$$

and for the y-momentum equation,

$$A_1 = - \frac{\mu}{J} \left(Fx_\eta^2 + y_\eta^2 \right)$$

$$A_2 = - \frac{\mu}{J} \left(Fx_\xi^2 + y_\xi^2 \right)$$

$$B_1 = \rho \tilde{u} - \frac{\mu}{J} \left[\left(Fx_\eta^2 + y_\eta^2 \right)_\xi - \left(Fx_\xi x_\eta + y_\xi y_\eta \right)_\eta \right]$$

$$B_2 = \rho \tilde{v} - \frac{\mu}{J} \left[\left(Fx_\xi^2 + y_\xi^2 \right)_\eta - \left(Fx_\xi x_\eta + y_\xi y_\eta \right)_\xi \right]$$

$$C = J\rho \frac{G}{\Delta t}$$

where G is 1 for first-order time derivatives and $\frac{3}{2}$ for second-order. By similar developments, we have for the energy equation (Equation 78),

$$A_1 = A_2 = \frac{\kappa}{J} (\alpha + \gamma)$$

$$B_1 = \rho \tilde{u} - \frac{\kappa}{J} (\alpha_\xi - \beta_\eta)$$

$$B_2 = \rho \tilde{v} - \frac{\kappa}{J} (\gamma_\eta - \beta_\xi)$$

$$C = J\rho \frac{G}{\Delta t}$$

Turbulence Model

111. The cumulative effect of turbulence and the correlation terms from the lateral averaging is modeled by using horizontal and vertical eddy viscosity and diffusivity coefficients. This is done by replacing the viscosity μ by $\mu + \rho D_{jj}$ (no summation) in the stress

elements σ_{ij} , and the conductivity κ by $\kappa + \rho \frac{\kappa}{\mu} C_j$ in the heat flux q . Thus, D_{11} and D_{12} are the horizontal and vertical eddy viscosities, respectively. Three variations of D_{11} and D_{22} are provided for input selection: (a) uniform values; (b) the model of Edinger and Buchak (1979), as given in Johnson (1981); and (c) the model of Kent and Pritchard (1959), as given in Brandsma and Divoky (1976).

112. The model of Edinger and Buchak is implemented in the present model as

$$D_{11} = 0.16 \left(\frac{h^2 d}{d_0} \right) \left| \frac{\partial |u|}{\partial y} \right| \quad (94a)$$

$$D_{22} = \begin{cases} \frac{D_{11}}{\sqrt{1 + 10R_1}} & R_1 > 0 \\ \frac{|y_\xi + y_\eta|^2}{2\Delta t} & R_1 \leq 0 \end{cases} \quad (94b)$$

$$C_1 = 1.33 D_{11} \quad (95a)$$

$$C_2 = \begin{cases} \frac{C_1}{(1 + 3.33 R_1)^{3/2}} & R_1 > 0 \\ C_2 = D_{22} & R \leq 0 \end{cases} \quad (95b)$$

The model of Kent and Pritchard is implemented as

$$D_{11} = 0.0086 d^2 \left(1 - \frac{d}{d_0} \right)^2 \frac{|u|}{d_0} \quad (96a)$$

$$D_{22} = \begin{cases} \frac{D_{11}}{(1 + 0.276 R_1)^2} & R_1 > 0 \\ D_{11} & R_1 \leq 0 \end{cases} \quad (96b)$$

$$C_1 = D_{11}$$

$$C_2 = D_{22}$$

113. In both of these, the Richardson number R_1 is given by

$$R_1 = - \frac{g \rho_y}{\rho \left| \frac{\partial |u|}{\partial y} \right|^2} \quad (97)$$

and d is the local depth, d_0 is the total depth, and h is the height above the bottom, i.e., $h = d_0 - d$. Also if $\left| \frac{\partial |u|}{\partial y} \right|$ is less than $0.7 \frac{|u|}{d_0}$, the former is reset to the latter value.

114. The model also includes an optional artificial eddy viscosity and conductivity in the form

$$D_{11} = D_{22} = \frac{|D|}{\rho B} \quad (98)$$

$$C_1 = C_2 = \frac{|D|}{\rho B} \quad (99)$$

where D is the mass residual (Equation 80) calculated with central differences.

PART VI: RESULTS

115. The discrete representation for the equations of motion, with the solution thereof, has been implemented in the computer code WESSEL (Thompson and Bernard 1985). Boundary-fitted curvilinear coordinate systems are generated numerically by a separate code, WESCOR (Thompson 1983), allowing boundaries of arbitrary shape to be used.

116. The WESSEL code was run for three comparison cases with distinct geometries:

- a. Selective withdrawal from a rectangular channel with linear stratification.
- b. Cold inflow into a flume with nonuniform width and depth.
- c. Flow over a crested weir, with and without stratification.

While this range of geometries and flow conditions is not exhaustive, it does afford a sampling of typical applications for the present model.

117. In the calculations discussed below, conservative upwind differencing was used for the convective terms, with second-order backward differencing for the time derivatives. Variable acceleration parameters were used for the momentum and energy equations, with the boundary-temperature acceleration parameter set at unity. The acceleration parameter for the Chorin pressure calculation was fixed at

$$\omega = 0.88$$

A value closer to unity might have improved convergence in some cases, but the chosen value proved satisfactory for all cases and geometries considered. Calculations were made without using artificial viscosity and conductivity, and the turbulence models were inactive unless otherwise noted. As previously stated, the coordinate systems are generated with twice as many points as the flow fields. The initial velocity field was always specified such that the initial flow was horizontal, with uniform flow rate.

118. Results are presented primarily in the form of velocity vectors and temperature (or density) contours at selected time steps.

All runs were made on the CRAY-1 computer at the Boeing Company, Bellevue, Wash.

Selective Withdrawal from a Rectangular
Channel with Linear Stratification

119. A pair of classic papers by Pao and Kao (1974) and by Kao, Pao, and Wei (1974) quantified the mechanisms associated with the establishment of selective withdrawal from reservoirs. The first comparison calculation in the present work duplicates the physical conditions for one of the experiments reported in Kao, Pao, and Wei (1974).

120. Consider a rectangular channel of uniform width and depth, with linear density stratification, such that

$$F = 0.014$$

where F is the densimetric Froude number given by

$$F = \frac{Q}{Nd^2}$$

with

Q = flow rate*

N = the Vaisala frequency

d = channel depth

$$N = \left(-\frac{g}{\rho_0} \frac{d\rho}{dy} \right)^{1/2}$$

The specified value of F was achieved herein by setting

* In this case (linear stratification), the flow is vertically symmetric. The values of Q and d specified here represent half of the total flow rate and vertical depth.

$$d = 1 \text{ ft}^\dagger$$

$$g = 32.2 \text{ ft/sec}^2$$

$$\rho_o = 1 \text{ gm/cm}^3 = 1.94 \text{ slug/ft}^3$$

$$\frac{d\rho}{dy} = 0.0071 \frac{\text{gm}}{\text{ft-cm}^3} = 0.0138 \text{ slug/ft}^4$$

$$w = \text{width} = 1 \text{ ft}$$

$$Q = 0.00684 \text{ ft}^3/\text{sec}$$

The experimental channel length was 30.5 ft, but for the calculation this was reduced to 23 ft, which was long enough for the comparison of results near the outlet. The coordinate grid used was 101 × 41 mesh, with a 51 × 21 flow field mesh (Figure 2), representing the top half of a vertically symmetric flow field. Figure 2 shows only the last 4 ft or so of the channel. The longitudinal grid spacing is uniform (0.1 ft) for the last 3 ft, and the vertical spacing is uniform (0.05 ft) everywhere in the flow field. Detailed results were desired only for the last 3 ft, so exponential spacing was used for the 20 ft upstream.

121. The reference or characteristic time is the inverse Vaisala frequency,

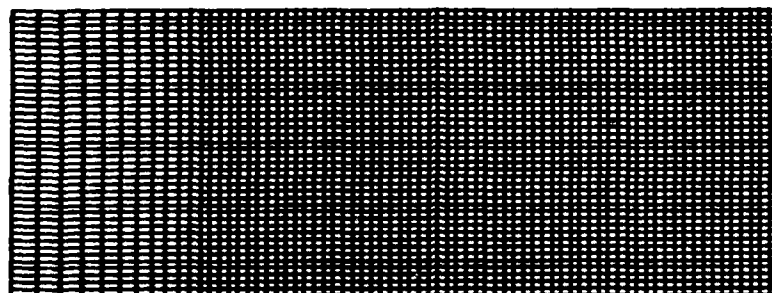
$$N^{-1} = 2.09 \text{ sec}$$

and the associated nondimensional time is

$$t^* = Nt$$

† A table of factors for converting non-SI units of measurement to metric (SI) units is presented on page 4.

Field System



Flow System

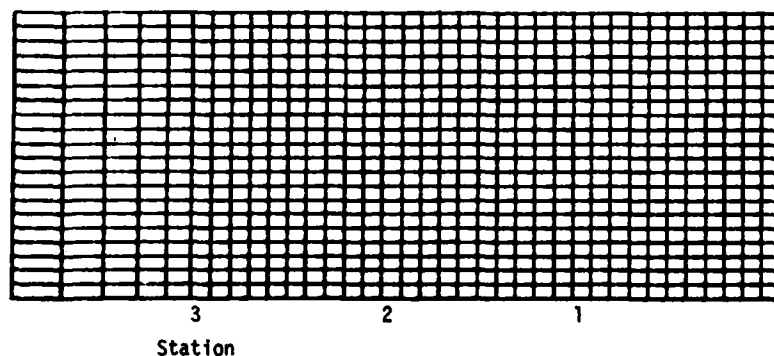


Figure 2. Coordinate system for rectangular channel

The reference velocity is

$$U = \frac{Q}{wd} = 0.00684 \text{ ft/sec}$$

so the nondimensional velocity is

$$u^* = u/U$$

122. WESSEL calculations were executed for times up to $t = 125 \text{ sec}$ ($t^* = 60$) with time steps of 2.09 sec ($\Delta t^* = 1.0$) and

0.209 sec ($\Delta t^* = 0.1$). Further reduction of the time step produced no significant change in the results. The number of iterations was fixed at 15 per time step.

123. The inflow boundary condition ($i = 1$) was extrapolated velocity and density with flow balance employed. The upper boundary ($j = 21$) was idealized as a no-slip wall with fixed density. The symmetry boundary ($j = 1$) was treated as a slip wall with fixed density. The downstream boundary ($i = 51$) was modeled as a no-slip wall with extrapolated density, except for the outlet ($i = 51, j = 1$ to 4) where the density was extrapolated and the velocity was held fixed. The initial condition was a uniform horizontal flow field ($u = 0.00684$ ft/sec).

124. Figure 3 shows comparisons of calculated and measured velocities versus time along the symmetry line ($j = 1$). Stations 1, 2, and 3 are, respectively, 1, 2, and 3 ft upstream from the outlet. Certain facts are readily obvious:

- a. The velocities at early times are correctly predicted.
- b. The steady-state velocities are underpredicted.
- c. Accuracy improves with distance from the outlet.
- d. The smaller time step ($\Delta t^* = 0.1$) provides better resolution of the transient behavior, but the larger ($\Delta t^* = 1.0$) achieves essentially the same accelerations (somewhat delayed) and steady-state velocities.

The deterioration of the symmetry-line velocity predictions with time, near the outlet, can be understood in part after an examination of the predicted and observed steady-state velocity profiles. Figure 4 shows the calculated and observed profiles at stations 1-3. The sharpest profile occurs nearest the outlet, where the highest acceleration occurs on the symmetry line. The numerical calculation underpredicts the maximum velocity primarily because the symmetry line ($j = 1$) is idealized as a slip wall, which means the horizontal velocity is extrapolated from the next line up ($j = 2$), so the code does not resolve the large velocity gradient between $j = 1$ and $j = 2$. Hence, as the slope of the observed profile becomes gentler upstream of the outlet, the agreement between calculation and experiment improves.

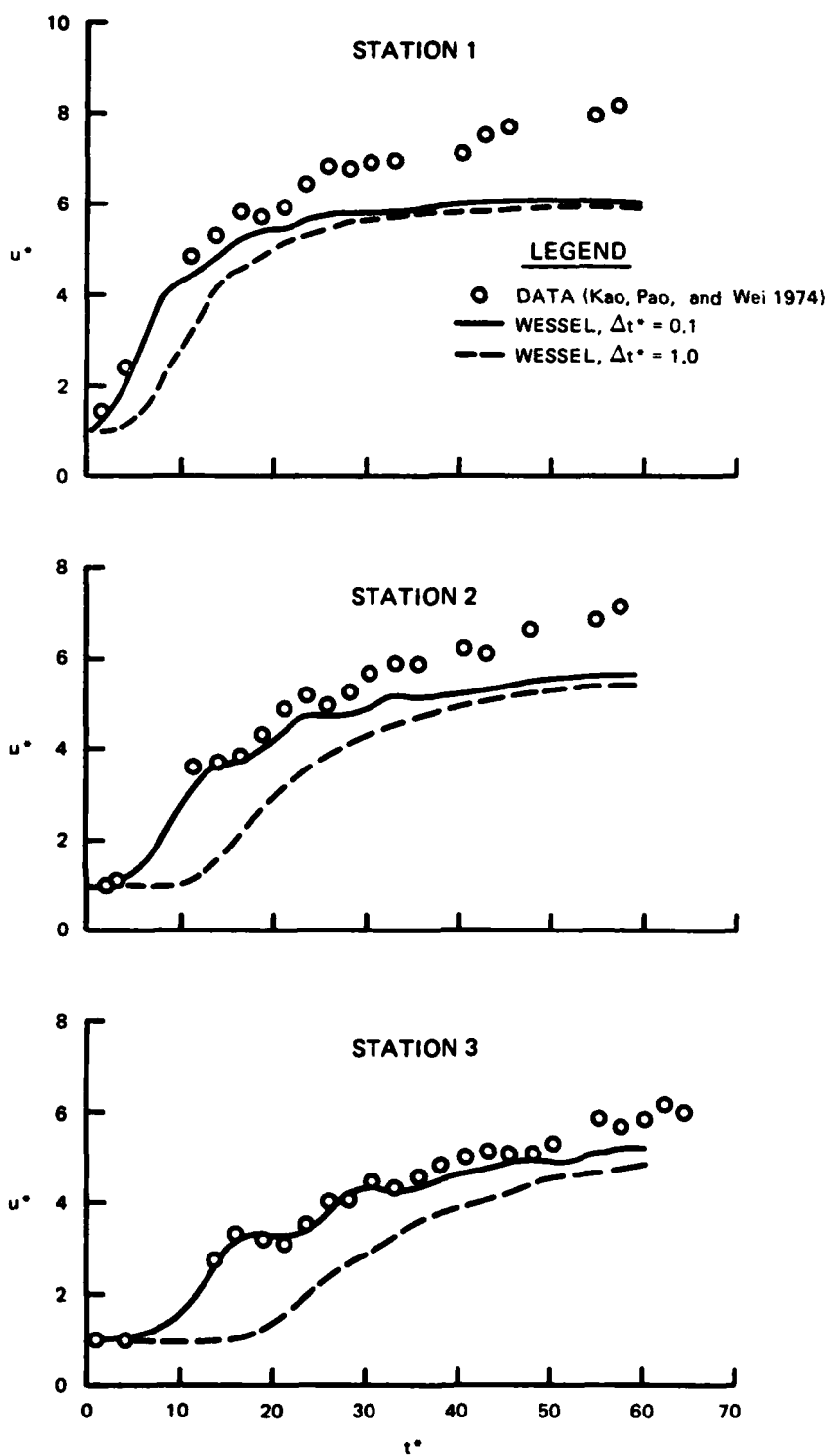


Figure 3. Nondimensional velocity versus time along line of symmetry for rectangular channel

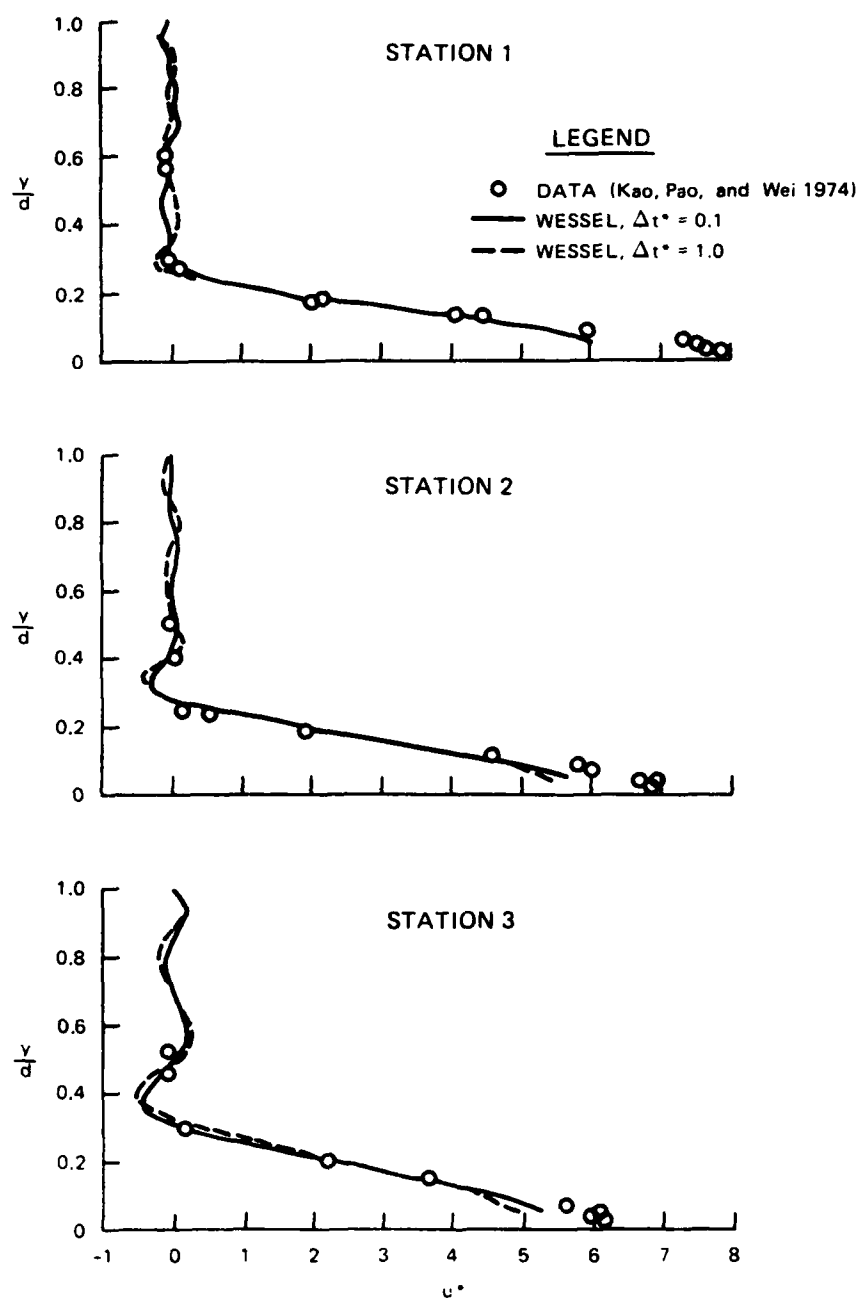


Figure 4. Nondimensional steady-state velocity profiles ($t^* = 60$) for selective withdrawal from rectangular channel

125. Figure 5 presents vector plots of the developing flow field between station 3 and the outlet. This shows clearly the growing region of circulation at $t^* = 10$ and $t^* = 20$, and the plot for $t^* = 60$ represents the steady state. The results in Figure 5 were obtained with $\Delta t^* = 0.1$

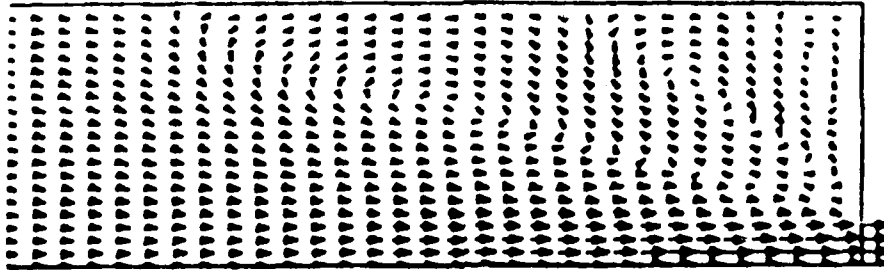
Cold Inflow into a Flume with Nonuniform Width and Depth

126. The experimental facility represented in this comparison is the Generalized Reservoir Hydrodynamics (GRH) flume at WES, described in Johnson (1981). The flume is 80 ft long with a 3- by 3-ft cross section at the downstream end. The cross section of the upstream end is 1 by 1 ft, and the width expands uniformly with length over the first 20 ft, to a cross section 1 ft deep and 3 ft wide. Thereafter, the width remains constant while the depth grows uniformly with length, to 3 ft at the downstream end. Plan and side views of the GRH flume appear in Figure 6.

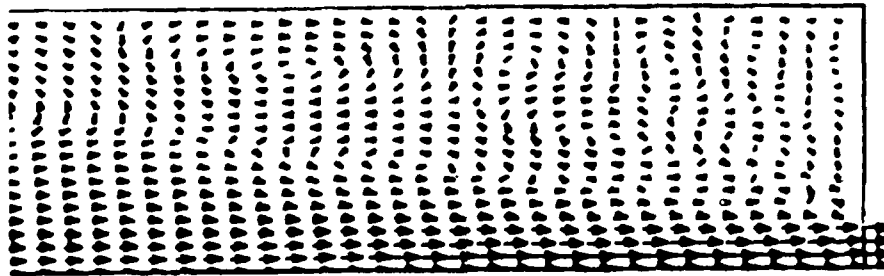
127. The water in the flume was at rest and homogeneous at the beginning of the test, with the temperature being 70.6° F. Cold water was input 1.5 ft from the upstream end at a temperature of 62.0° F. A baffle restricted the cold water to enter through the lower 0.5 ft of the cross section. The inflow rate was 0.022 cfs, with the outflow rate at the downstream end being the same. The outflow was removed from a 1-in.-diam port located 0.5 ft above the bottom of the flume and 1.5 ft from either side. The flow was observed to be relatively smooth and was probably laminar, or at least only in the transition range to turbulent flow. Numerical results from several codes are compared with experimental results in Johnson (1981).

128. For simulation with the WESSEL code, a 33×25 coordinate grid was used, with a 17×13 flow field grid (Figure 7). The inlet was specified as the lower 0.5 ft ($i = 1$, $j = 1$ to 7) at the upstream end,

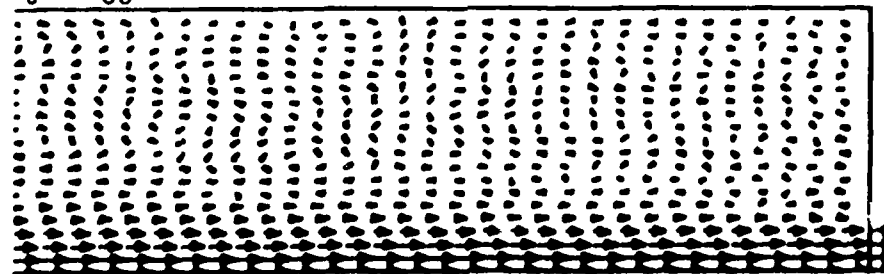
$$t^* = 10$$



$$t^* = 20$$



$$t^* = 60$$



3
2
1
Station

Figure 5. Velocity vectors for selective withdrawal from rectangular channel

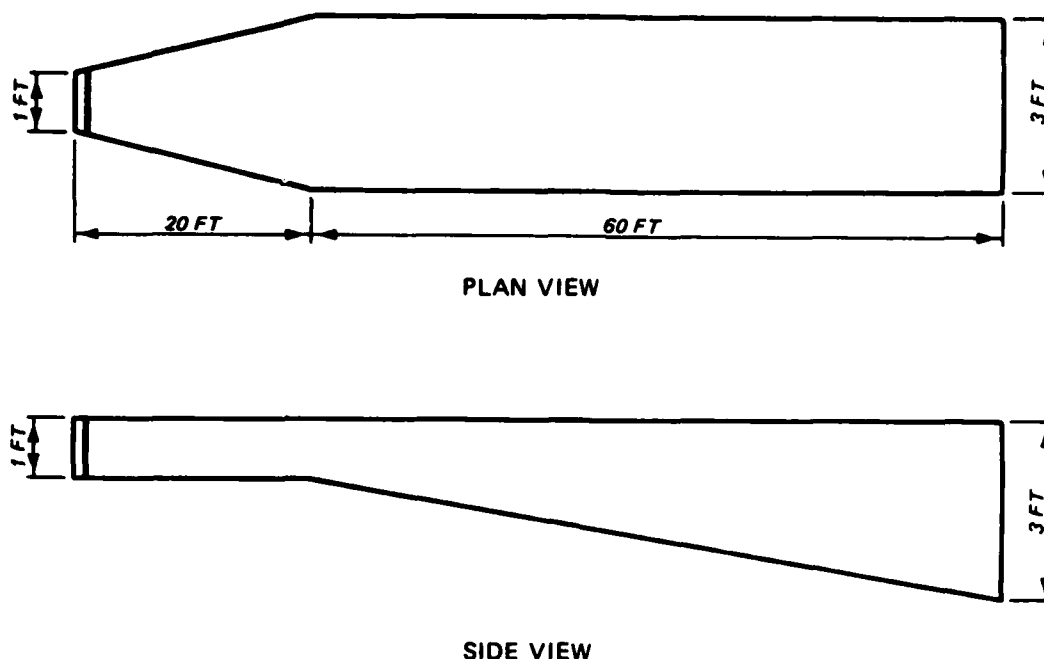


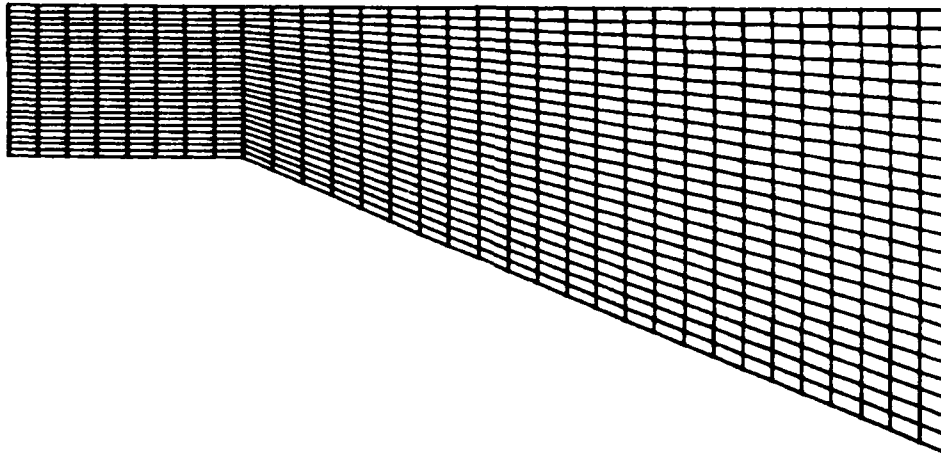
Figure 6. Plan and side views of GRH flume

and the outlet was idealized as a single grid space ($i = 17, j = 3$) 0.5 ft from the bottom at the downstream end. Velocities were held fixed at the inlet and outlet, with the initial (horizontal) velocity field specified such that the flow rate was 0.022 cfs everywhere in the flume. The temperature was fixed at the inlet and extrapolated at all other boundaries. The free surface was modeled as a slip boundary, and the no-slip condition was employed on the walls.

129. Calculations were made for (a) laminar flow, (b) the Kent turbulence model, and (c) the Edinger turbulence model. In each case, the time step was set at 5 sec with a limit of 50 iterations per time step, and the code was run for 500 time steps.

130. Figure 8 shows a comparison of the WESSEL results with experimental data and with predictions of the LARM code of Edinger and Buchak (1979). The underflow front position is correctly predicted by the laminar calculation and by the calculation using the Kent turbulence model. The total drop in outlet temperature is underpredicted, possibly

Field System



Flow System

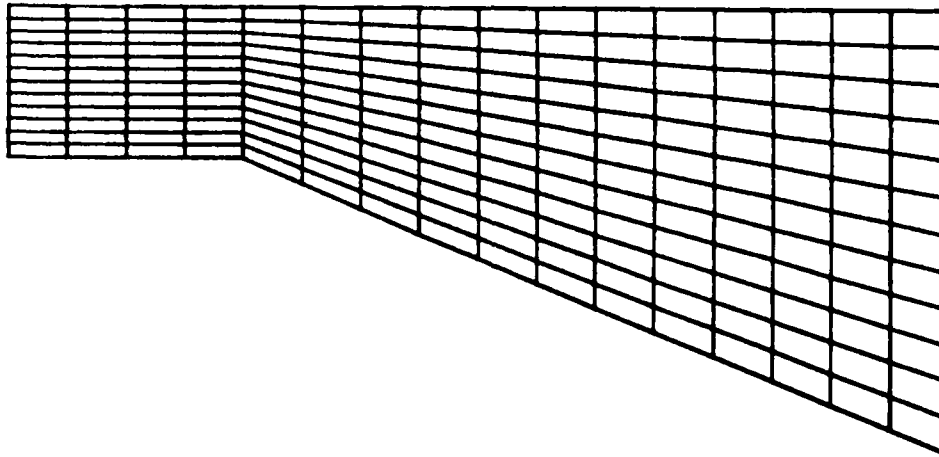


Figure 7. Boundary-fitted coordinate system for GRH flume

due to the coarse grid and rather crude treatment of the outlet itself. Furthermore, while the rate of temperature drop is initially correct, the onset is probably delayed by the diffusive effects of upwind differencing. Evidence for this can be seen in the calculation with the Edinger turbulence model, which is far more diffusive than the Kent

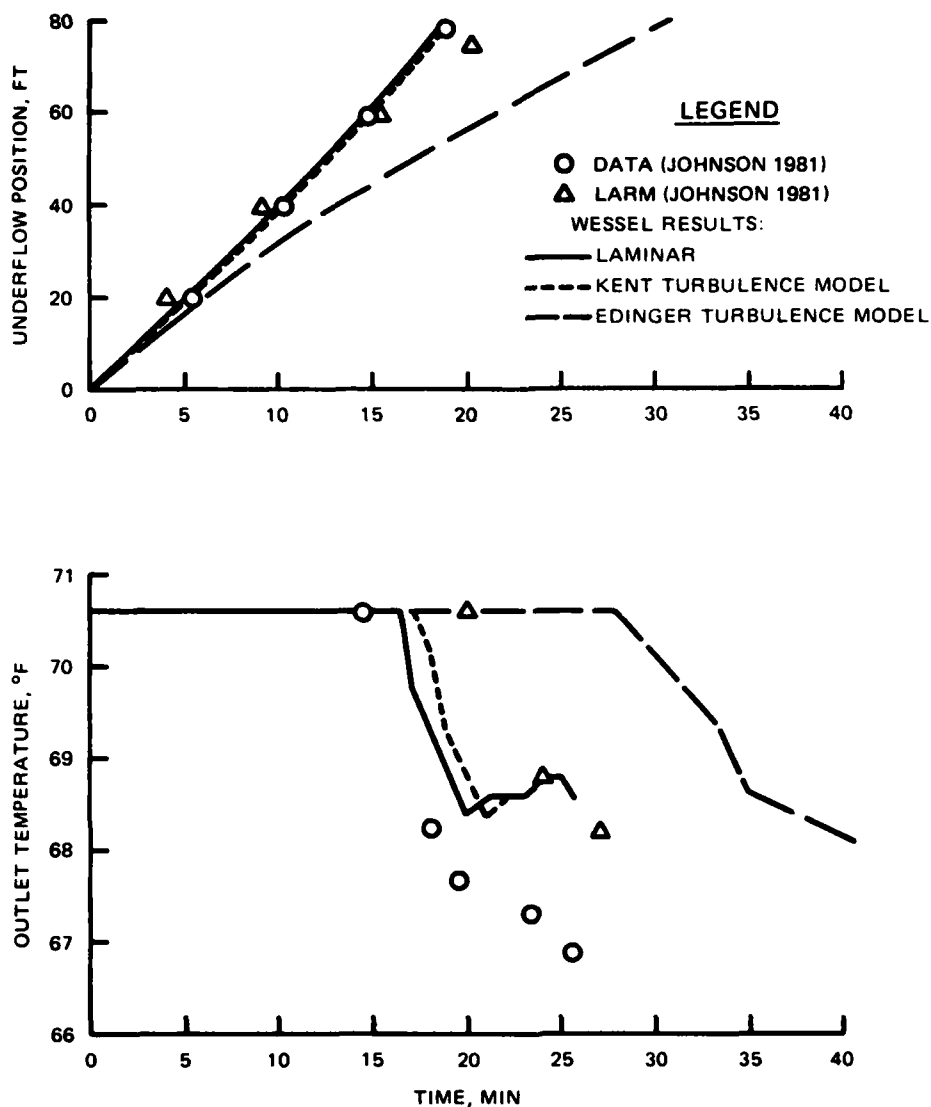


Figure 8. Comparison of results for cold underflow in GRH flume

model. Here the large eddy viscosity of the Edinger model severely retards the motion of the underflow front as well as the onset of temperature drop at the outlet.

131. Flow field development with time (velocity vectors and temperature contours) for the three flume calculations can be seen in

Figures 9-14.* The laminar case (Figures 9 and 10) is almost indistinguishable from that with the Kent turbulence model (Figures 11 and 12). The cold water flows along the bottom to the outlet, causing recirculation in the warm water, with a cooling effect that eventually works its way upstream. The Edinger turbulence model (Figures 13 and 14) produces results that are quite different from the first two cases. Instead of flowing just along the bottom, the cold water diffuses, forming a thicker and slower-moving underflow front. This delays the temperature drop at the outlet but causes more cooling in the flume as a whole.

Flow over a Crested Weir

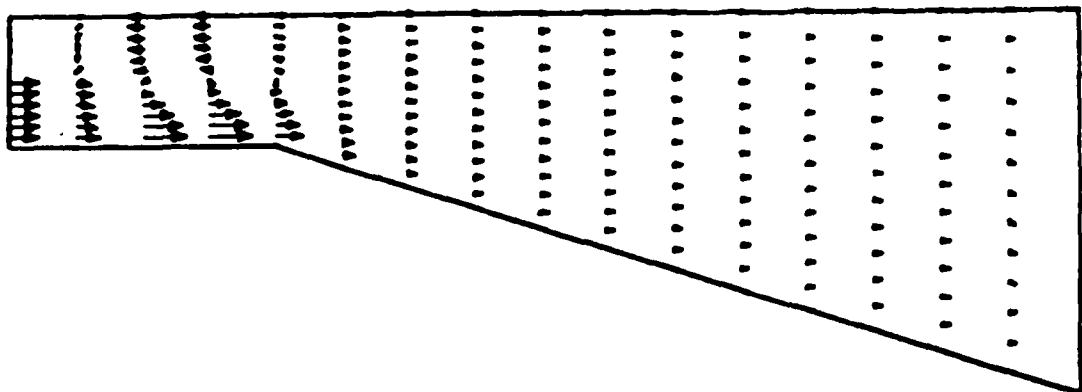
132. As a final example, consider a rectangular channel of uniform width (1 ft) with a crested weir (Figure 15). Flow tests were conducted for this configuration to verify a finite-element model.** In one test, the flow (0.074 cfs) was initially stratified upstream of the weir, but unstratified downstream. In another test, the flow (0.7 cfs) was unstratified throughout the channel. Figure 16 shows the density profile for the stratified case, 4 ft upstream of the weir crest.

133. WESSEL calculations were made for (a) constant density with total discharge $Q = 0.7$ cfs, and (b) initial density stratification on both sides of the weir with $Q = 0.074$ cfs. In the latter case, the initial density profile was that given in Figure 16. The boundary-fitted coordinate system (Figure 17) consisted of a 101×35 grid, with a 51×18 flow field grid. The no-slip condition was employed on the channel walls, and the free surface was idealized as a slip boundary. Density was extrapolated at all boundaries. The outlet was 0.6 ft high

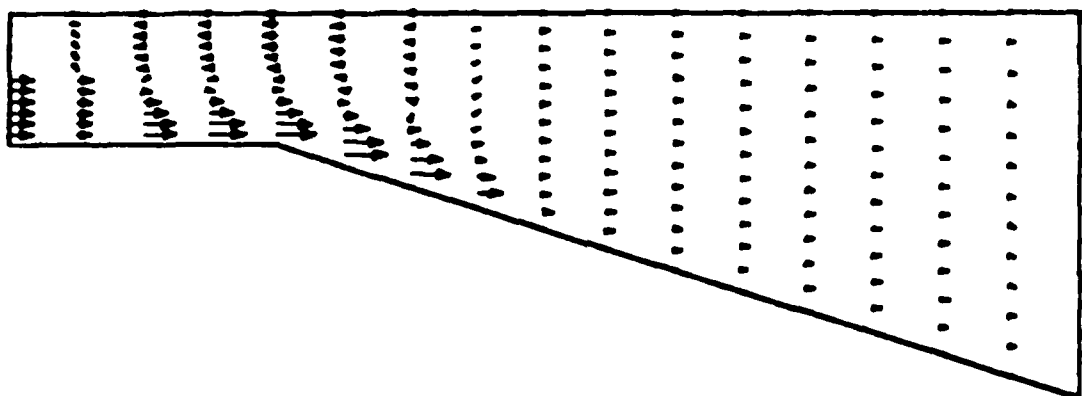
* The velocity vectors along the bottom are actually parallel to the bottom. They do not appear so in the vector plots because the flume is not drawn to scale. This also steepens the apparent horizontal temperature gradients in the contour plots.

** Personal Communication, 1983, J. L. Grace, Jr., Hydraulics Laboratory, US Army Engineer Waterways Experiment Station, Vicksburg, Miss.

250 Seconds



500



750

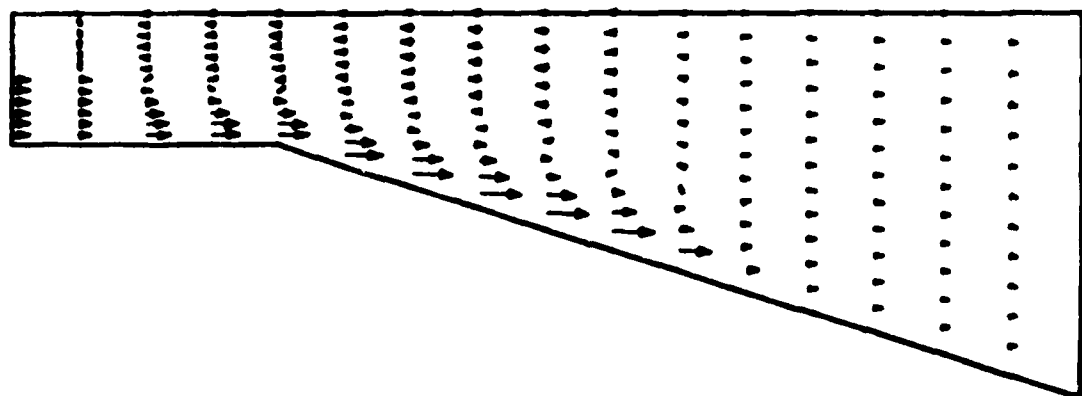
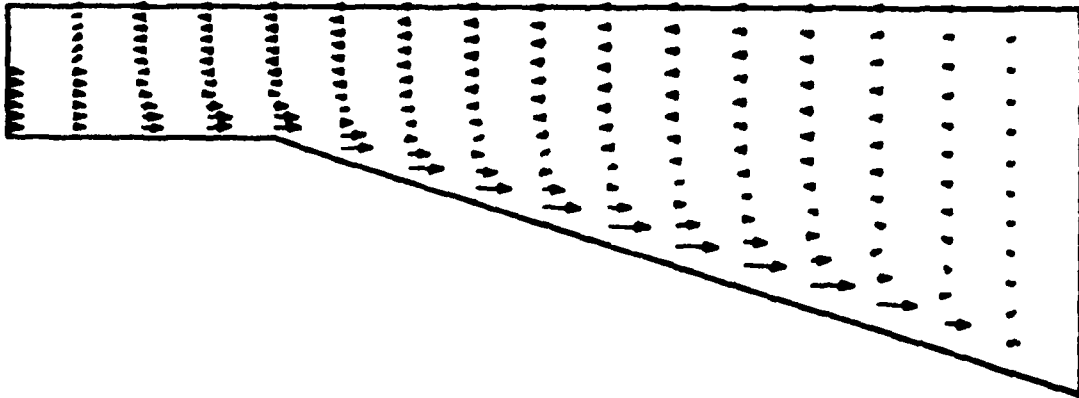
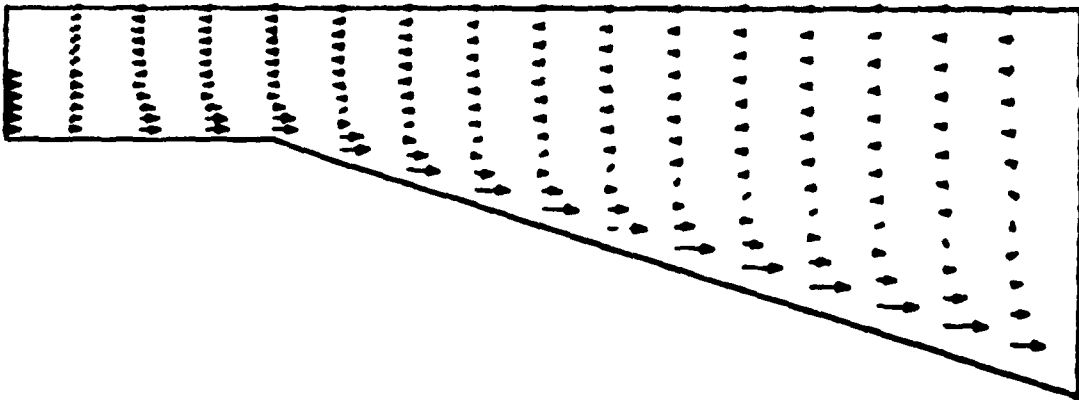


Figure 9. Velocity vectors for laminar flow calculation in GRH flume (Sheet 1 of 3)

1000



1250



1500

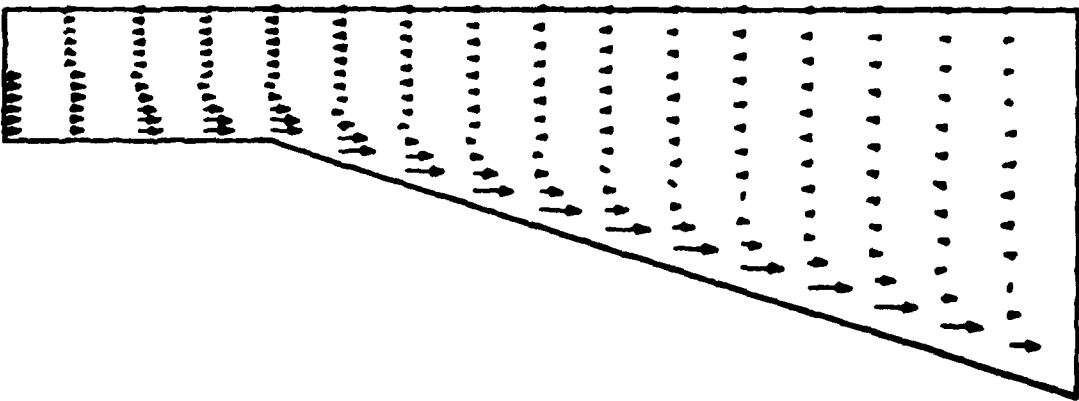
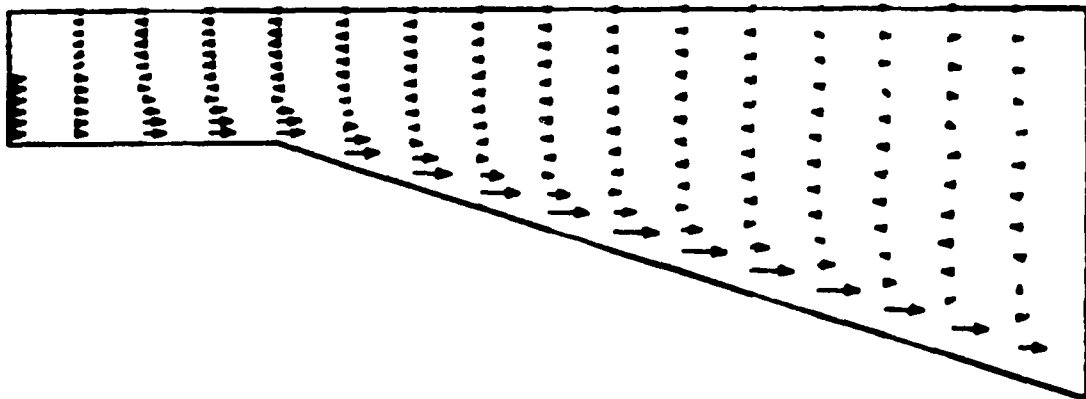
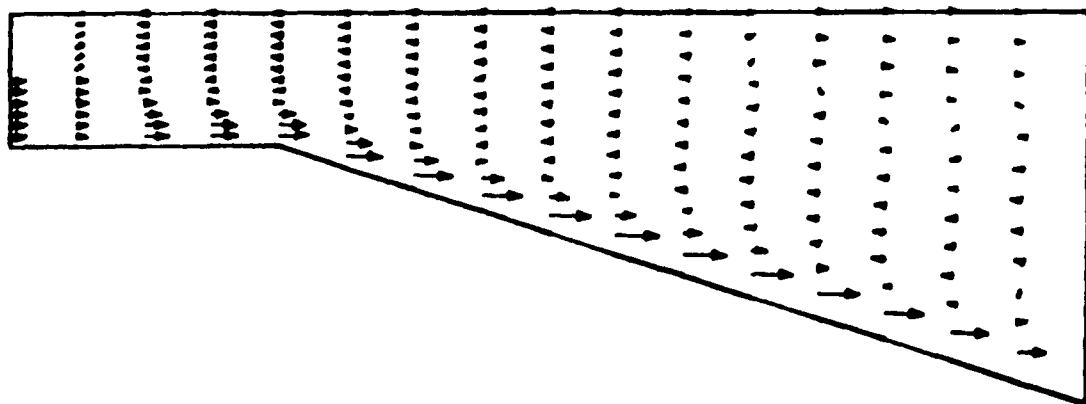


Figure 9. (Sheet 2 of 3)

1750



2000



2500

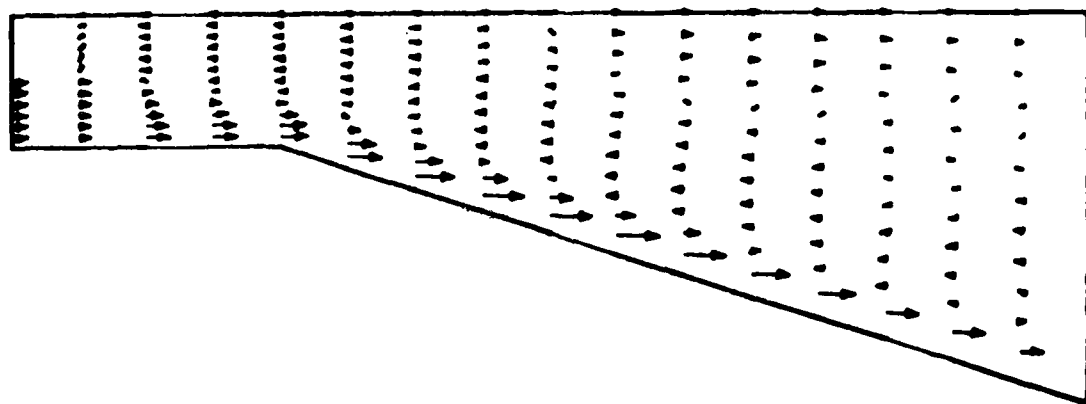
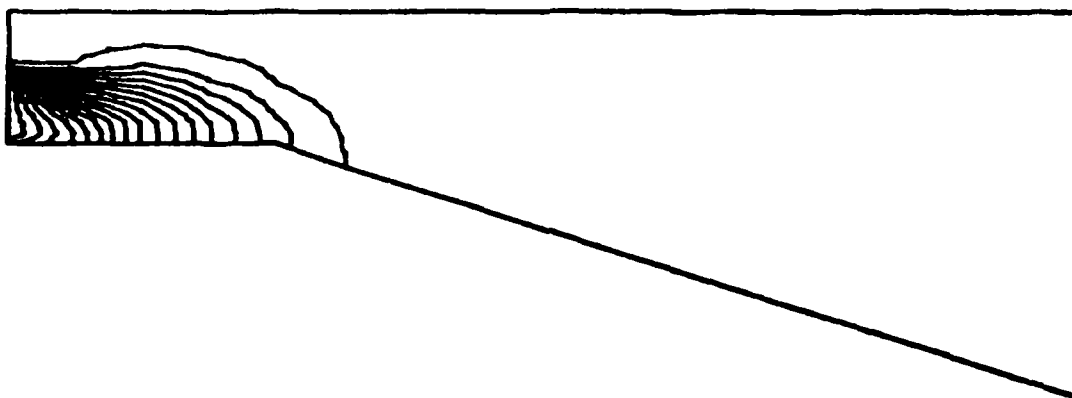
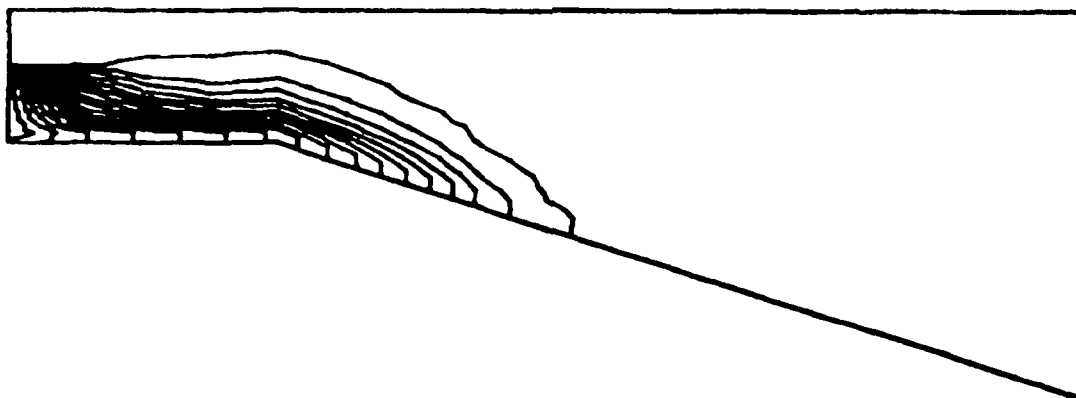


Figure 9. (Sheet 3 of 3)

250 Seconds



500



750

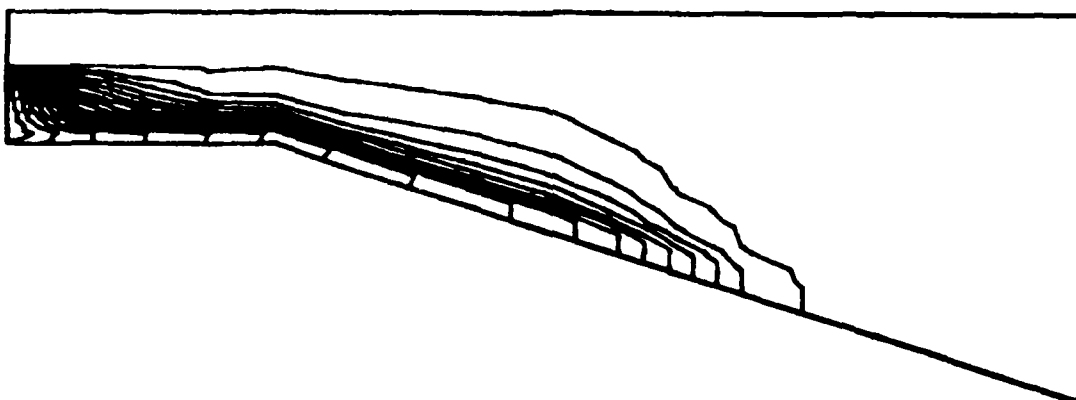
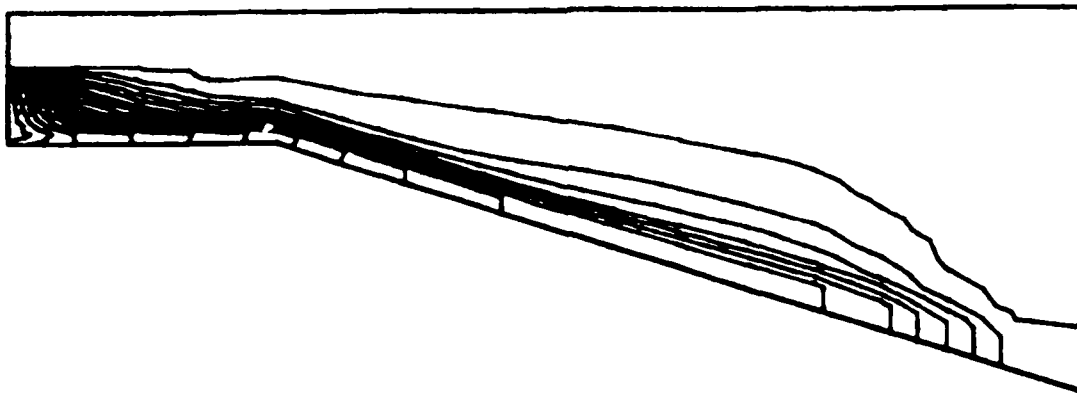
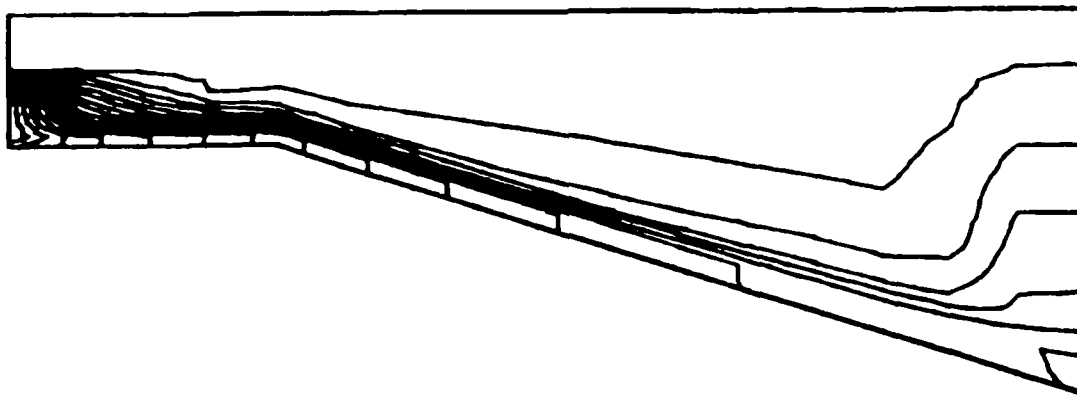


Figure 10. Temperature contours for laminar flow calculation in GRH flume (contour interval = 0.5°F) (Sheet 1 of 3)

1000



1250



1500

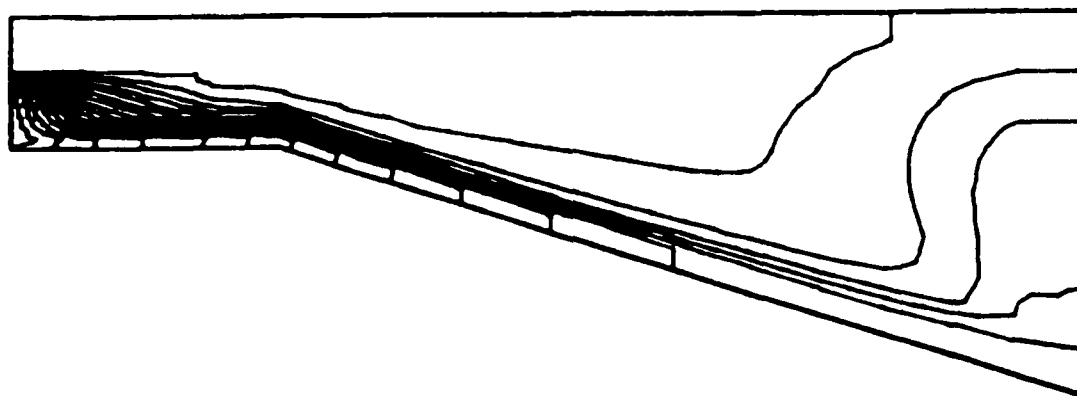
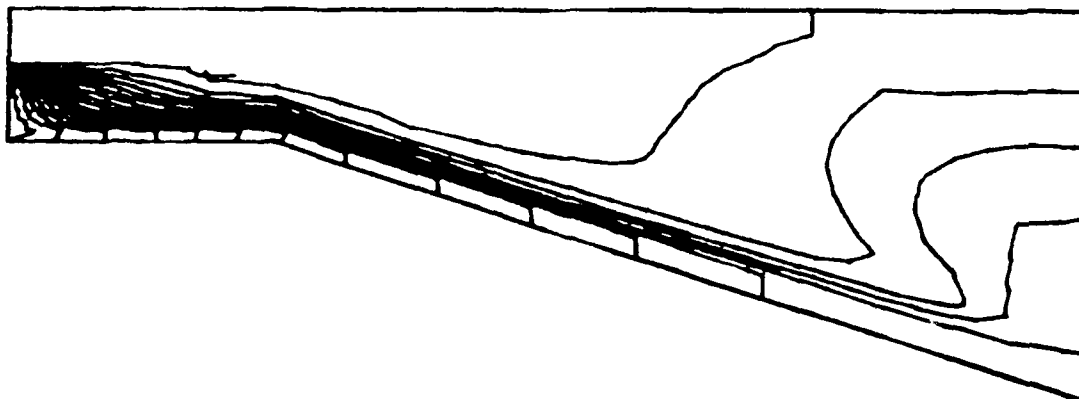
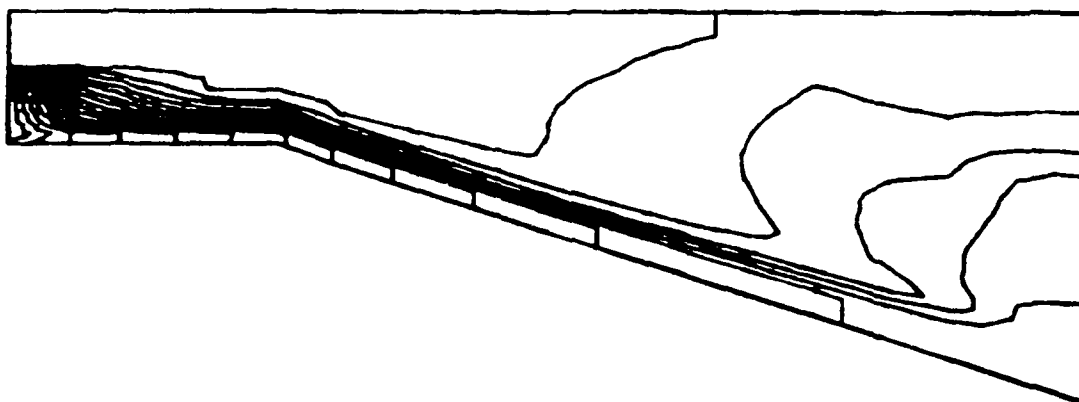


Figure 10. (Sheet 2 of 3)

1750



2000



2500

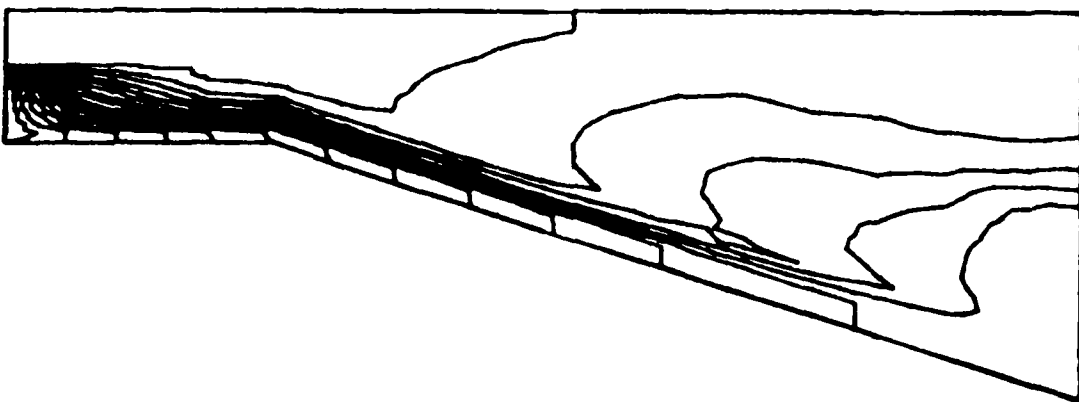
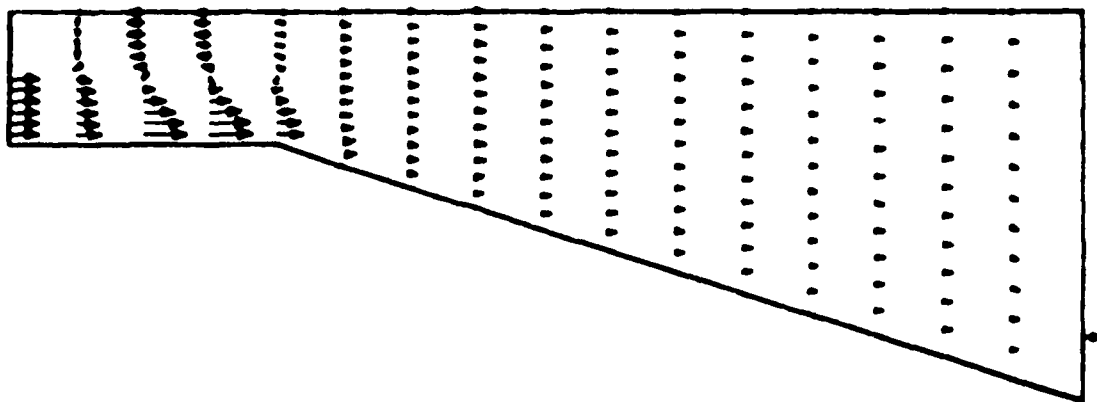
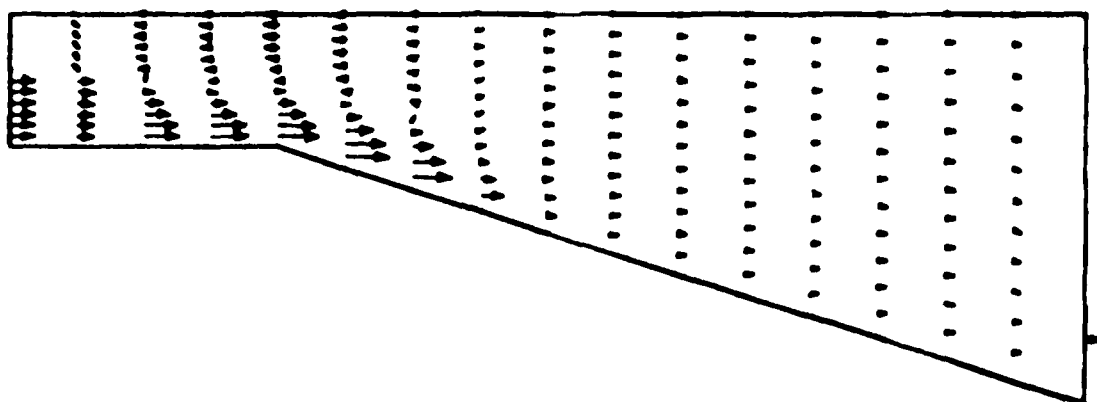


Figure 10. (Sheet 3 of 3)

250 Seconds



500



750

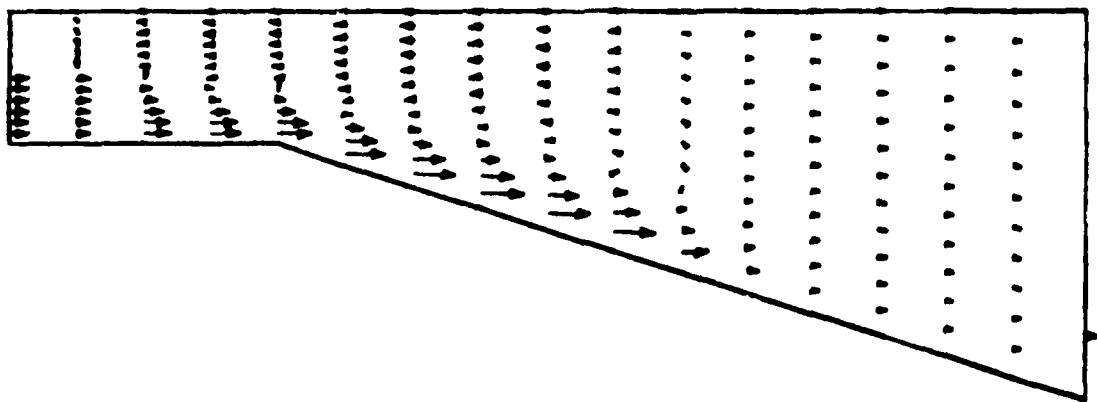
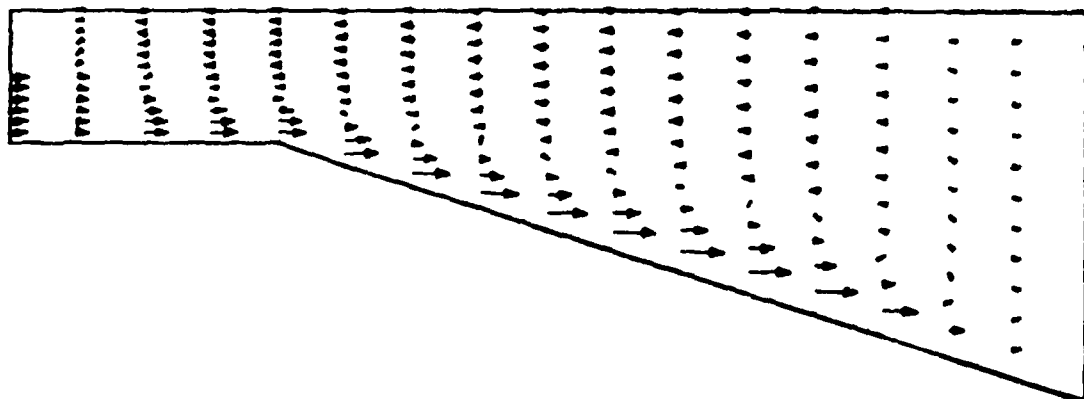
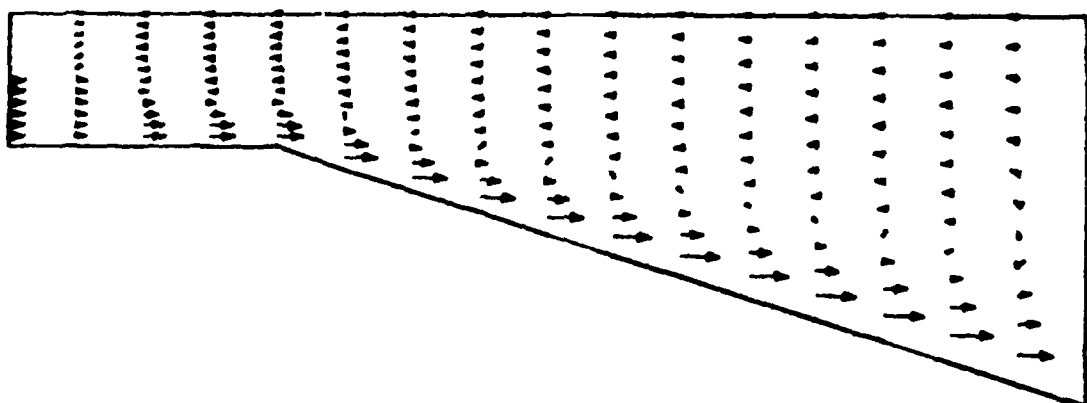


Figure 11. Velocity vectors for calculation with Kent turbulence model in GRH flume (Sheet 1 of 3)

1000



1250



1500

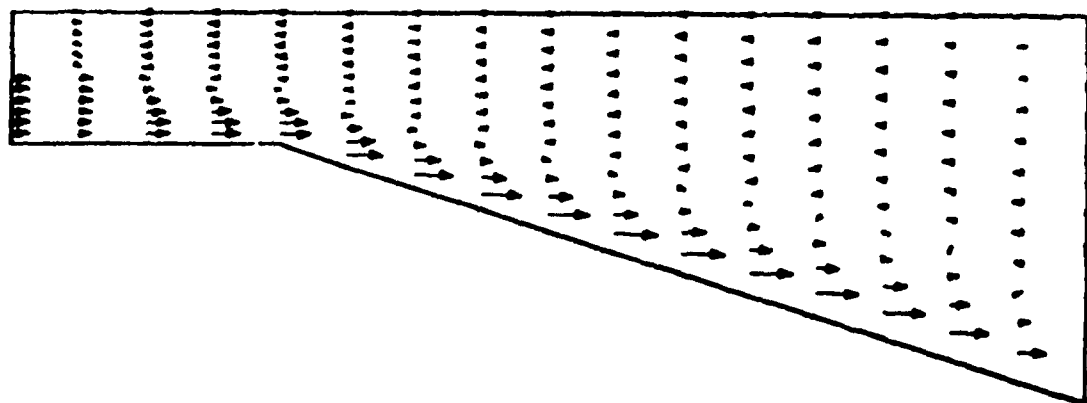
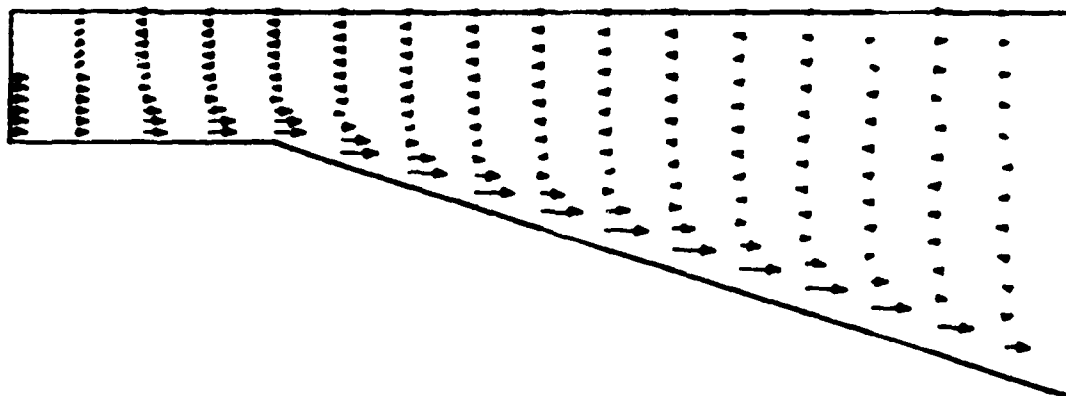
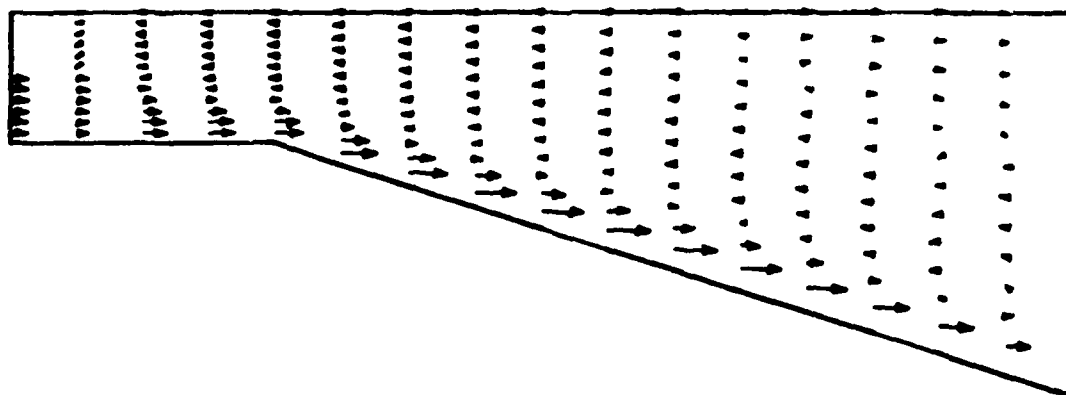


Figure 11. (Sheet 2 of 3)

1750



2000



2500

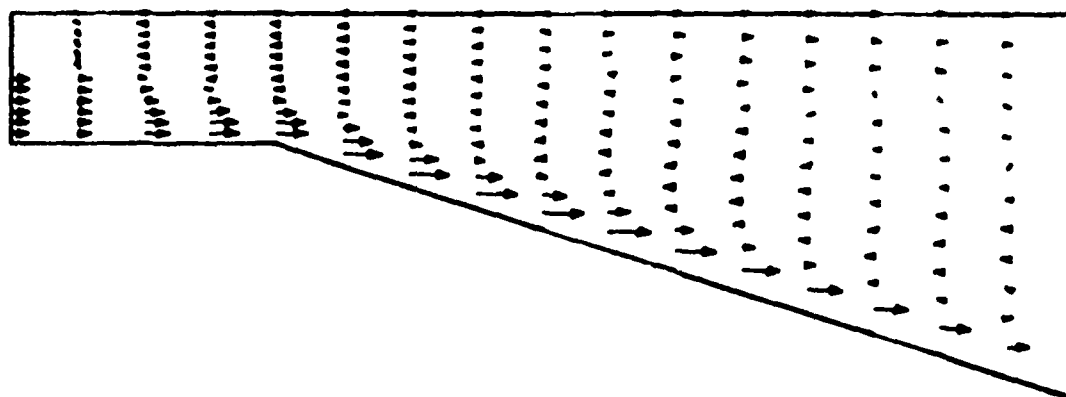


Figure 11. (Sheet 3 of 3)

AD-A160 991 NUMERICAL MODELING OF TWO-DIMENSIONAL WIDTH-AVERAGED
FLOWS USING BOUNDARY (U) MISSISSIPPI STATE UNIV

2/2

NUMERICAL MODELING OF TWO-DIMENSIONAL WIDTH-AVER
FLOWS USING BOUNDARY (U) MISSISSIPPI STATE UNIV

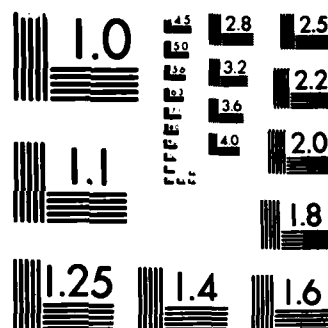
UNCLASSIFIED J F THOMPSON ET AL AUG 85 WES/TR/E-85-9

MISSISSIPPI STATE DEPT OF AEROPHYSICS A
J F THOMPSON ET AL AUG 85 WES/TR/E-85-9

F/G 20/4

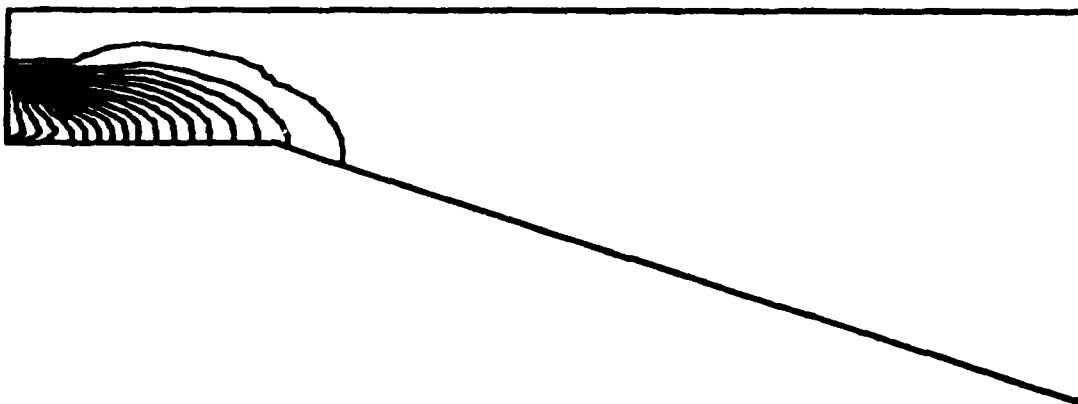
NL

[illegible]

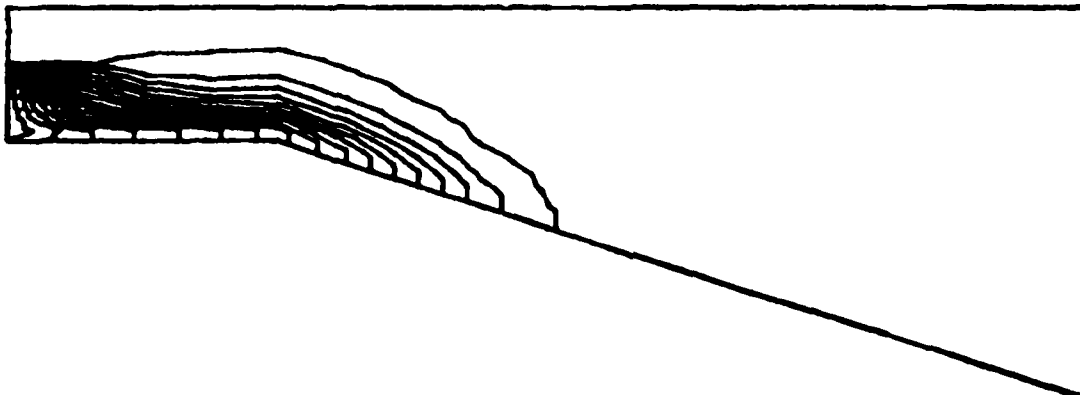


MICROCOPY RESOLUTION TEST CHART
NATIONAL BUREAU OF STANDARDS-1963-A

250 Seconds



500



750

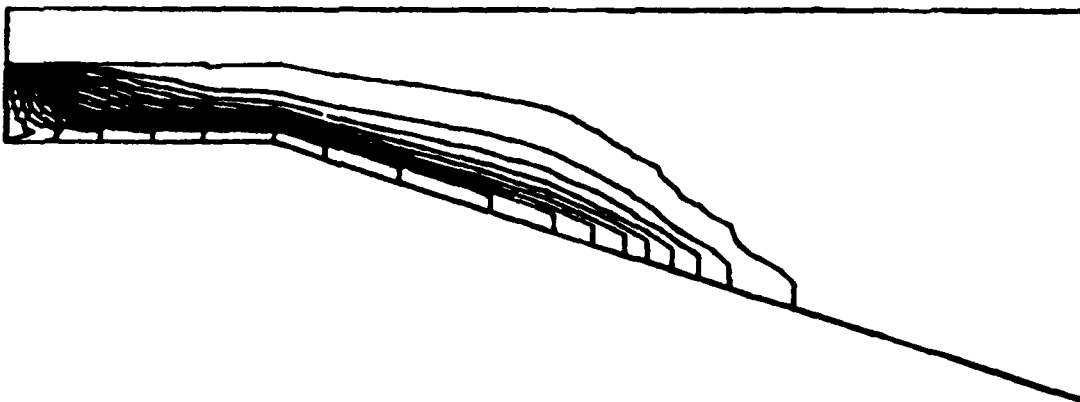
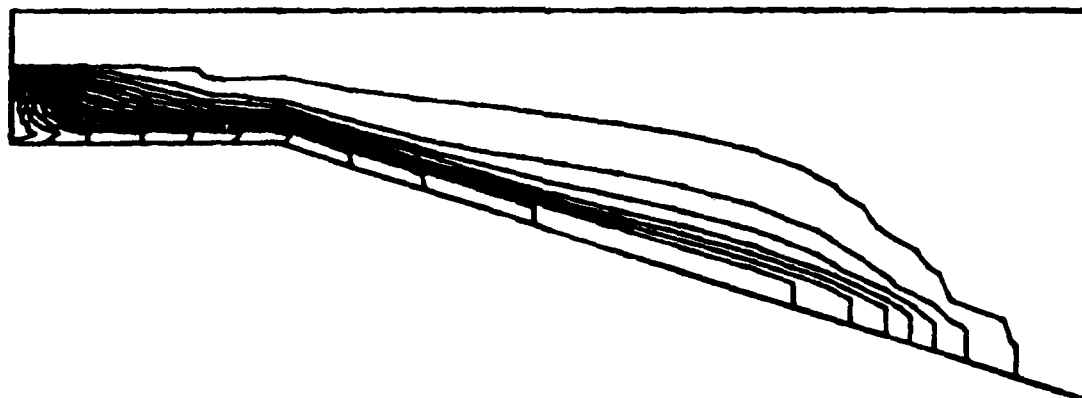
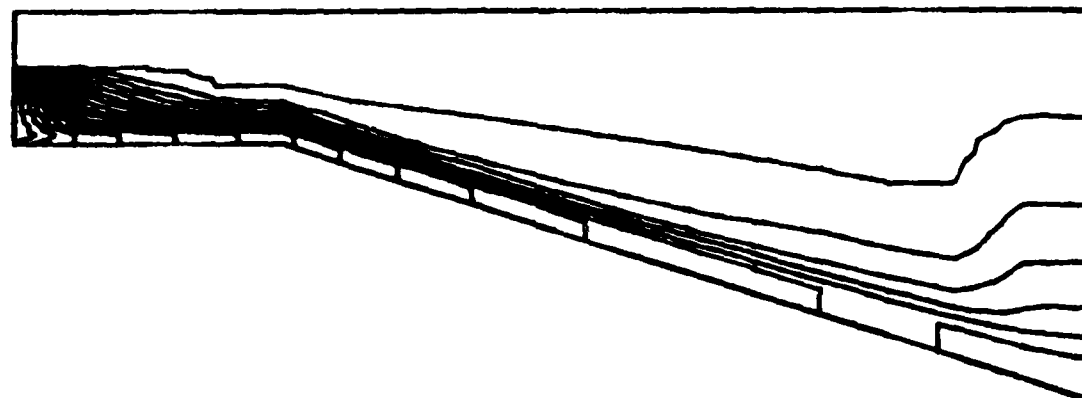


Figure 12. Temperature contours for calculation with Kent turbulence model in GRH flume (contour interval = 0.5° F)
(Sheet 1 of 3)

1000



1250



1500

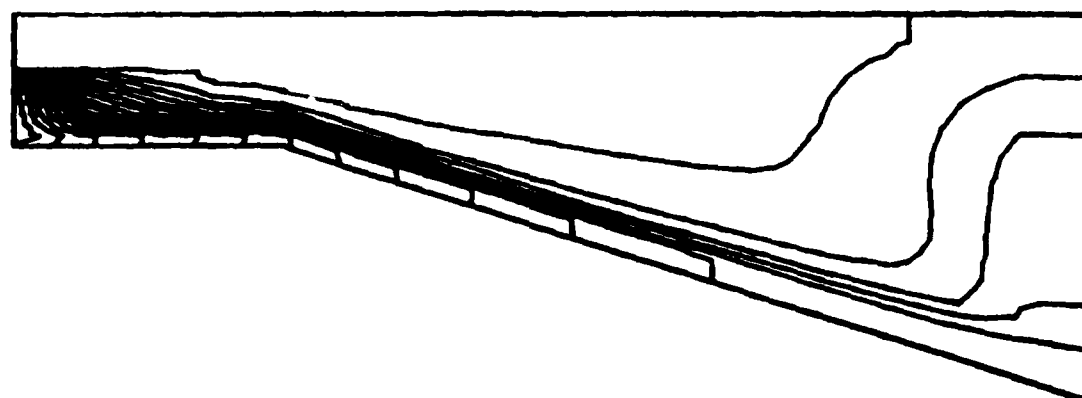
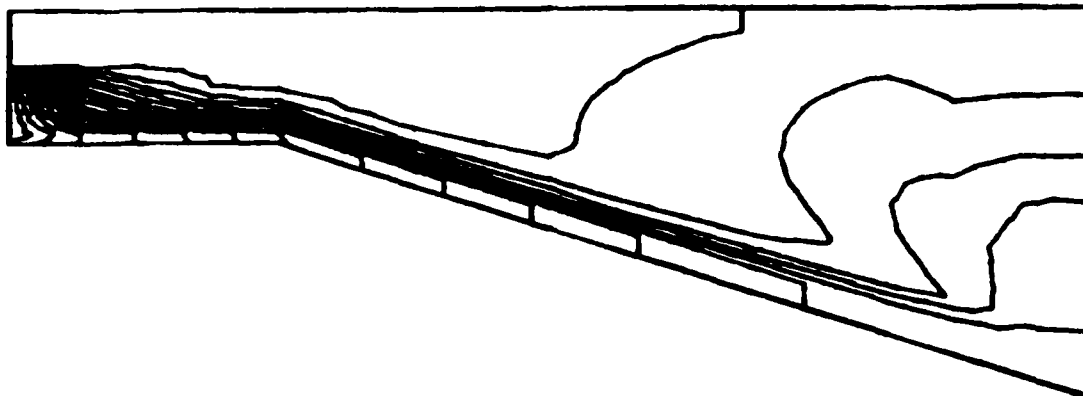
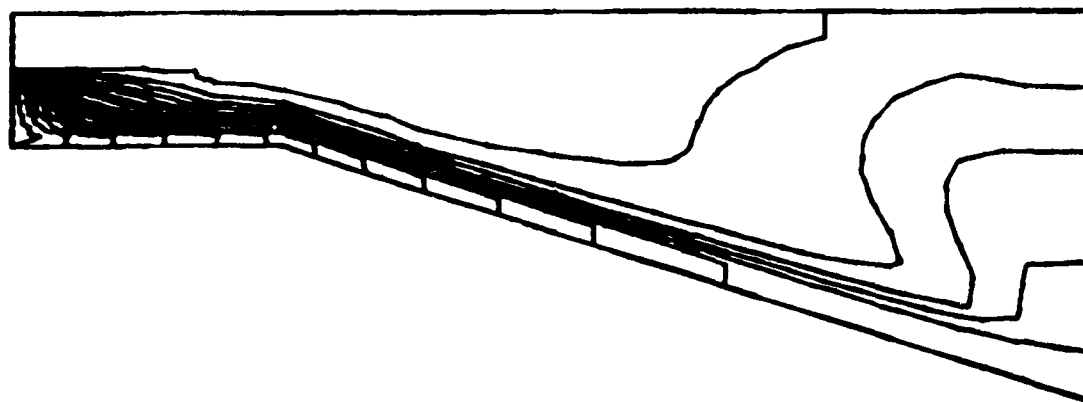


Figure 12. (Sheet 2 of 3)

1750



2000



2500

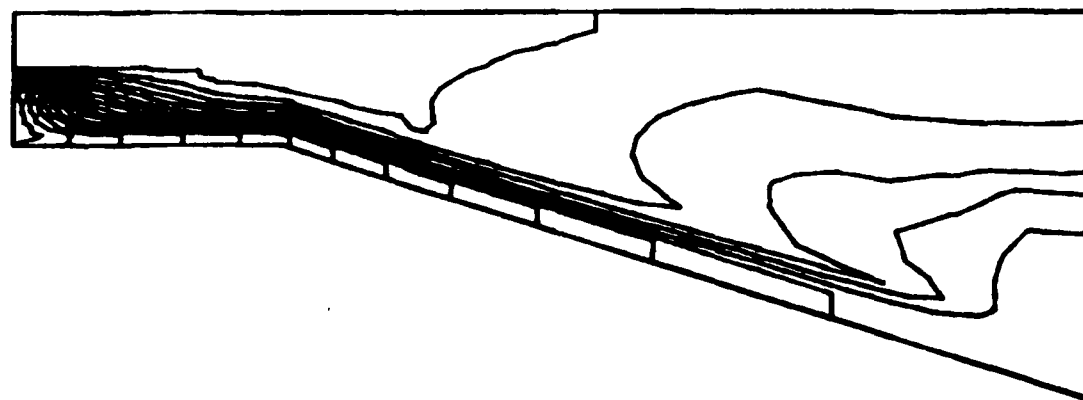
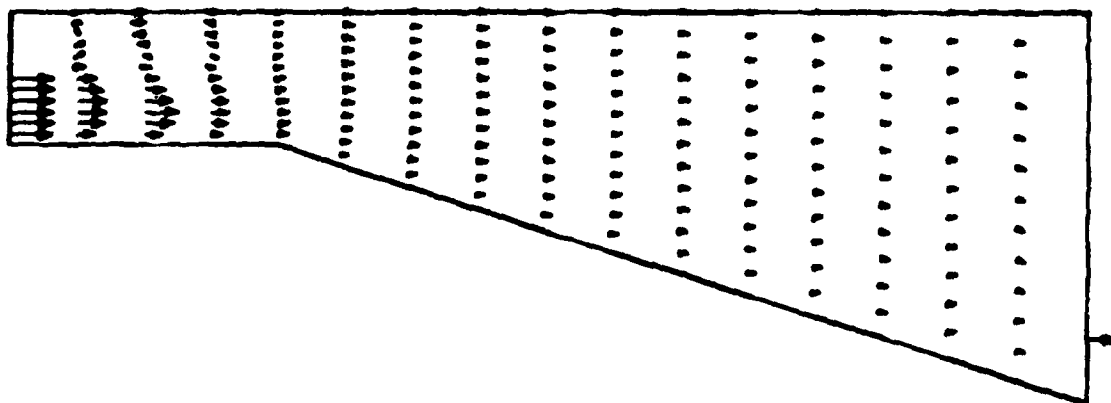
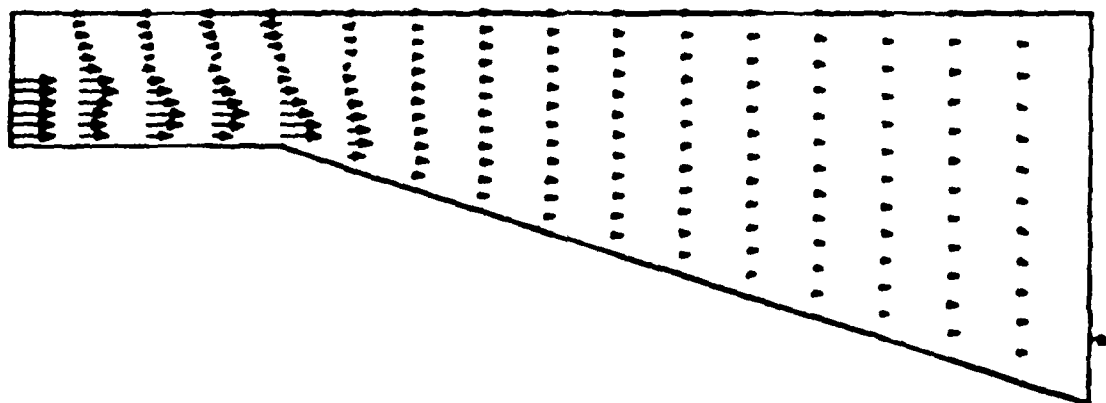


Figure 12. (Sheet 3 of 3)

250 Seconds



500



750

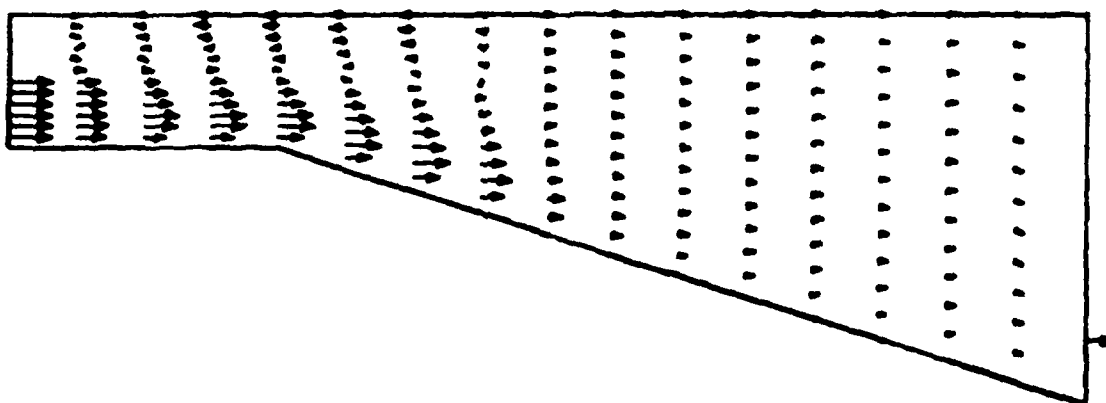
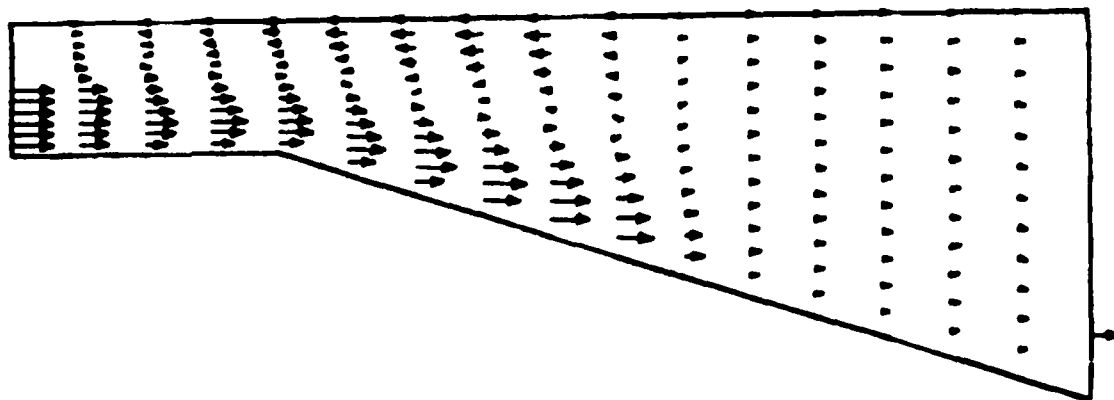
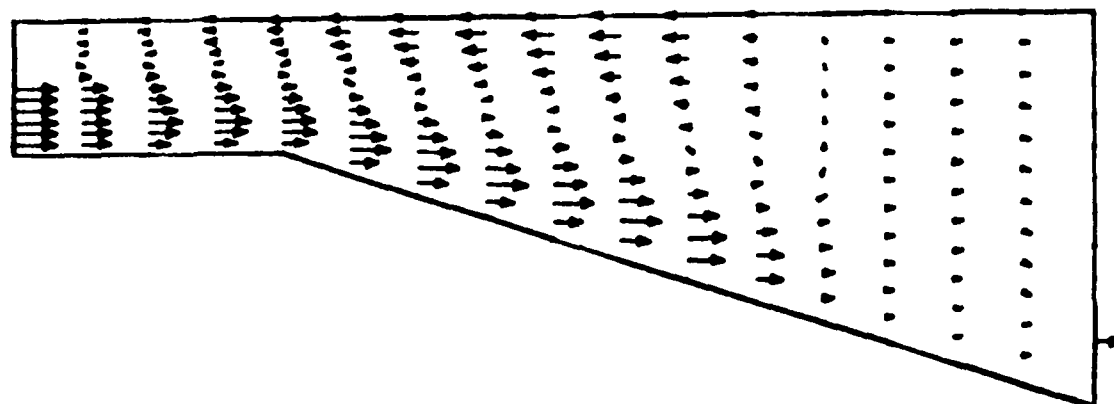


Figure 13. Velocity vectors for calculation with Edinger turbulence model in GRH flume (Sheet 1 of 3)

1000



1250



1500

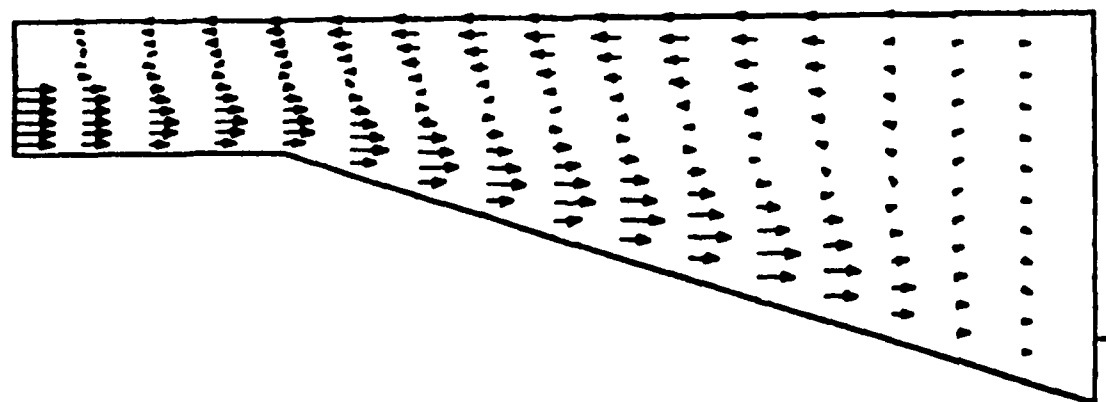
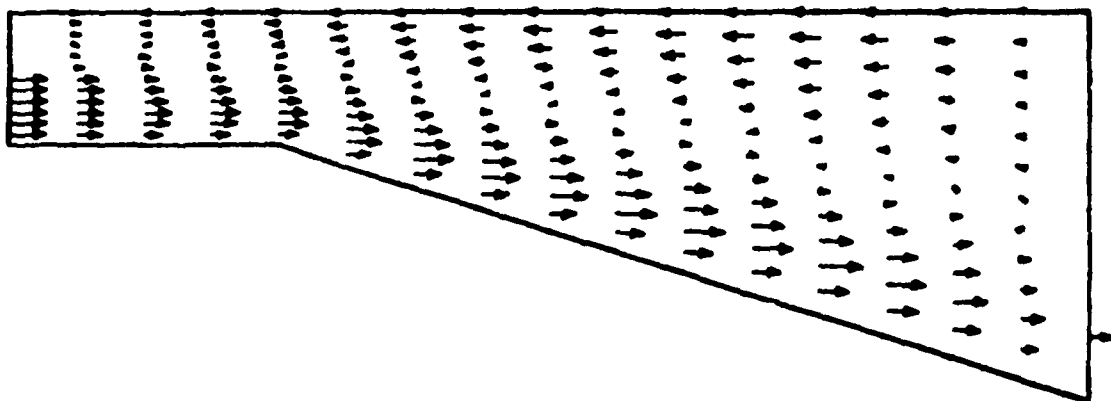
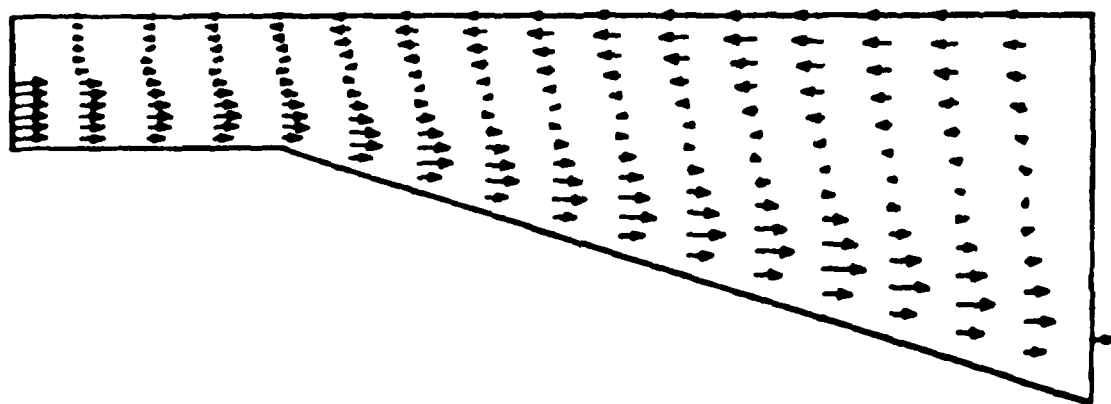


Figure 13. (Sheet 2 of 3)

1750



2000



2500

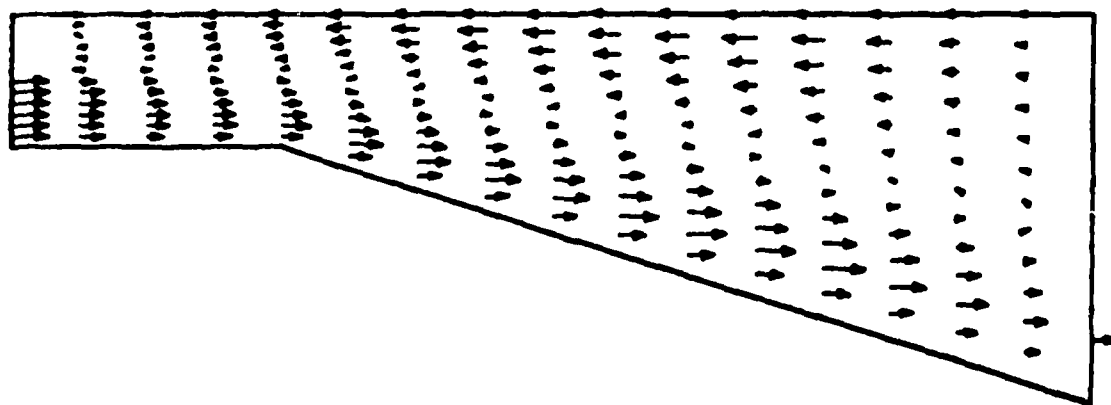
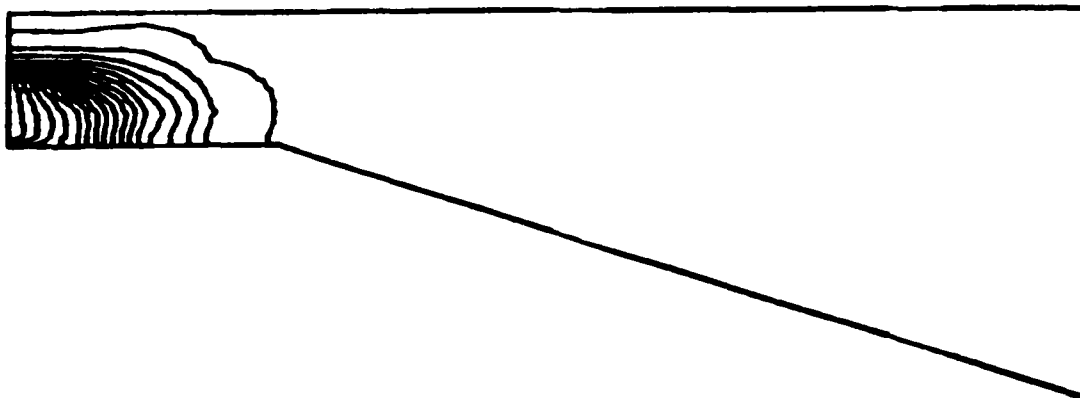
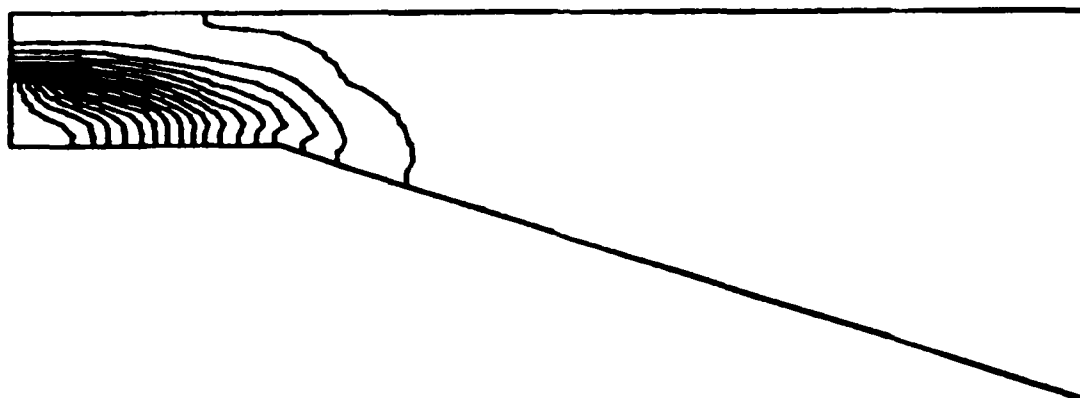


Figure 13. (Sheet 3 of 3)

250 Seconds



500



750

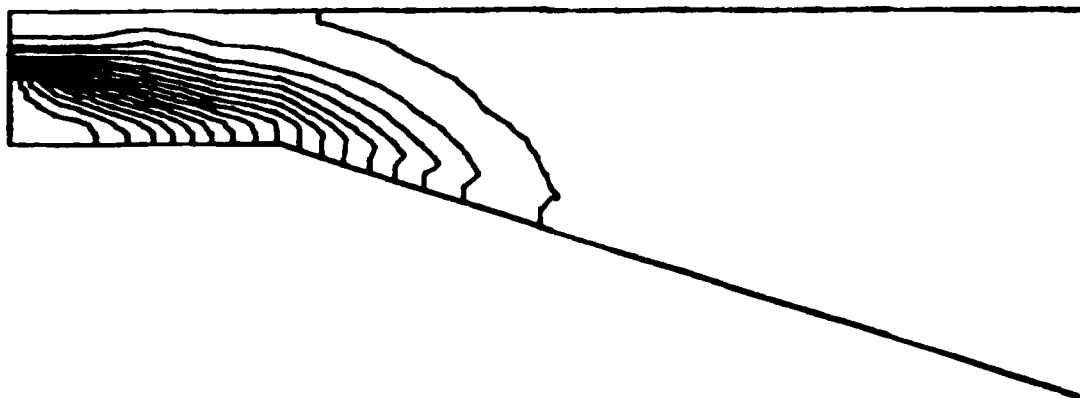
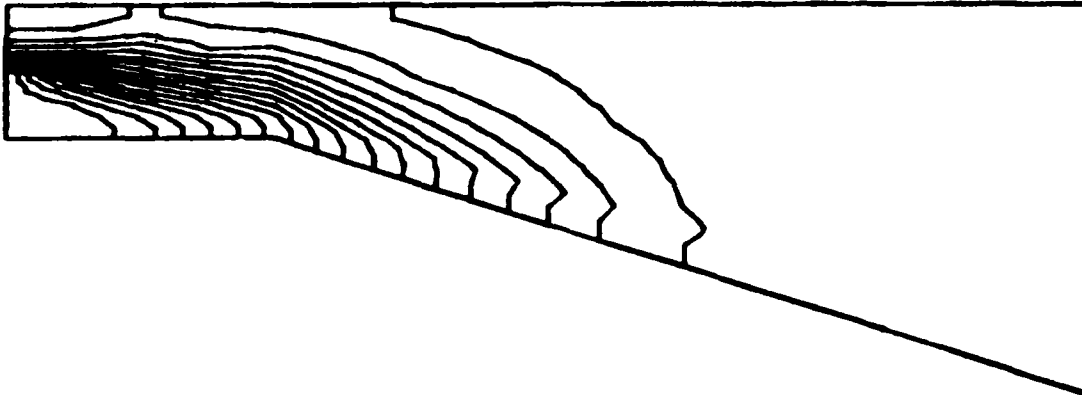
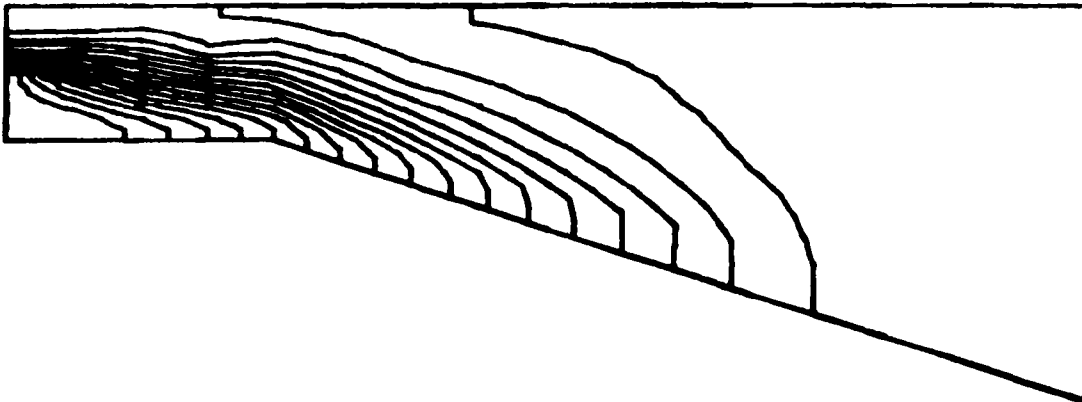


Figure 14. Temperature contours for calculation with Edinger turbulence model in GRH flume (contour interval = 0.5°F)
(Sheet 1 of 3)

1000



1250



1500

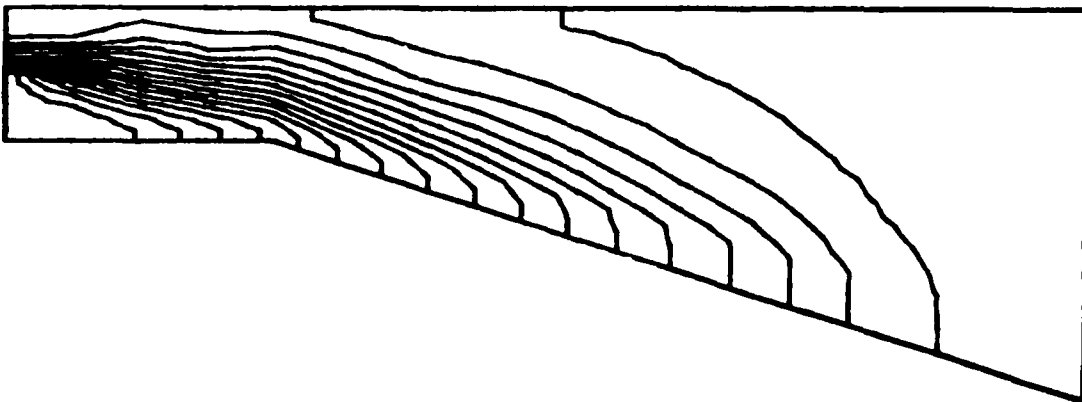
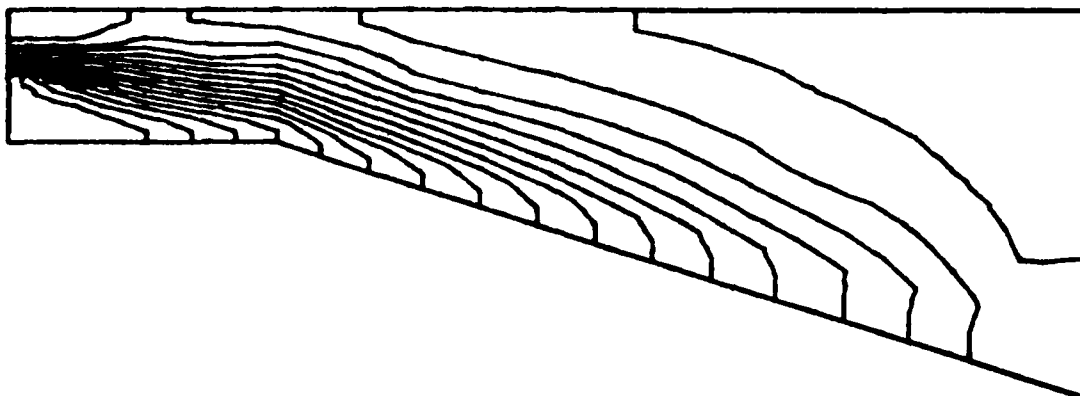
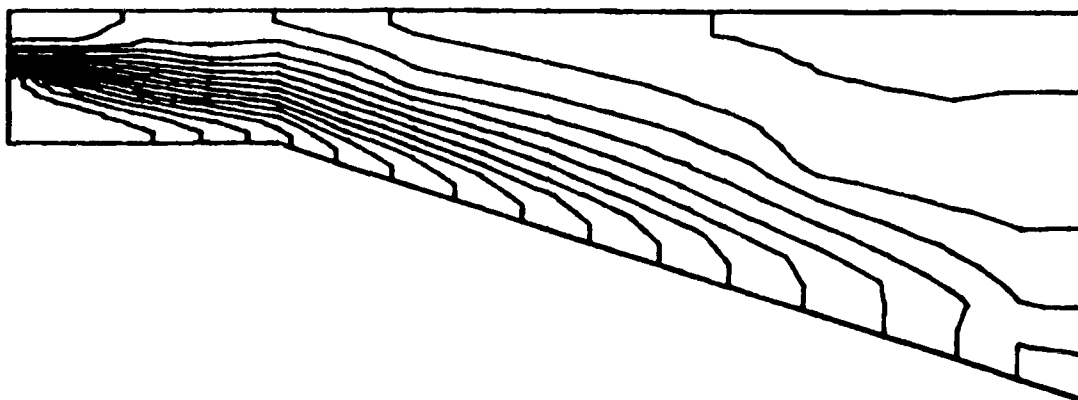


Figure 14. (Sheet 2 of 3)

1750



2000



2500

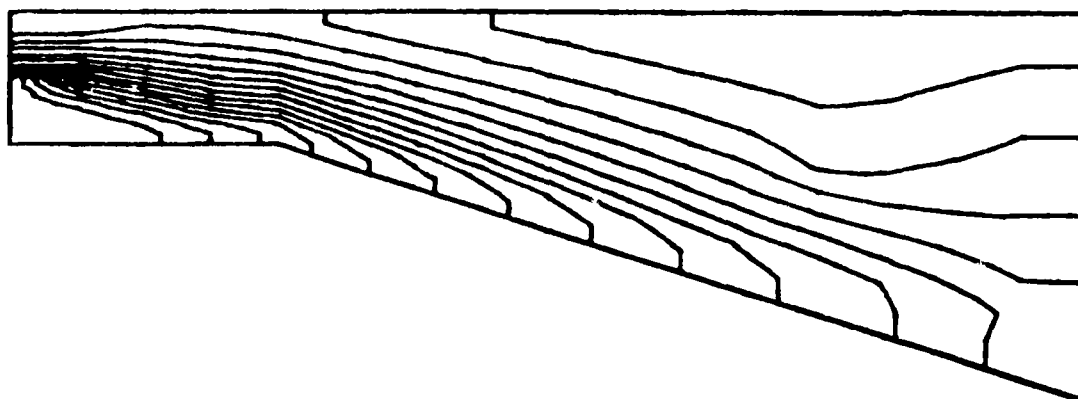


Figure 14. (Sheet 3 of 3)

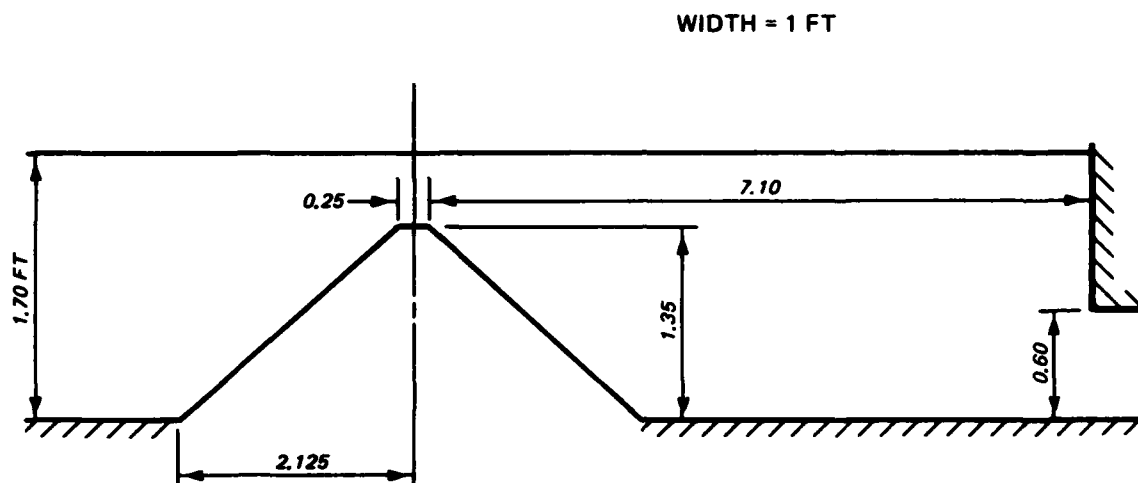


Figure 15. Side view of channel with crested weir

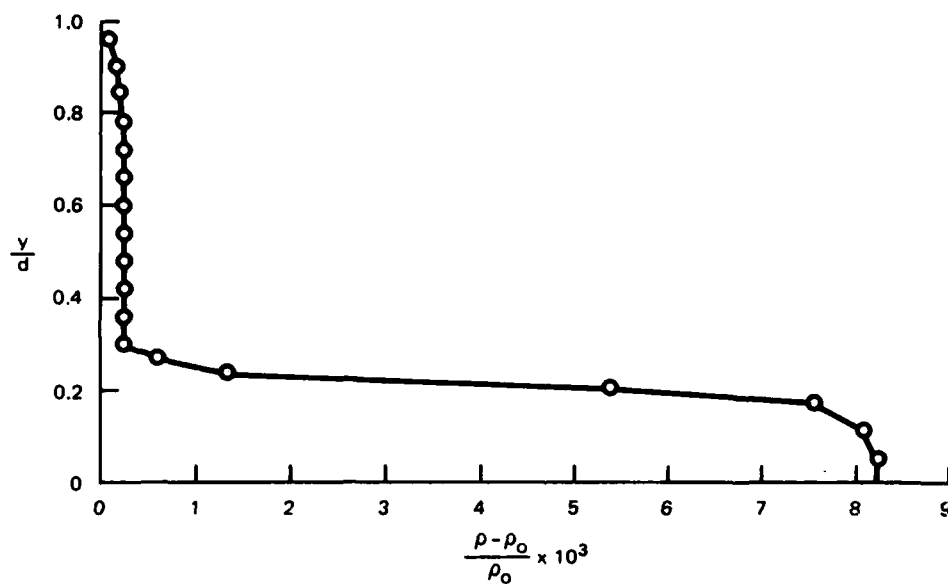
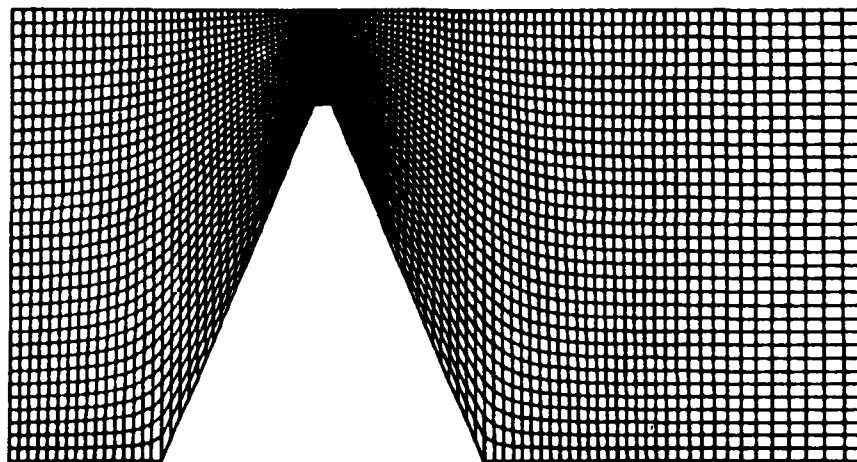


Figure 16. Initial density profile for stratified channel with crested weir

Field System



Flow System

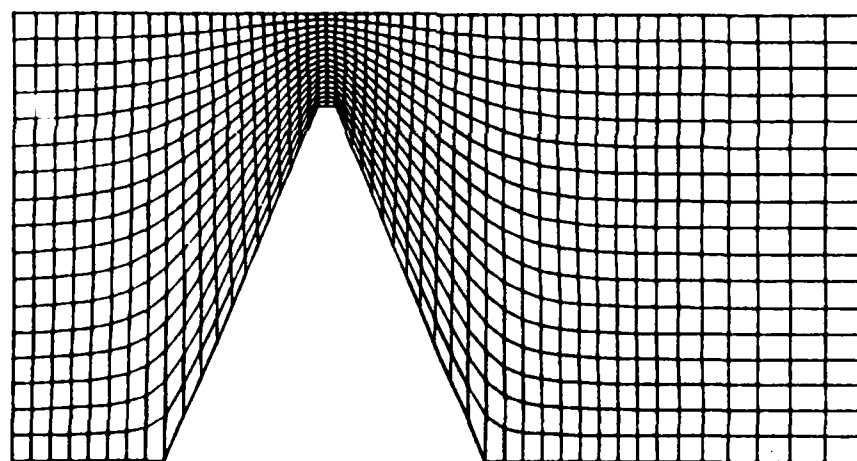


Figure 17. Boundary-fitted coordinate system for channel with crested weir

($j = 1$ to 7) at the downstream boundary ($i = 51$), and the outflow velocities were held fixed and uniform in both cases. The inlet was taken to be the entire upstream vertical boundary (1.7 ft high, $i = 1$, $j = 1$ to 18). The inflow velocities were held fixed and uniform for the unstratified calculation. In the stratified case, however, the inflow

velocities were extrapolated, using the flow balance option, to accommodate possible inflow variations caused by density changes upstream of the weir. The time step for both cases was set at $\Delta t = 0.1$ sec , and the number of iterations was limited to 25 per time step for the first 50 steps, and 15 per time step thereafter.

134. Figures 18 and 19 present comparisons of the measured* and calculated velocity profiles, at the upstream toe of the weir, for the unstratified and stratified cases, respectively. The calculated unstratified profile shows a stronger velocity gradient than the data near the bottom, because the inlet condition (uniform velocity) was specified too close to the weir (4.125 ft from weir crest) for a parabolic profile to develop. The stratified calculation (Figure 19) exhibits better agreement, but the backflow in the dense layer near the bottom was not observed experimentally. Again, this is probably due to (a) the proximity of the computational inflow boundary to the weir, and (b) the extrapolated inflow-velocity boundary condition. Improved results might be obtained by adding a longer upstream section to the grid, with fixed inlet velocity and density.

135. Figure 20 shows a comparison of calculated and observed velocity profiles 3.5 ft downstream of the weir crest, for unstratified flow. The data are taken from the measurements for $Q = 0.074$ cfs , since no downstream results are available for $Q = 0.7$ cfs . The calculated results represent a unit discharge of 0.074 cfs, but they exhibit the same general behavior as the data for 0.7 cfs.

136. Direct comparisons of velocity vector plots are shown for the stratified and unstratified calculations in Figures 21-23. These illustrations show clearly the dramatic contrast between the flow patterns for the two cases. Figure 24 shows time-lapse pictures of the developing circulation downstream of the weir crest for the unstratified

* Personal Communication, J. L. Grace, Jr., op. cit.

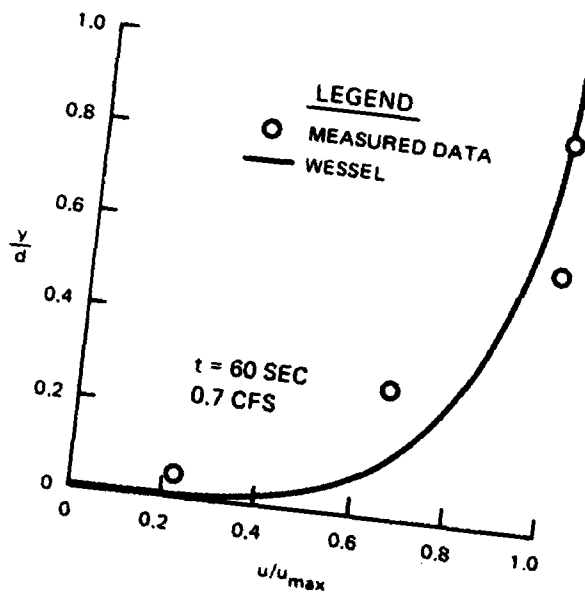


Figure 18. Velocity profile for unstratified flow at upstream toe of weir

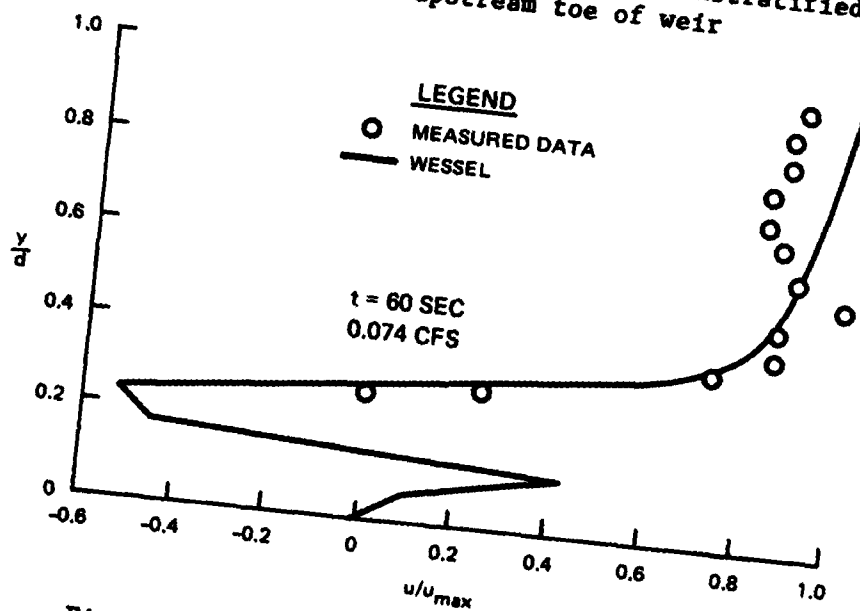


Figure 19. Velocity profile for stratified flow at upstream toe of weir

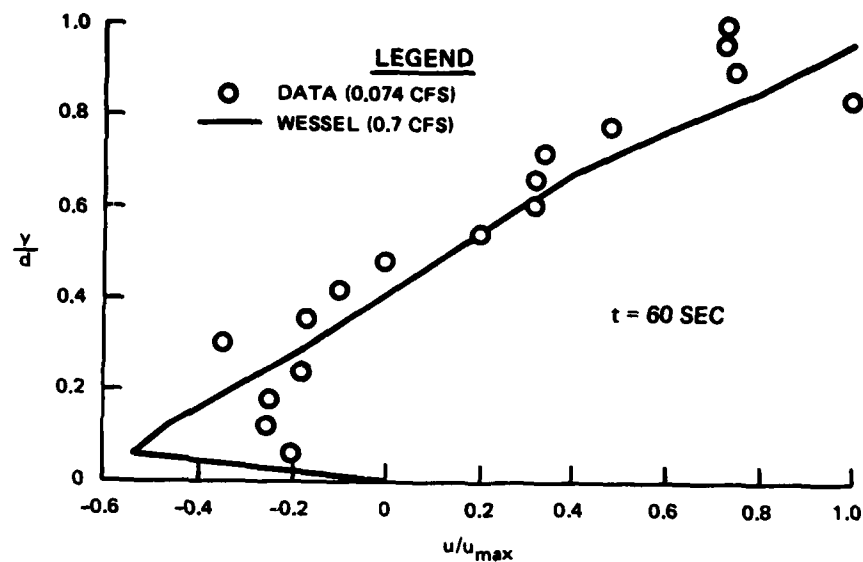


Figure 20. Velocity profile for unstratified flow 3.5 ft downstream of weir crest

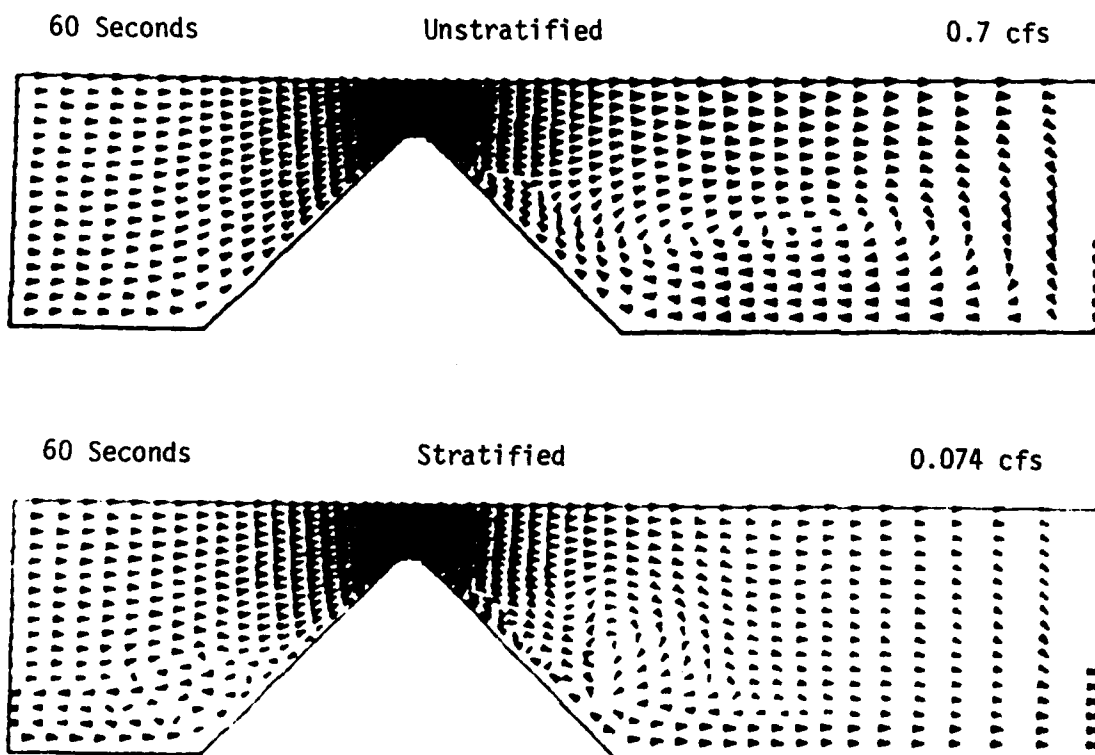
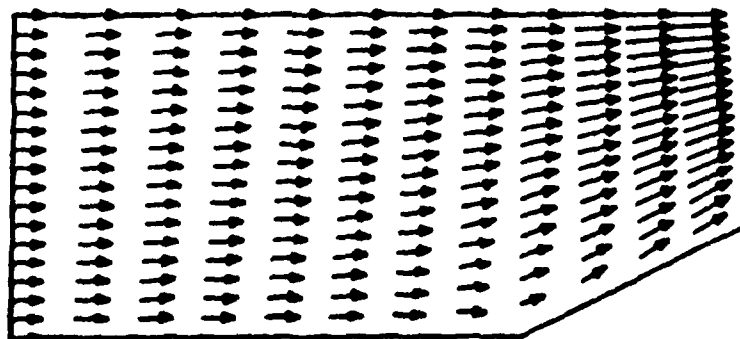


Figure 21. Comparison of velocity vectors for stratified and unstratified flow in channel with crested weir

60 Seconds

Unstratified

0.7 cfs



60 Seconds

Stratified

0.074 cfs

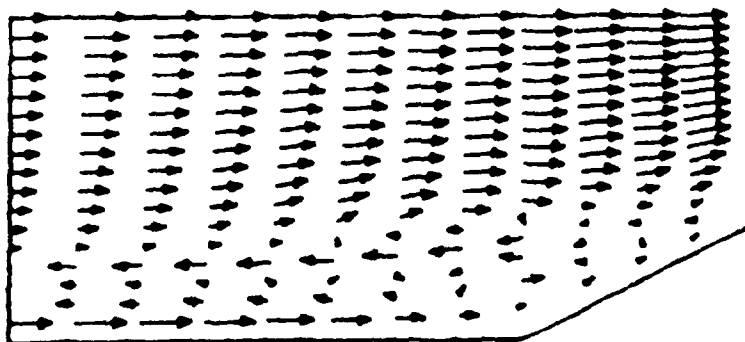


Figure 22. Comparison of velocity vectors for stratified and unstratified flow upstream of weir crest

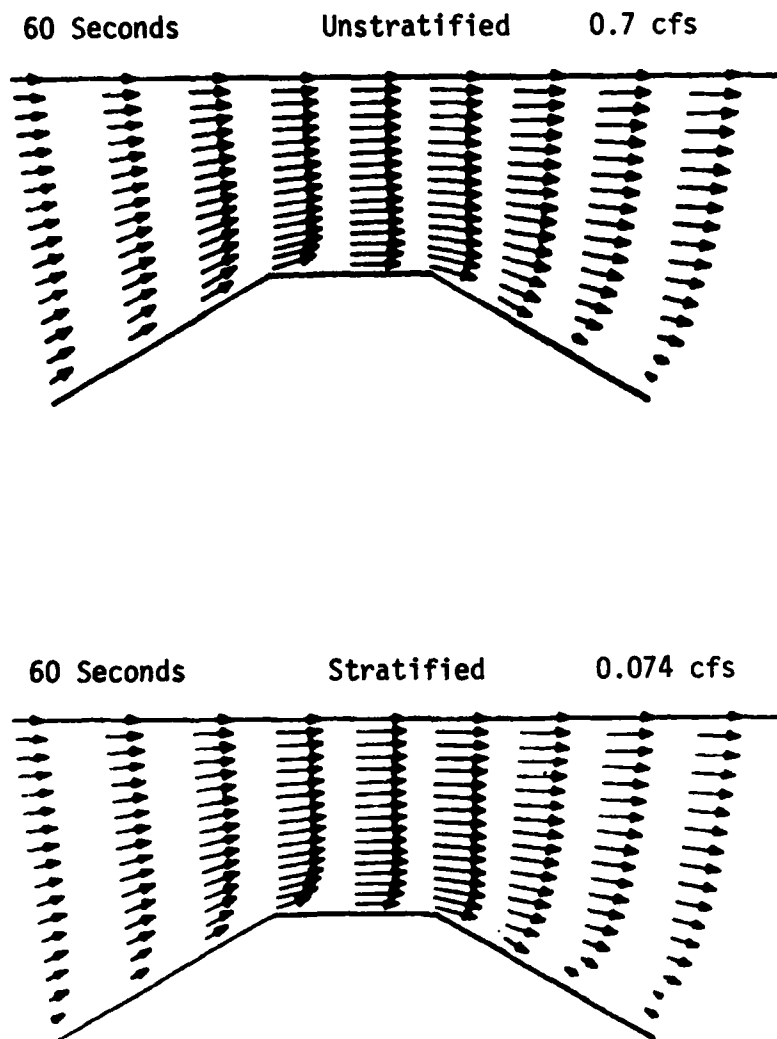
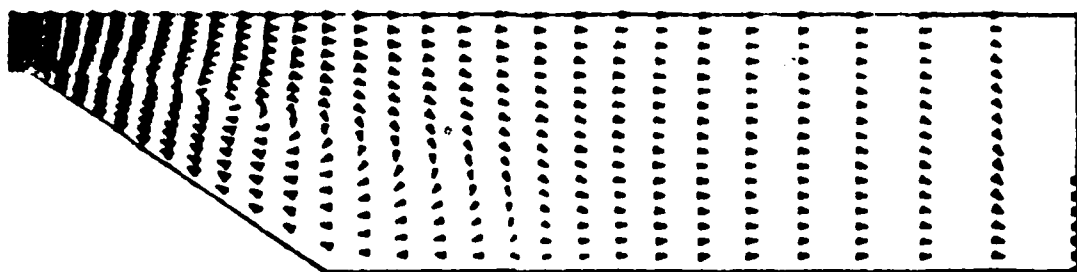
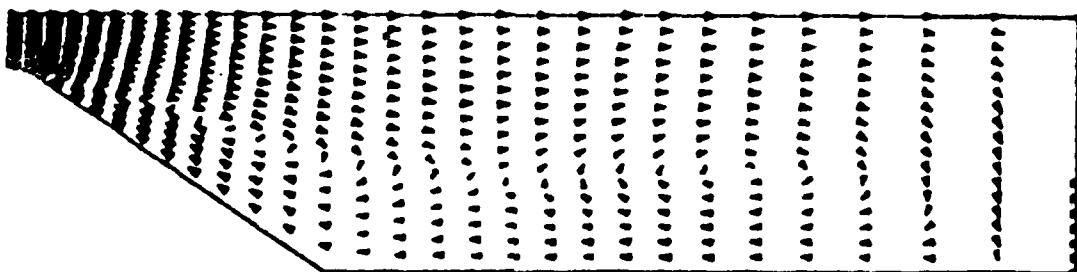


Figure 23. Comparison of velocity vectors for stratified and unstratified flow at weir crest

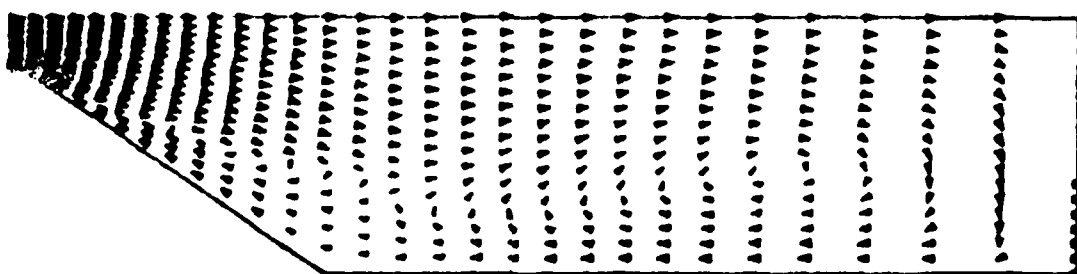
5 Seconds



10



15



20

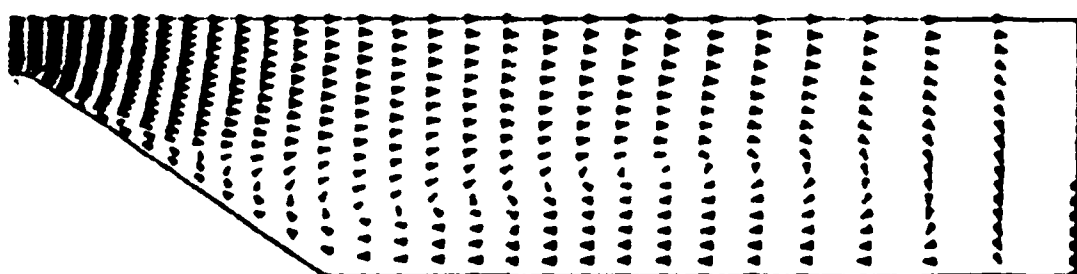
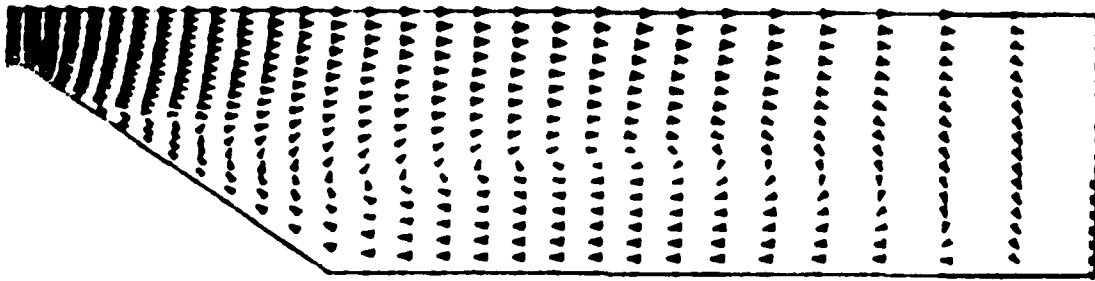
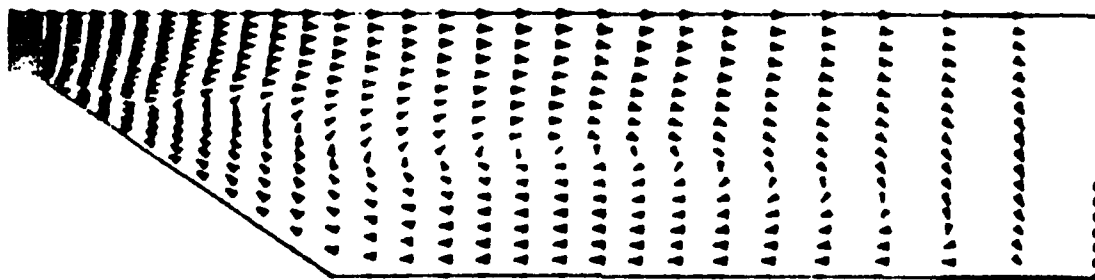


Figure 24. Velocity vectors for unstratified flow downstream of weir crest (Continued)

25



30



60

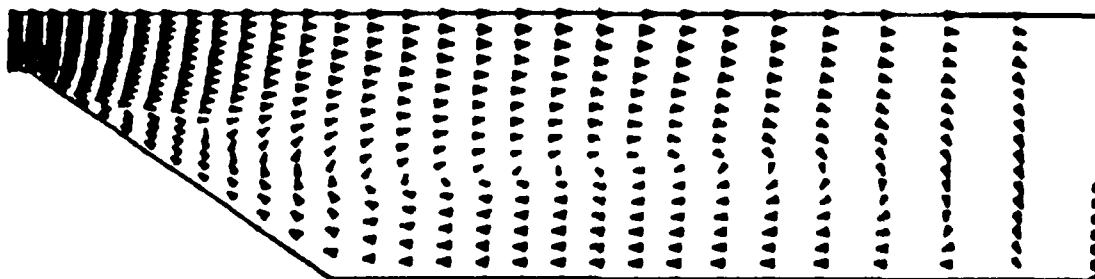
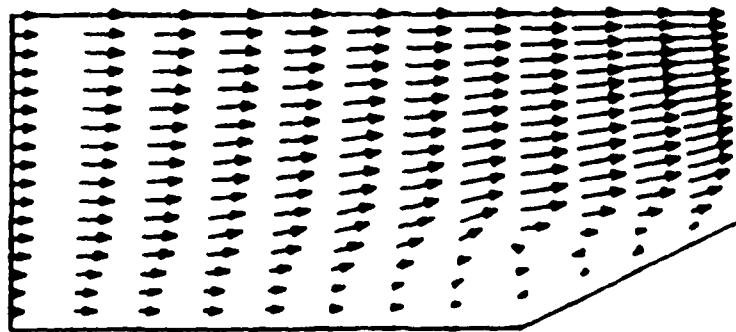


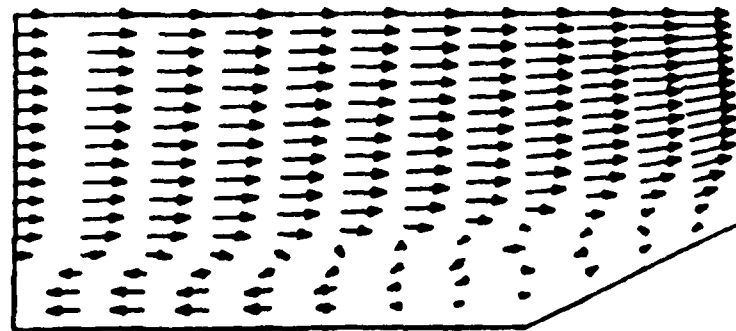
Figure 24. (Concluded)

flow. Figures 25 and 26 present the same sequence of events, on both sides of the weir for the stratified case. As pointed out above, the backflow in Figure 25 is apparently caused by the specified inflow-velocity boundary condition. Density contours for the stratified flow appear in Figure 27.

10 Seconds



20



30

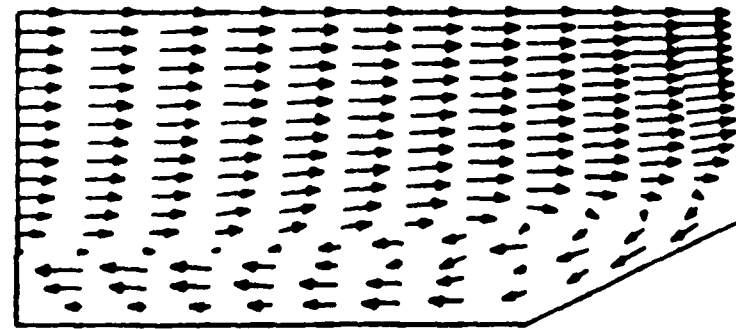
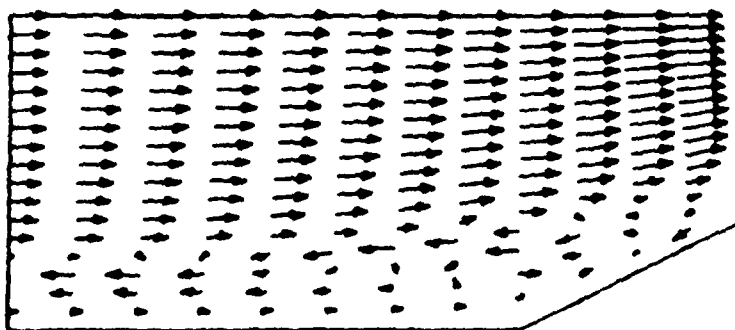
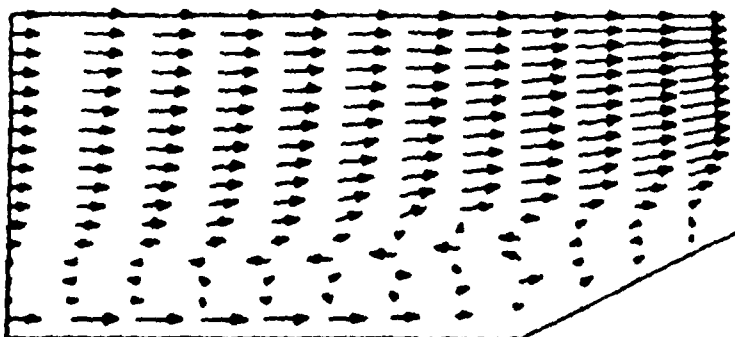


Figure 25. Velocity vectors for stratified flow upstream of weir crest (Continued)

40



50



60

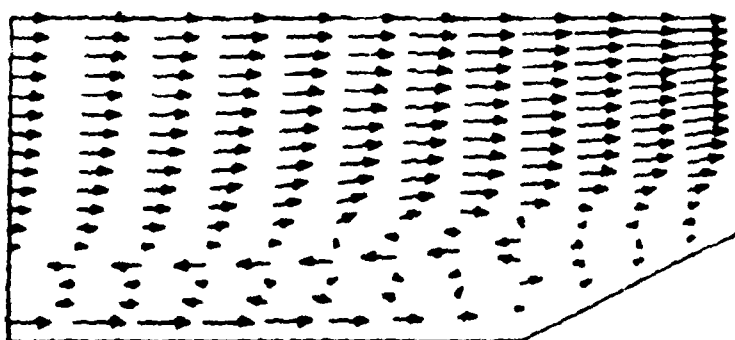
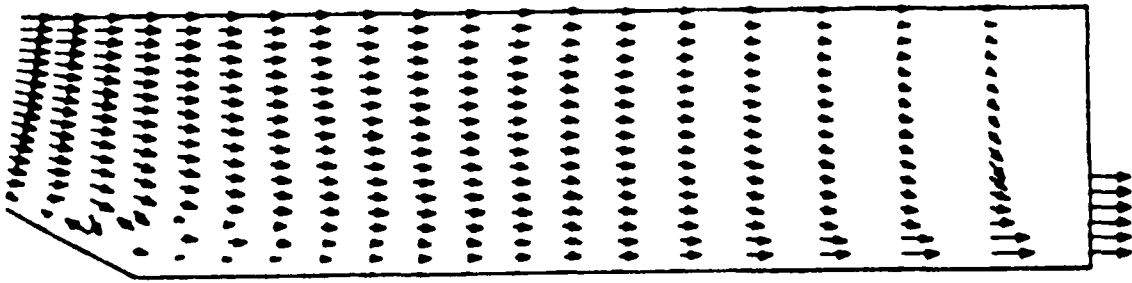
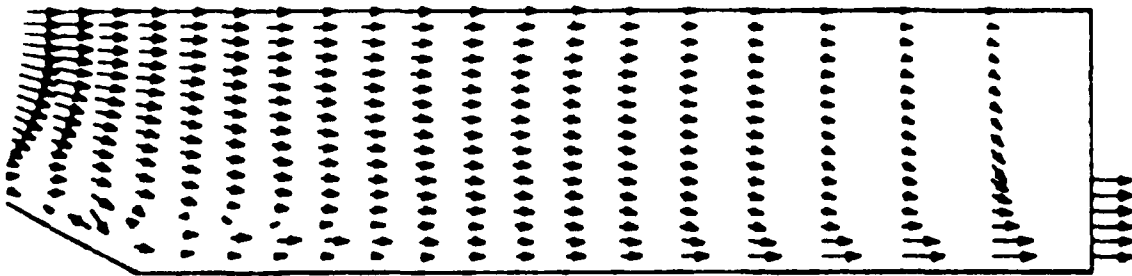


Figure 25. (Concluded)

10 Seconds



20



30

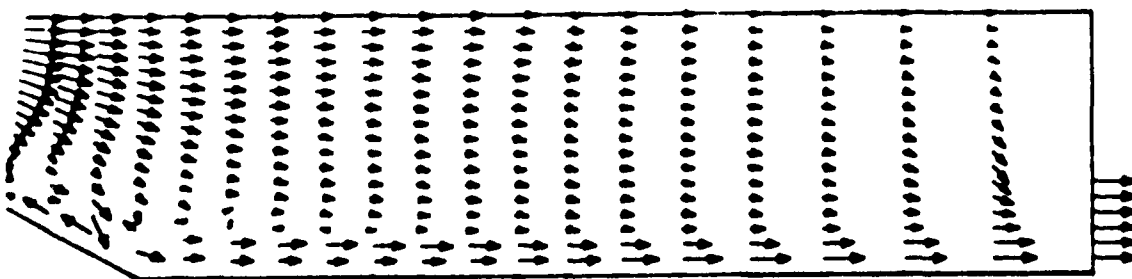
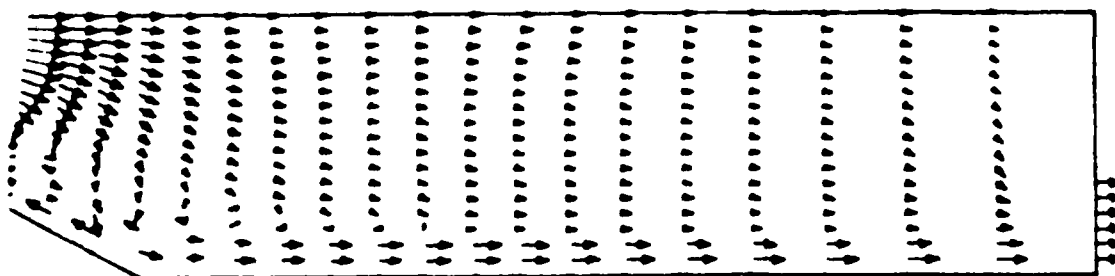
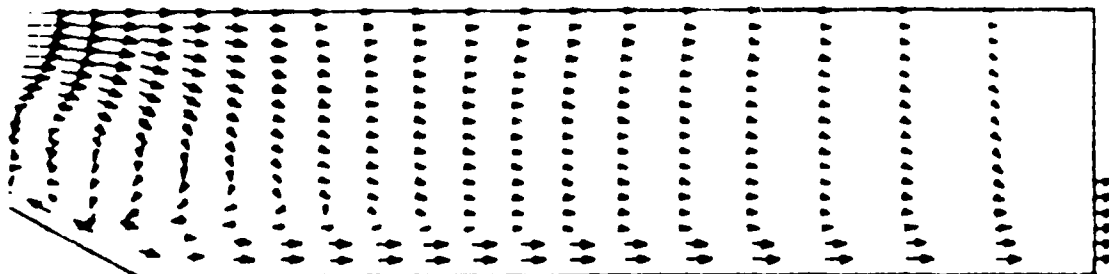


Figure 26. Velocity vectors for stratified flow downstream of weir crest (Continued)

40



50



60

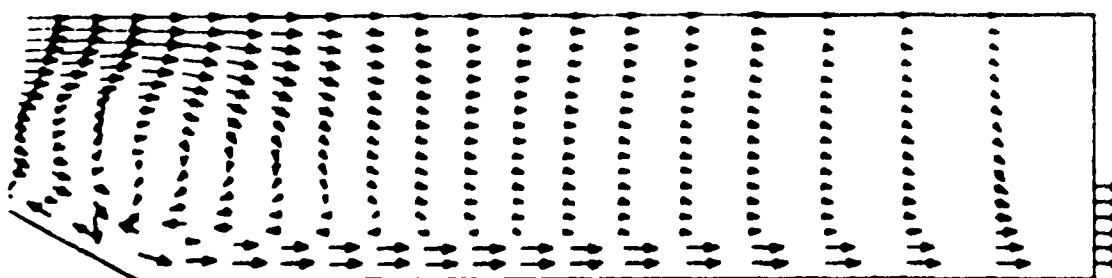
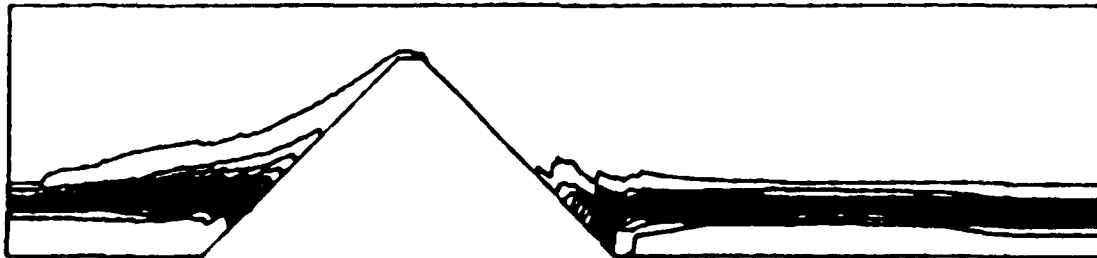
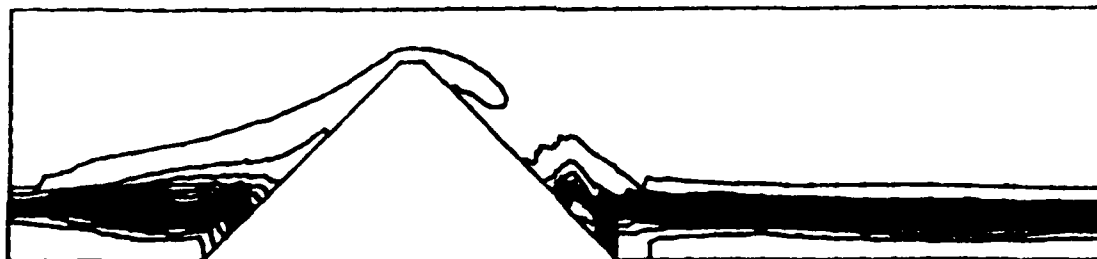


Figure 26. (Concluded)

10 Seconds



20



30

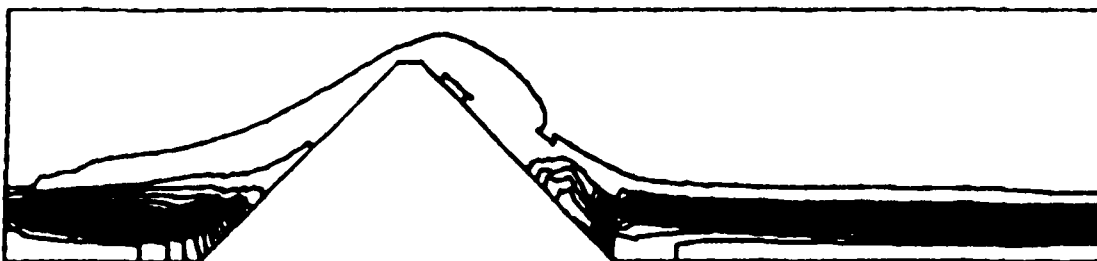
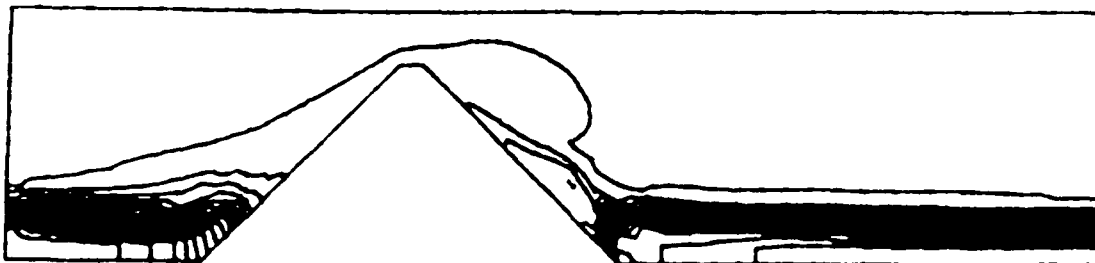
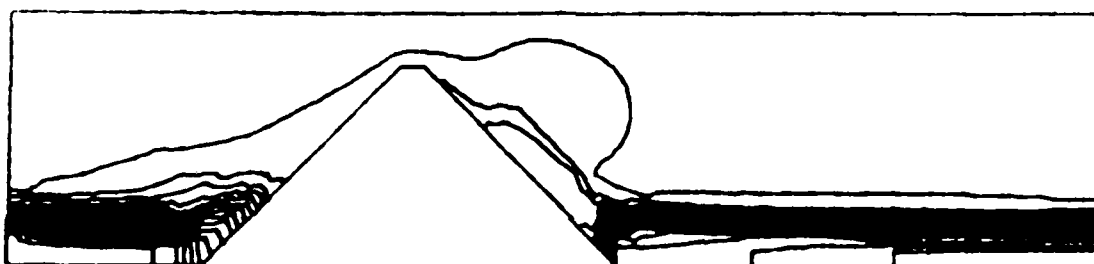


Figure 27. Density contours for stratified flow in channel with crested weir (contour interval = 0.0005 gm/cm^3) (Continued)

40



50



60

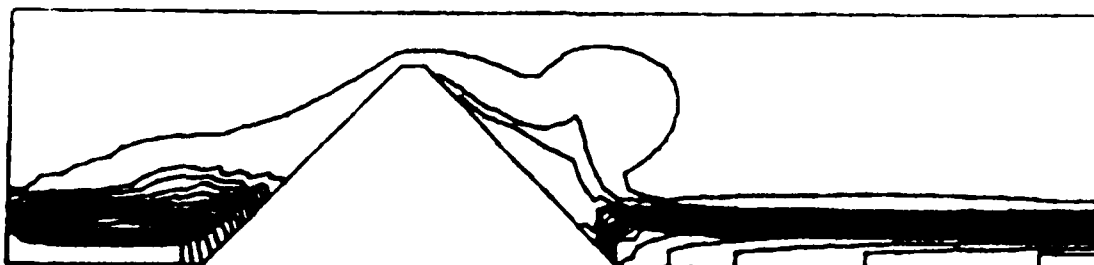


Figure 27. (Concluded)

PART VII: CONCLUSION

137. The WESSEL code is applicable to two-dimensional, time-dependent, width-averaged, variable-density flow in arbitrary regions with multiple inlets, internal obstacles, and boundary intrusions. Changes in the physical configuration can be made easily via input. At present, however, the code is not capable of simulating true free surface behavior.

138. WESSEL solves the Navier-Stokes equations without assuming the pressure to be purely hydrostatic, and this feature sets it apart from most hydraulic codes now in use. Thus, WESSEL provides a needed addition to the mathematical modeling capability of the Corps of Engineers, offering a means of simulating fully convective flow easily and economically. Potential applications include selective withdrawal, spillway approach flow, outlet works design, and pump station analysis.

139. The accuracy of the time-dependent predictions can be expected to improve with further experience in the use of the code. Since WESSEL is written to be very general in application, its operation is slowed somewhat by this generality. As it now stands, about 1 sec of CRAY computer time (scalar mode) is required to execute 15 iterative sweeps on a 50×20 grid. A faster code of more limited scope could be obtained by deleting a number of contingency checks in the present version. Further development and evaluation is planned along these lines. A new version of the code, using stream function and vorticity, has already been developed and will be documented in the future.

140. The one-sided differencing scheme for the continuity equation arose from a discussion at WES.* This scheme allows the use of a regular grid,** while retaining the point-to-point velocity and pressure coupling of a staggered grid.† A more extensive investigation of the method is anticipated in future work.

* Personal Communication, 1983, R. S. Bernard, J. F. Thompson, and P. J. Roache, US Army Engineer Waterways Experiment Station, Vicksburg, Miss.

** Pressure and velocity calculated at the same grid points.

† Pressure and velocity calculated at alternate grid points.

REFERENCES

1. Brandsma, M. G., and Divoky, D. J. 1976. "Development of Models for Prediction of Short-Term Fate of Dredged Material Discharged in the Estuarine Environment," Contract Report D-76-5, US Army Engineer Waterways Experiment Station, Vicksburg, Miss.
2. Chorin, A. J. 1967. "A Numerical Method for Solving Incompressible Viscous Flow Problems," Journal of Computational Physics, Vol 2, No. 12.
3. Edinger, J. R., and Buchak, E. M. 1979. "A Hydrodynamic Two-Dimensional Reservoir Model: Development and Test Application to Sutton Reservoir, Elk River, West Virginia," prepared for US Army Engineer Division, Ohio River, Cincinnati, Ohio.
4. Johnson, B. H. 1981. "A Review of Numerical Reservoir Hydrodynamic Modeling," Technical Report E-81-2, US Army Engineer Waterways Experiment Station, Vicksburg, Miss.
5. Kao, W. K., Pao, H. P., and Wei, S. N. 1974. "Dynamics of Establishment of Selective Withdrawal of a Stratified Fluid from a Line Sink, Part 2. Experiment," Journal of Fluid Mechanics, Vol 65, No. 689.
6. Kent, R. E., and Pritchard, D. W. 1959. "A Test of Mixing Length Theories in a Coastal Plain Estuary," Journal of Marine Research, Vol 18, No. 62.
7. Pao, H. P., and Kao, W. K. 1974. "Dynamics of Establishment of Selective Withdrawal of a Stratified Fluid from a Line Sink, Part 1. Theory," Journal of Fluid Mechanics, Vol 65, No. 657.
8. Thompson, J. F., ed. 1982a. Numerical Grid Generation, Proceedings of a Symposium on the Numerical Generation of Curvilinear Coordinate Systems and Their Use in the Numerical Solution of Partial Differential Equations, North-Holland Company, New York.
9. _____. 1982b. "General Curvilinear Coordinate Systems," Numerical Grid Generation, North-Holland Company, New York, pp 1-30.
10. _____. 1982c. "Elliptic Grid Generation," Numerical Grid Generation, North-Holland Company, New York, pp 79-105.
11. _____. 1983. "WESCOR - Boundary-Fitted Coordinate Code for General Two-Dimensional Regions with Obstacles and Boundary Intrusions," Technical Report E-83-8, US Army Engineer Waterways Experiment Station, Vicksburg, Miss.

12. Thompson, J. F., and Bernard, R. S. 1985. "WESSEL: Code for Numerical Simulation of Two-Dimensional Time-Dependent Width-Averaged Flows with Arbitrary Boundaries," Technical Report E-85-8, US Army Engineer Waterways Experiment Station, Vicksburg, Miss.
13. Thompson, J. F., Thames, F. C., and Mastin, C. W. 1977. "TOMCAT - A Code for Numerical Generation of Boundary-Fitted Curvilinear Coordinate Systems on Fields Containing Any Number of Arbitrary Two-Dimensional Bodies," Journal of Computational Physics, Vol 24, No. 274.
14. Thompson, J. F., Warsi, Zahir U. A., and Mastin, C. W. 1983. "Boundary-Fitted Coordinate Systems for Numerical Solution of Partial Differential Equations - A Review," Journal of Computational Physics, Vol 47, pp 1-108.
15. Zalesak, S. T. 1981. "High Order ZIP Differencing of Convective Terms," Journal of Computational Physics, Vol 40, No. 497.

APPENDIX A: NOTATION

B	Lateral width
D	Mass residual
e	Internal (thermal) energy per unit mass
F	Densimetric Froude number
f	Arbitrary function
g	Gravitational acceleration
g_i	Components of gravity vector
h	Enthalpy per unit mass
i, j	Unit vectors in x- and y-directions, respectively
J	$x_\xi y_\eta - x_\eta y_\xi$
N	Vaisala frequency
n_i	Components of surface-normal vector
\underline{n}	Surface-normal vector
n	Superscript indicating time-step number
p	Pressure
p_H	Hydrostatic pressure
p_o	Reference pressure
Q	Flow rate
q_i	Components of heat flux vector
\underline{r}	Position vector
S(t)	Surface of moving volume V(t)
T	Temperature
t	Time
t^*	Nondimensional time

U_i	Components of surface velocity
u_i	Components of fluid velocity
\underline{u}	Fluid velocity vector
u^*	Nondimensional velocity
u, v	x- and y-components of \underline{u} , respectively
\tilde{u}, \tilde{v}	Fluxes of \underline{u} through surfaces of constant ξ and constant η , respectively
x_i	Components of cartesian position vector
x, y	Cartesian coordinates
α	$x_\eta^2 + y_\eta^2$
β	$x_\xi x_\eta + y_\xi y_\eta$
γ	$x_\xi^2 + y_\xi^2$
δ_{ij}	Kroniker delta
∇	Gradient operator
∇^2	Laplacian operator
Δ	Incremental operator
μ	Dynamic viscosity
μ'	Bulk viscosity
κ	Thermal conductivity
ρ	Density
ρ_s	Initial density
ρ_o	Reference density
σ_{ij}	Components of stress tensor
τ_{ij}	Components of shear stress tensor

ξ, η Curvilinear coordinates

ω Acceleration parameter

END

FILMED

12-85

DTIC